Foam geometry and structural design of porous material

Gabbrielli, Ruggero

Award date:
2009

Awarding institution:
University of Bath

Foam geometry
and structural design of porous material

Ruggero Gabbrielli

A thesis submitted for the degree of Doctor of Philosophy

University of Bath

Department of Mechanical Engineering

Submitted: April 2009

Revised: August 2009

Contents

All the text, illustrations and ideas contained in this work, unless differently specified, are original work of Ruggero Gabbrielli.

Everything that is really great and inspiring is created by the individual who can labor in freedom.

A. Einstein. Out of my later years, 1950

Acknowledgments

I would like to thank my supervisors Irene Turner and Chris Bowen for the guidance and the support received in these three years at the Centre for Orthopaedic Biomechanics at the University of Bath, UK. I wish to thank all the staff from the Department of Mechanical Engineering that helped me while using manufacturing equipment and optical instruments, Peter Taylor, Frank Hammett, Ian Trussler, Chris Arnold and Andrew Green.

I wish to thank Thomas Hales for the interesting discussions on sphere coverings and on the Kelvin problem.

A special thank you goes to Ken Brakke, whose invaluable help with his program, the Surface Evolver, has been fundamental. A large part of the code used in this work has been written by himself from scratch on the basis of needs arose by myself during the modelling of foams.

An enormous thank you goes to John Sullivan. I owe a relevant part of my results to his Voronoi constructor vcs and to his code for dealing with periodic foams in the Surface Evolver.

I thank Olaf Delgado-Friedrichs, who introduced me to the computational tiling theory and the powerful applications he developed, 3dt and Systre, that have been necessary tools in the development of this work. He supplied me with an algorithm that made possible the discovery of a wide number of completely new partitions of space whose surface area has been

calculated in this work for the first time. I also wish to thank the people who contributed to the search for a counter-example to Kelvin's conjecture with their individual computer resources: Michael Ayers, Giacomo Bagnoli, Frances Baxter, Michela Bonsignori, Ferruccio Gabbrielli, Francesco Gabbrielli, Tim Holsgrove, Toby Jameson, Russell Mckenna and Sarah Sydney.

I wish to say thank you to Michael O'Keeffe, whose help and guidance have been highly constructive, for having me introduced to symmetry and for the interesting and useful discussions we had, often starting points for new thoughts.

I would like to thank Davide Proserpio for his advice and his continuous support on file conversion, the CILEA supercomputer facility in Milan and James Davenport and the supercomputing facility in Bath for the help received in carrying out most of the computational work. Thanks also to the Numerical Algorithms Group for their support on MPI.

Thanks to Stephen Hyde and Barry Ninham who gave me the chance to show the most important achievement I was able to reach in these three years to a very heterogeneous audience last year in Canberra. I will not forget it.

Thanks to Bernd Sing, who created the web page containing the graphical output of the main results found by Olaf's algorithm. I will miss the productive meetings we had during our collaboration on foam modelling.

I am profoundly grateful to Michael Cross, whose online demonstrations on pattern formation have the power of sharing to the world the behaviour of a family of partial differential equations using an interactve visual interface. This applet gave me the idea for the method that produced the counter-example to Kelvin's conjecture contained in this thesis.

I wish to thank David Lloyd who provided the bi-dimensional solver

written for Matlab^{TM}, that I extended to the three-dimensional case. His support and guidance have been - and currently are - fundamental.

The initial code for the generation of the periodic nodal surfaces has been written by Michael Carley, specifically for this application, and it has been used for the first batch of samples realized on the rapid prototyping equipment at the Department of Mechanical Engineering at the University of Bath. Thank you, Michael.

Thanks to Randall Kamien and his group for sharing their projects with me and for the interest shown in the application of pattern formation to spatial partitions: Gareth Alexander, Bryan Chen, Tom Haxton, Xiaoming Mao, Sabetta Matsumoto and Vincenzo Vitelli.

I thank Simon Cox for the generation of files with the geometry of individual polyhedra.

I would like to thank Denis Weaire, Stefan Hutzler and the PhD students at the Foams & Complex Systems Research Group at the Trinity College for the pleasant day spent in Dublin and the fruitful debates about their projects.

This work was supported by the University of Bath, UK and the programme Bridging the Gaps, funded by the EPSRC.

To my father Fiornando.

Abstract

This work considers the geometry of foams, their relation to three-dimensional patterns and a set of idealized structures intended to model highly porous materials for structural applications.

Foams are aggregates of bubbles, normally of different sizes. The problem handled in this work refers to an ideal state in which all the bubbles have the same volume. Since the process of foam formation is driven by energy minimization and since the energy decreases with decreasing surface area, the structure that would best represent the geometry of foams is thought to be that of lowest surface area. This translates into the geometrical question of how to divide space into equal volume cells with minimum partitional area, which is known as the Kelvin problem. Various approaches to solve this question have led to a number of new structures.

A combinatorial algorithm for the tessellation of polytopes based on face-matching rules has been developed. Although only the outline of the algorithmic idea has been shown, its manual implementation already produced a new tiling with unusual properties that engendered a multitude of questions about the degree of symmetry of systems made of self-similar subunits.

A partial differential equation used in the science of pattern formation has been successfully linked for the first time to a number of different problems in geometry including the Kelvin, the sphere packing, the covering and the quantizer problem, producing new non-lattices in three-dimensional

space and providing a new method for future investigations in arbitrary dimension. New crystallographic patterns with associated space-filling polyhedra have been discovered. This approach also produced new counter-examples to Kelvin's conjecture, showing a link with the experimental evidence derived from the inspection of cellular solids such as foams and aggregates of cells, soft particles or soap bubbles. The existence of partitions with lower energy than that conjectured by Lord Kelvin containing quadrilateral rings has been proved numerically for the first time in this work.

A family of surfaces - derived by the minimal surfaces - has been adapted for use in the modelling of highly porous materials for structural applications. The addition of a linear term to the mathematical expressions of the surfaces in implicit form has been shown to model the geometry of functionally graded materials (FGM). A model has been proposed for a typical problem in orthopaedic implants, the fixation of an acetabular cup to a human pelvis.

Statement of aims

This work is divided into two parts. The first part, which contains the most innovative - and theoretical - results, is a multi-approach methodology for the solution of a problem in optimal geometry, directly related to the shape of bubbles in foams and froths. The second part is an innovative approach to the three-dimensional modelling of highly porous materials for load bearing applications, intended to be fabricated by a Solid Free Form (SFF) technique. The structures described in this work are therefore of two different types: structures that closely resemble foam-like geometries, some of which have been discovered within this study [1, 2], and high-porosity structures derived from the Periodic Nodal Surfaces (PNS) [3].

Two are the goals set for this thesis.

The first goal is to solve the Kelvin problem [4, 5]. This would give a unique foam model able to represent the ideal structure of foams. The Kelvin problem is in fact the mathematical expression of the physical principle of energy minimization which foams are characterized by during their formation process. The problem is currently believed to have an ordered, crystalline solution [6] but this clashes with the experimental evidence arising from the geometry of monodisperse foams, systems characterized by high disorder [7]. There are already a few works that describe the possible geometrical structure of foams, but they either exclude evidence coming from

visual inspection of real systems [8], such as the presence of polyhedra with 13 faces in foams [7, 9], either rely on purely random approaches in the hope that the condition of optimality will be at some point reached [10]. The fact that the theoretical work on the Tetrahedrally Close Packed structures [6, 8] did not match the experimental observations of real foams [11, 9], made scientists wonder about the order (crystallinity) of the solution to the mathematical problem. A recent work based on random packing algorithms [10] showed topological results in agreement with the experimental observations but not with the energy minimization, since foam energies (or costs) were higher than those found in Sullivan's work on the TCP structures.

The total lack of structures containing the *right* polyhedra has moved the author to consider the problem in its formal statement and to spare no effort in creating and finding new algorithms for the generation of new geometrical foams. This work aspires to find structures that are combinatorially similar to the experimental results yet preserving the low system energy that characterizes foams.

The new foam models here described are defined by their combinatorial expression. The structure of real foams is somewhat elusive, always affected by the manufacturing process used, the variables in the process like temperature and pressure, and the material properties, let alone the engineering errors that always arise from the acquisition of such complex morphological data, usually performed with three-dimensional physical scans. In order to accomplish the second goal and to avoid the inconsistencies above described, a large part of this work has been dedicated to methods able to perform combinatorial and geometrical searches for idealized foam models.

The complexity of the problem is very high and specific algorithms and methods that can directly move towards the minimal solution are hard to

find. Given the enormous computing resources that would be required to solve it, scientists say a proof will not come for years [12].

Three are the methods that have been used. The first method is based on the combinatorial tiling theory. It provides an exhaustive search for nets and tilings with given symmetry. The second method uses an assembly algorithm for polyhedra, called Corona algorithm. The third method starts from a pattern forming partial differential equation known as the Swift-Hohenberg equation . All these methods will be described in detail in Chapter 4.

The second goal is to show the potential of porous material based on the PNS for load bearing applications by comparing their stress concentration characteristic to that of models for foamed materials under applied static load in an elastic linear model. This has been done numerically, with the aid of a computer.

Summarizing, the aims are:

- To solve the Kelvin problem, or at least to find new counter-examples to Kelvin's conjecture, with the perspective of this leading to a formal understanding of the nature of disorder in foams and aggregates of cells

- To show that porous materials based on the Periodic Nodal Surfaces can represent an efficient and adaptable way to model porous materials for structural applications

Chapter 1

Introduction

What is the shape of foams? What is the most economical way to arrange matter in space so it can still stand up to a static load? This work is an attempt to answer the first question and to propose a solution for the second.

In the first part of this work the geometry of foams is investigated thoroughly, based on the physical principle that bubbles in dry foams tend to minimize their surface area for a given volume.

In the second part a method to model the geometry of highly porous materials for structural applications is presented.

The definition of an *ideal* geometry for highly porous media subject to loads is a complex problem, mainly depending on the boundary conditions of the system under study. In this thesis, a general definition of porous materials has been initially given (Chapter 2). Then the focus moves onto the morphology of foams, the most common class of industrially produced porous materials. A large amount of time and resources in this project were spent in finding a universal foam model that could be used in the future by professionals and researchers that deal with foamed materials. Details of the previously known models are given in Chapter 3, whilst the adopted

approaches for the discovery of the new models, and their formal descriptions, are given in Chapter 4. This part constitutes the core of this work. It also contains the most notable results on space partitions and tessellations. Finally, a very simple set of equations describing surfaces that can be successfully used to model porous media with extremely low solid volume fraction is presented (Chapter 5). A numerical bending test showing a direct comparison between the stress spatial rate on nodes extracted from the generated foam models and the PNS having the same solid volume fraction is included (Chapter 6).

The geometrical results on foams can be easily applied to different materials, for structural, fluid dynamics or even combined and multiphysics numerical analyses. Polymers, metal alloys and ceramics, all of these can be either foamed or made porous via a large number of different techniques [13, 14, 15], for an even larger number of applications.

Open-porous polymeric foams are widely used in the packaging industry, for padding, and for cushions. Their good energy absorption and relatively low cost have resulted in the manufacturing industry to opt for these materials in this kind of applications.

Open-porous metal foams can be efficiently used in biomechanical prostheses to lower the mechanical stiffness of implants made out of solid titanium or solid steel to match that of bone and to provide fixation. The case study to be considered in this thesis refers to an acetabular cup, used in the total hip joint replacement. In the aerospace industry the most prominent application is in the core of sandwich structures. Another relevant field is the automotive sector, where high energy absorption capability joined with sufficient stiffness to allow self-support is required. Bumpers are often realized in aluminium alloy foams [16].

Open-porous ceramic foams are also widely used, in applications that range from biomedical to renewable energy, to heat resistant filtering devices [15]. Calcium phosphate porous materials are used as scaffolds for the substitution of damaged, or the integration of missing, osseous tissue in living organisms, especially in the human body. In the renewable energy sector, zirconia electrodes for fuel cells require high surface area per unit volume. Foams with such property are the optimal solution for molten metal and hot gas filters as well as for catalyst supports [16].

Foams are not the only open-porous materials that can be produced. Nowadays it is possible to create porous materials with a microstructure that is not touched by the shape constraints imposed by any foaming process. The Solid Free Form fabrication industry is provided with machines able to manufacture three-dimensional objects of arbitrary shape out of a wide choice of materials including metals and ceramics [17]. Solid Free Form fabrication is a technique for manufacturing solid objects by the sequential delivery of energy and/or material to specified points in space, sometimes still referred to as rapid prototyping. The geometrical results on PNS constitute a tool for the generation of this class of materials.

Chapter 2 of this work gives a definition for porous matter. A general method for the description of pore geometry in structures requiring interconnected channels like trabecular bone is sketched. The method sets some fundamental parameters, such as volume fraction, element dimension and connectivity, that are essential for comparative purposes among different structures.

Chapter 3 illustrates the background information that has been necessary to develop the methods presented in Chapter 4. Section 3.1 is an overview of foams, their formation mechanism and their geometry is described and

used as a starting point for the developments of the models. A review of the geometrical models for foams and froths is presented, and an in-depth analysis of the problem of partitioning the space into cells of equal volume is also illustrated. The benefits and drawbacks of using these models are discussed thoroughly. Section 3.2 is a review of the combinatorial tiling theory, a work initiated by Andreas Dress, continued and implemented on computers by Olaf Delgado-Friedrichs in the computational tiling theory. Section 3.3 describes a family of partial differential equations used in the science of pattern formation.

Chapter 4 contains three completely new approaches to the modelling of foam geometry. The first approach, based on the combinatorial tiling theory, has produced a very large number of new tilings with interesting properties and with the possibility of extrapolating data for more complex structures. A second approach has been used successfully to find suitable partitions of space with restricted given set of polyhedra. It produced a new simple tiling by a polyhedron with 14 faces, proving the existence of a tiling simultaneously monotypic and non-isohedral, the first of its kind. In the third approach a new family of counter-examples to Kelvin's conjecture on space partitions has been discovered. The method used a numerical evaluation of the 3D Swift-Hohenberg equation in a periodic boundary with pseudorandom initial conditions. The most common patterns known to crystallography, plus a few new ones, can be formed starting from random data simply driving the solution of the differential equation to its stationary state.

Chapter 5 presents a set of truss-like periodic structures each characterized by a different topology, derived from the PNS. A task of this work is to evaluate the difference in performance between the open-cell foam models

and a group of lattice structures that include stretch-dominated structures [18] and bending-dominated truss-like structures derived from the triply periodic minimal surfaces (TPMS) [19, 20] developed in a previous study [21] and already found in orthopaedic applications [22]. Parameterized and tailored new structures are illustrated and the functions adopted for their generation are described. An application of these structures to an acetabular cup is shown.

Chapter 6 deals with numerical techniques applied to the modelled structures. In order to evaluate their mechanical properties Finite Element Analysis software has been used. The stress leveling point response, within the elastic region, has been acquired. Quantitative data for the new porous models are extracted and compared with that obtained from the foam-like models produced in this work.

Chapter 7 concludes with a description of the two main results achieved in this thesis. Firstly, the P42a structure, obtained from a new method capable of facing an age-old problem in geometric measure theory. Secondly, as an application of the mathematical models introduced in in Chapter 5 to orthopaedic implants, an acetabular cup with a new kind of body-implant porous interface.

Chapter 8 presents the work planned for the future. The interest of scientists in the method for the generation of the new foam models has directed research efforts toward the study, the implementation and the optimization of the method itself.

From a scientific point of view, the core result contained in this work represents a tool for mathematicians working in geometric measure theory, sphere packings and coverings, group theory and pattern formation, but also for physicists and crystallographers interested in dimension related disorder,

three-dimensional lattices and non-lattices, patterns and tilings.

From an engineering point of view, this work suggests a fast route to the modelling of highly porous materials for structural applications, with the main aims being their use in computer simulations and their generation by Solid Free Form techniques.

Chapter 2

Porous Materials

The use of the term *porous* to indicate materials that presents internal void spaces is quite unfortunate. A more rigorous classification would have been that of composite materials, since porous materials are made of at least two different phases, solid and void. This on the other hand might lead the reader to some confusion. Although for a composite material the interest is directed on the properties of both the phases and also on the interaction between the two, here the attention is focussed on the first phase only, aware of the fact that the system being studied only models the solid phase and therefore represents an approximation of real systems (like trabecular bone).

The etymology of the word *pore*, from the Greek word $\pi o \rho \acute{o} \varsigma$, which means passage, linguistically recalls the verb *to fare* [23]. If the porosity is open, interconnected channels through a porous medium can be identified and discerned. This is particularly easy for samples with a very high solid volume fraction. The idea of a passageway or a duct that allows fluid flow through the medium is then quite direct and can instinctively be comprehended without the need to recur to bold circumlocutions. More in general, the channels might be so flat that instead of a duct one might spot a sepa-

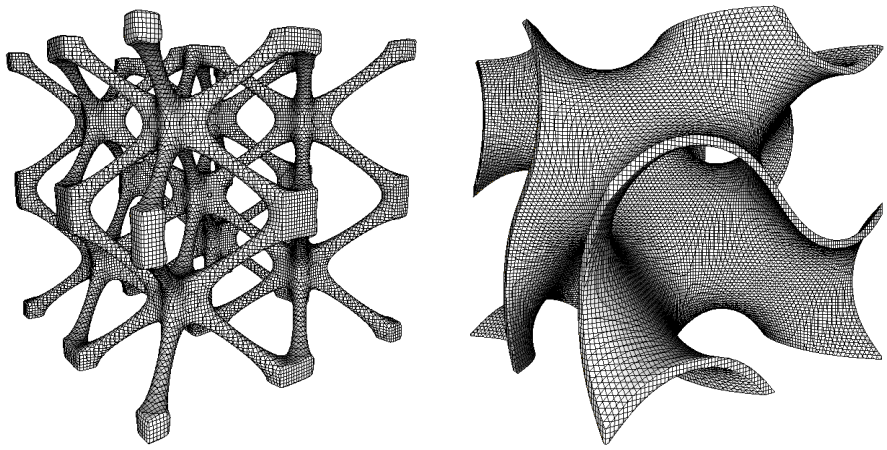

Figure 2.1: Two examples of models of porous materials. A strut-like and a shell-like periodic structure having the same volume fraction but different spatial arrangement, yet preserving interconnectivity of the solid phase. The images have been generated with the application K3DSurf [24].

ration surface. It is possible to imagine the reverse samples of those shown in Figure 2.1, the first sketching interconnected channels, the second a continuous surface dissecting a solid. It is of interest to note that the word pore in modern English generally refers to any kind of porosity, including that of materials with isolated pores (a very short *fare* in this case).

Many authors have used in the past the term *cellular* to identify solids that show various kinds of porosity [25]. The use of this term is unfortunately as misleading as the previous one. The word *cell* has its roots in the Latin word *cella* which means *small apartment, room* [23]. Although this term might be appropriate when dealing with foams and periodic frameworks, it cannot be used to univocally identify random lattice structures, which also are porous materials, neither a large amount of periodic nets. It will be shown in the next chapter how *polyhedral cells* can be identified inside the reticular structure of real foams and how material defined as periodic can still

have a *periodic unit cell* (here the word *cell* is referred to a periodic unit, with a completely different meaning) that is able to represent the whole structure. To avoid confusion, the word *tile* or *polyhedron* instead of *cell* will be used, the latter being reserved to the periodic unit of a space-filling arrangement of geometrical elements.

It is not an easy task to label such a vast category of materials as what are called porous materials, that it is out of the scope of this work to look for the most appropriate term. Instead, the definitions of some of the parameters commonly used to characterize porous matter are given, with the addition of simple examples, yet in a rigorous way.

The definition of *volume fraction*, as reported below, is valid for a generic biphasic material, irrespective of its phase interconnectivity. Let two phases named A and B fill a cubic region of volume $V = V_A + V_B$. The volume fraction of the phase A is given by $v_A = V_A/V$. Since only the solid phase is taken into account in this study, the symbol v will be used in this work to identify the volume fraction of the solid phase, which can vary from 0 to 1.

The complex lattice of a porous matter sample can intuitively be subdivided in smaller single elements such as struts or rods and shells or sheets. This visual partitional approach can also be formalized in a more rigorous way by the use of the parameter called *element dimension*. In an n-dimensional space it is possible to arrange k-dimensional elements where $0 < k < n-1$. Since 0-dimensional elements, known as points, are incapable of defining a three-dimensional lattice on their own, the use of 1-dimensional (linear or strut-like) and 2-dimensional (planar or shell-like) elements will be necessary. The materialization of these elements into three-dimensional ones requires a further parameter, this time related to the volume creation. Linear elements will then be characterized by a diameter and planar ones by

a thickness. Figure 2.1 illustrates two samples built using linear and planar features respectively, both samples having exactly the same volume fraction of 0.06, which - as it will be shown in the next chapter - is a typical value for a reticulated foam.

It is possible to mix linear and planar elements, this way increasing the complexity of the lattice. However, for a better understanding of the influence of the two different kinds of elements, investigations were carried out on sample with only one kind at a time. It is interesting to note that an infinity of different configurations can be built, even using elements all of the same dimension.

A parameter developed from graph theory is used, which defines *connectivity* of a lattice as the number of struts per unit node. A node is a 0-dimensional element where more than 2 struts meet. For shell-like materials this number corresponds to the maximum number of paths available from an arbitrary point in the void space.

Strut-like structures only are considered in this work. Two main classes are illustrated, structures based on the Periodic Nodal Surfaces and structures based on the shape of real foams, the last being obtained as a result of a search for the solution to a problem known as the Kelvin problem [4].

This problem, in its formal statement, asks for the partition of space in regions of equal volume having the least interfacial area.

It is relevant to note that the formal problem proposed by Lord Kelvin touches many more disciplines than those related to the morphology of foams [26]. On a smaller scale, the problem is of interest in soft condensed matter physics [27], in biphasic systems [28] and microgravity fluid dynamics [29]. In chemistry the problem is directly related to the chemical structure of a group of a wide class of materials known as zeolites, that today have

many applications including catalytic cracking and water and gas purification. But applications are not limited to the material world. In cosmology, according to an evolutionary theory, the shape of the universe resemble that of a packing of polyhedral soap bubbles, where matter aggregates along the edges of the polyhedra. Optimization of wireless networks and data compression in computer science [30], optimal lattice quantizers in mathematics [31] are other areas that would potentially gain from a definitive answer to the Kelvin problem. On a theoretical point of view, such a result would be an extremely important step forward in Geometrical Measure Theory, a branch of mathematics that deals with the measure of manifolds .

The new models found in this work may be useful to scientists and engineers who are in the need of simple geometrical models for foams, without the need of performing physical scans of real foams. The purpose may be various: structural, fluid dynamic (flow through porous media), thermal, optical, informational. Any application that requires a reference standard for foam-like materials or, more generally, for minimal partitions of the three-dimensional space into regions having the same volume, could be a potential beneficiary of these models. Computer scientists working on data sampling, engineers designing a wireless network for large areas (when compared to a single antenna's domain) will find the foam models described in this work of undisputed value.

Chapter 3

Literature review

This chapter is divided into three parts. The first part describes the structure of real foams and the related formal problem known as the Kelvin problem. The second part introduces the Delaney symbols for tilings and the computational tiling theory. The third part is a brief review of a partial differential equation known in pattern formation, the Swift-Hohenberg equation.

3.1 Foam geometry

Foams represent a wide class of engineering materials. In this work the interest is focussed on the morphology of open-cell foams, but the results obtained are mainly topological and can therefore be easily extended to any kind of monodisperse foams.

A review of engineering foams and the geometrical aspects connected with the foaming process is briefly presented below. Initially their use in technology will be presented and at the same time a first idea of what they look like will be shown. Then the focus will move onto open-cell foams.

Historically, the need for foamed materials arose when engineers were

looking for an inexpensive manufacturing method for fabricating porous materials. These materials exhibited global properties that none of the existing ones could ever possess. The idea of reducing the volume fraction of material simply by adding empty space to a liquid phase and then obtaining the solid phase via a chemical or thermal process, made possible the realization of materials with properties that could match specific applications. Metal foams in particular found applications in hot gas filtering, catalytic supports, energy storage devices, where the high surface to volume ratio was the primary requirement, but also energy absorption, like bumpers for cars [16].

Whatever foaming technique used, foamed materials appear to be constituted by an assembly of smaller units, very similar each other in many aspects. These units are called bubbles, in order to avoid confusion with the word cell, which is used to identify a crystallographic unit cell in periodic structures of the kind illustrated later in this chapter.

Consider now a solid, continuous material. The porosity of such a material is zero. Imagine now the addition of a second phase (void), shaped as many small spherical bubbles at random locations in space. The value of porosity, which can also be called the volume fraction of the void phase, is now positive. The bubbles (or void phase) will not be able to touch each other yet as their concentration is still too low. If the bubbles are further inflated so that the void phase fraction increases, at some point two or more bubbles will touch each other. At this point a spatial rearrangement of the bubbles is necessary. Bubbles move and set into a new position where they can keep their spherical shape, and doing so they fill the space in a presumably more efficient way.

Now the first question arises on the arrangement of points in the initial

configuration.

3.1.1 Open-cell foams

When not only low density is a requirement but also high permeability to fluids is crucial to the application and fundamental for the function accomplished by the product, foams are realized with interconnected cavities and are called open-cell foams. This can be achieved in different ways, depending on the base material used. Open-cell foams are produced today in all the three different classes of materials: polymers, metals and ceramics. Only polymer foams are produced from the bulk material whilst metallic and ceramic ones are often generated from a polymer foam template [13]. Polymeric foams are commonly manufactured starting from a diisocyanate and a diol (often polyethylene glycol) in presence of a catalyst and a foaming agent. The reaction is a polymerization which gives rise to a polyurethane, in this case the extra presence of a substance that volatilizes (the foaming agent) during the process, leads to the formation of bubbles of gas which then collide and create the interconnectivity. The variation of parameters such as pressure and temperature gives the possibility of obtaining foams with different pore sizes. The bubbles generated by the foaming process are in tight contact each other as in a packing of soft spheres. The geometrical shape of a single cell can then be represented by a polyhedron. Since the microstructure of open-cell foams has a noticeable effect on their mechanical properties [32], an examination of their morphology will be the first step in this study.

3.1.2 Microstructural morphology

A systematic investigation of these shapes can be only conducted if the number of parameters in the models is finite. In order to obtain parametrized models for foams, it is necessary to have a closer look to the bubble formation and foam setting mechanism involved in the process. Foam agents generate gas bubbles in the curing resin. This then polymerizes and sets making the foam evolve from a wet condition, in which spherical bubbles touch each other on points, to a dry one, where bubbles have polyhedral shapes [32] whose faces are shared with adjacent bubbles. Repeated experiments [33] show how bubbles of monodisperse (cells of equal volume) wet foams place themselves in an orderly fashion, precisely hcp (hexagonal close packed), fcc (face centered cubic) or rhcp (random sequence of hcp layers).

During the drying phase of a wet foam, spherical bubbles assume polyhedral shapes and settle in configurations believed to minimize the total surface area of the film, in the same way it happens in agglomerates of soap bubbles. The general structure of singularities of soap bubbles (films meeting at edges, edges meeting at vertices) has been thoroughly investigated by Jean Taylor [34]. If the bubbles are considered to have all the same volume, then a problem can be stated in a formal way, and this is what Lord Kelvin did in 1887 [4].

3.1.3 Kelvin's problem

The geometrical problem of partitioning three-space into regions of identical volume with the least total interfacial area is known as the Kelvin problem [5].

The equivalent problem in two dimensions is much easier to visualize therefore it will be presented first. Fig. 3.1 shows three periodic partitions of

the two-dimensional Euclidean space - the plane, respectively by equilateral triangles, by squares and by regular hexagons with one coloured cell (Fig. 3.2).

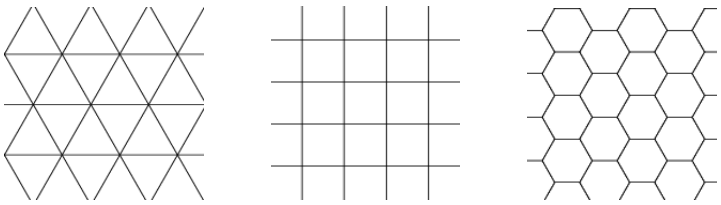

Figure 3.1: Three grids with cells of different shape but having same area.

Note that not only does each single pattern contain congruent cells but also the three different patterns have cells of exactly the same area when compared one to the other. Now consider a representative cell for each pattern and give an expression for what intuitively is its sphericity. In physical terms, this magnitude is called cost of a foam or partition. The cost c for two-dimensional partitions can be defined as the ratio of half the perimeter of a cell p to the square root of its area A, but this ratio can be extended to any dimension, included the three-dimensional Euclidean space [35].

$$c = \frac{p}{2\sqrt{A}} \tag{3.1}$$

It can be noted that this ratio is dimensionless, which means that is size-independent. If the cells are not congruent it will be necessary to take the minimum number of cells that constitute the periodic unit. Two cells are congruent if one can be transformed into the other by an isometry, such as translations, rotations or reflections. This can be done only if the structure is periodic by isolating the translational unit. A similar and better known ratio in geometry, which gives exactly the same information, is the isoperimetric

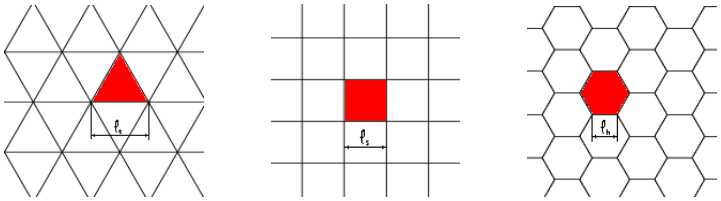

Figure 3.2: The representative cell for each pattern.

quotient. This in simple terms tells how far from the circularity of a circle is a given closed curve. The isoperimetric quotient Q of a closed curve is defined as the ratio of the curve area A to the area of a circle A_c with same perimeter as the curve p [36].

$$Q = \frac{A}{A_c} = \frac{A}{\pi(\frac{p}{2\pi})^2} = \frac{4\pi A}{p^2} \tag{3.2}$$

Cost and isoperimetric quotient are related through Eq. 3.3:

$$Q = \frac{\pi}{c^2} \tag{3.3}$$

For the purpose of this study, and without losing in generality, the cost will be used instead. The area of the cells is fixed equal to 1 and their perimeter P, which with this assumption coincides with their cost, is calculated. For triangles (t), squares (s) and hexagons (h) this gives:

$$A_t = 1 = \frac{\sqrt{3}}{4} l_t^2 \qquad l_t = \frac{2}{\sqrt[4]{3}} \qquad P_t = 3l_t = 2\sqrt{3\sqrt{3}} \approx 4.6 \tag{3.4}$$

$$A_s = 1 = l_s^2 \qquad l_s = 1 \qquad P_s = 4l_s = 4 \tag{3.5}$$

$$A_h = 1 = \frac{3\sqrt{3}}{2} l_h^2 \qquad l_h = \sqrt{\frac{2}{3\sqrt{3}}} \qquad P_h = 6l_h = 2\sqrt{2\sqrt{3}} \approx 3.7 \tag{3.6}$$

The third pattern, a honeycomb, has the lowest perimeter. Additionally, any partition of the plane into regions of equal area has perimeter at

least that of the regular hexagonal grid, as it was conjectured by Pappus of Alexandria [37] and recently proved by Thomas Hales [38].

The analogue problem in three-dimensional space has only a conjectured solution, which is the Weaire-Phelan structure [6, 39]. In two dimensions the perimeter of the partition and the area of the cell were considered, here the focus is on the surface area of the partition interface and the volume of the cells. The cost of a foam is given by Equation 3.7:

$$c = A/V^{2/3} \tag{3.7}$$

where A is the average interfacial area per tile and V is the volume of each tile. A correct way to state the problem is then as follows: what partition of three-space in equal volume cells has minimal surface area? The question is very similar to the two-dimensional case mentioned above, therefore it can be stated in a similar way: what partition of two-dimensional space in equal area cells has minimal perimeter? Extending this to a generic dimensional space, one might ask: what partition of n-space in equal n-dimensional finite regions has minimal (n-1)-dimensional interfacial boundary? This problem and its fundamental theoretical background have been touched on by many mathematicians and physicists in the past [4, 40, 41, 42, 6, 8, 10]. A recent step forward has been taken by Morgan, who proved the existence of such a partition [43]. The search has been limited to the three-dimensional case here, as the main interest is to find a mathematical expression for the shape of monodisperse (equal-volume cells) real foams.

A detailed review of the past efforts to solve the problem and results obtained is presented below, and a wide spectrum of tools and methods that have been used to perceive the complexity of the question is illustrated.

More than a century ago, in 1887, Sir William Thomson - better known

as Lord Kelvin - conjectured that the space-filling arrangement of cells of equal volume with minimal surface area was made of a periodic structure whose units were similar to a truncated octahedron, or orthic tetrakaidecahedron [4], a polyhedron with eight hexagons and six squares. The units only differed from the actual polyhedron by the fact that its edges were not linear and its faces not planar, as shown in Fig. 3.3. The structure is known as the Kelvin cell, or, in accordance with the Reticular Chemistry Structure Resource, for short RCSR [44], **sod**, as in the mineral sodalite. The symbols of the structures as they appear in the RCSR are in bold fonts.

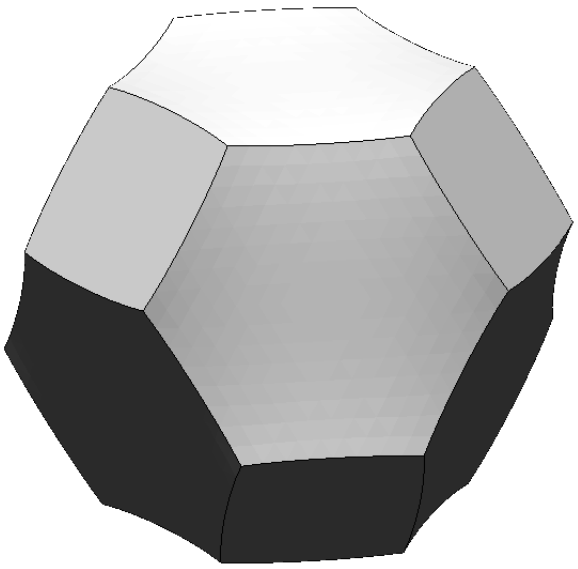

Figure 3.3: The Kelvin cell, a version of the truncated octahedron with slightly curved edges and non planar faces, net symbol **sod**. The graphical output, produced with the Surface Evolver, shows the gentle curvatures of the surfaces in this minimal partition of space.

More recently Weaire and Phelan [6] gave a counterexample to Kelvin's conjecture using a periodic structure found in certain chemical compounds

called clathrates. The translation unit is made of eight cells. There are two different polyhedra in this structure: a tetrakaidecahedron containing twelve pentagons and two hexagons, and an irregular pentagonal dodecahedron (Fig. 3.4), in which only the hexagons were planar faces. This structure's net symbol is **mep** (as in the mineral melanophlogite), and the spatial arrangement of the centres of the bubbles shown is know as the $A15$ pattern.

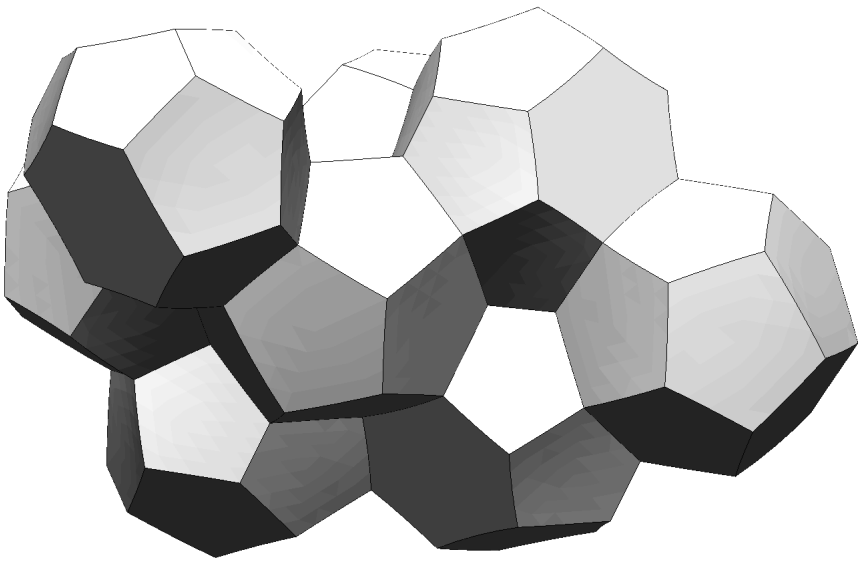

Figure 3.4: The periodic unit of the Weaire-Phelan structure, also called $A15$, net symbol **mep**, is made of two [0-12-0] and six [0-12-2].

These cells are repeated periodically in the space so they can completely fill it. The periodic unit is made of six tetrakaidecahedra and two dodecahedra. Using the Surface Evolver by Ken Brakke [45], they measured the area of a wide range of structures, all containing only pentagons and hexagons. Together with the structure described above, other structures have been obtained and their cost calculated. Some of them showed lower cost than

sod but none lower than **mep**. There are 24 known crystalline structures called tetrahedrally close packed (TCP), or Frank-Kasper phases, which are related to different types of clathrates [46, 47].

A clathrate is a chemical compound whose structure resembles an assembly of cages. One kind of molecule is usually trapped in a lattice or net composed by a second kind of molecule. Gas clathrate (or clathrate hydrates) are made of hydrogen bonded water molecules trapping a gas, typically methane or carbon dioxide. There are three different types of clathrates, the main two resembling the structure of **mep** (Type I) and **mtn** (Type II).

A deeper look into the family of structures from Weaire and Phelan showed that an infinite number of new structures can be generated as a convex domain [8] of the three structures **mep**, **zra-d**, referred to as Z in Sullivan's work, and **mtn**, referred to as $C15$ (Fig. 3.5).

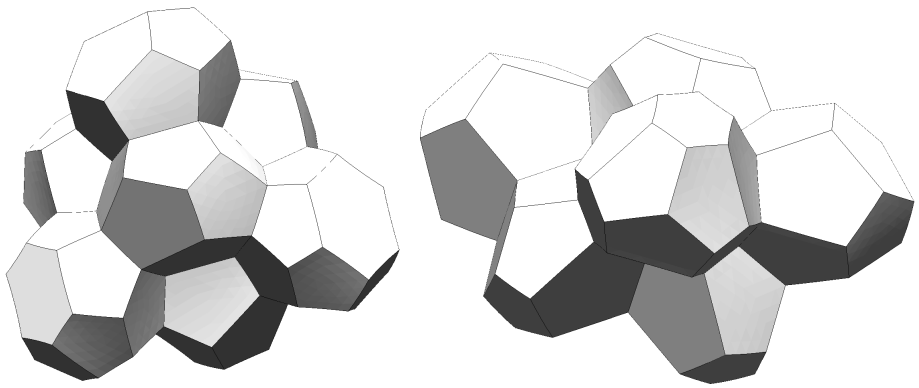

Figure 3.5: The periodic units of the other two basic structures belonging to the TCP range: Z, net symbol **zra-d**, made of seven cells (three 12-hedra, two 14-hedra and two 15-hedra), and $C15$, net symbol **mtn**, made of six cells (two 12-hedra and four 16-hedra).

3.1.4 Topology

Area-minimizing problems are typically those in which a three-dimensional closed curve is given and the surface of minimal area touching that curve is calculated. If the curve lies in a plane, the obvious result will be planar, whatever the shape of the curve. For a three-dimensional curve the minimal surface lies in 3-space and for simple geometries can be obtained analytically. When the geometry of the system being studied is more complex, the numerical approach is the only solution. Surface Evolver is an interactive program for the modeling of liquid surfaces shaped by various forces and constraints. Another class of area-minimizing problems is given by those related to bubble packing (soft-sphere packing), where the minimum surface area for an infinite number of solid regions is searched. If the regions are supposed to be all of the same volume, the problem is equivalent to the Kelvin problem.

3.1.5 The structure of random foams

The structure proposed by Lord Kelvin as the minimal partition of space in cells of equal volume, **sod**, has been beaten by **mep**, the counter-example presented in Weaire's 1992 paper [6]. Recent attempts to find structures with even lower cost, or at least a second counter-example to Kelvin's conjecture not belonging to the range of the TCP structures, have used models generated via random sequential adsorption or random close packing methods. This modelling technique produced computer generated random monodisperse foams which have been subsequently *annealed* in order to get the lowest possible value of cost [10]. The average number of faces of these foams had a minimum of 13.68, a value extremely close to that encountered by Matzke in his physical experiments with 600 soap bubbles of 13.70 [7].

Unfortunately, it has not been possible to push their cost below the value of 5.324 (the value for **sod** is 5.306, largely below this limit).

3.2 Tiling theory

The combinatorial tiling theory deals with the transcription of the information contained in periodic tilings into a connected graph (Delaney graph). The computational tiling theory provides concise and efficient data structures able to represent periodic tilings by a simple sequence of integers (Delaney symbols). What follows is a detailed description of the Delaney symbols and how these can be obtained from a given tiling, taken from a fundamental work by Delgado-Friedrichs [48].

A periodic tiling is a subdivision of an n-dimensional space into regions called tiles. The periodicity of the tiling implies that a finite set of tiles, called periodic unit, can represent the whole configuration, which can be obtained by translation of the periodic unit.

Consider now a tiling of the plane. A barycentric subdivision of the tiling can be constructed by choosing a point in the interior of each edge and each tile. Then the points chosen in the tile can be connected to its vertices and to the points in the interior of its edges, as shown in Figure 3.6.

A triangulation will result from this operation where each triangle, called chamber, has three types of vertices, namely a vertex of the original tiling, a point on an edge and a point inside a tile. These are labelled as 0, 1 and 2 respectively. The edges are labelled the same as the vertices opposite to them. In Figure 3.6 edges labelled 0, 1 and 2 are shown dashed, dotted and solid in this order. Each chamber has three neighbours, distinguished by the type of edge they share with it. These chambers are named $s_0(t)$, $s_1(t)$ and $s_2(t)$.

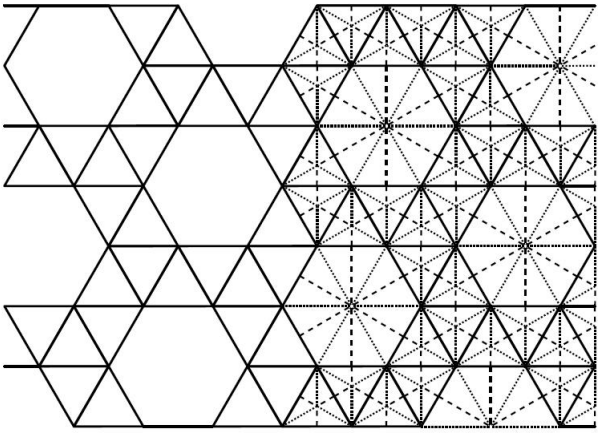

Figure 3.6: A tiling with its barycentric subdivision. The picture is from Delgado-Friedrichs [48].

Two chambers are symmetry equivalent if there is a symmetry of the tiling mapping one onto the other. The chambers are shown in Figure 3.7. The information contained in the tiling can now be converted into a graph (right hand side of Figure 3.7), called the Delaney graph. This is basically a map of chamber adjacencies, where the kind of connection between two elements in the graph is determined by the kind of edge between the two chambers in the barycentric subdivision of the tiling.

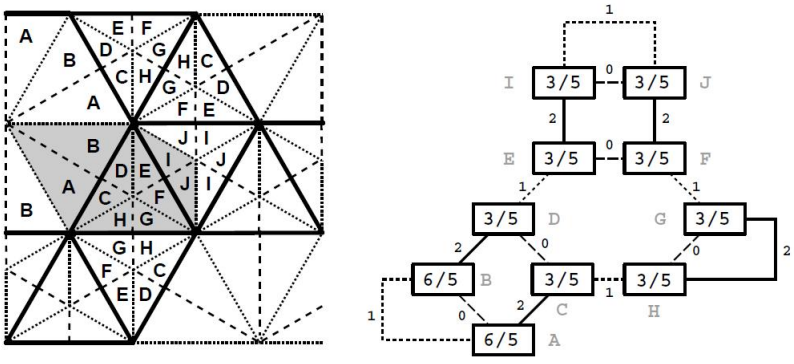

Figure 3.7: Chamber classes and the Delaney symbol. The picture is from Delgado-Friedrichs [48].

The Delaney graph does not uniquely determine the tiling. The archimedean solid shown in Figure 3.8 has exactly the same Delaney graph as the previous planar example, but it contains squares instead of hexagons.

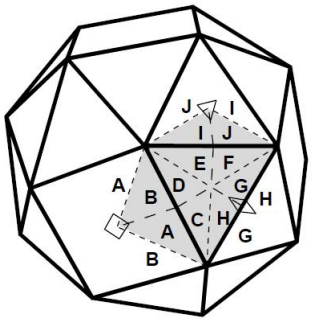

Figure 3.8: An archimedean solid. The picture is from Delgado-Friedrichs [48].

For this reason two numbers are added to the Delaney graph. The first one represents the number of vertices of the tiles containing chambers of this class and the second gives the degree of the vertices (number of meeting edges) adjacent to chambers of this class. These two numbers are shown inside the rectangles representing the chambers of the Delaney graph in Figure 3.7.

This augmented Delaney graph can be converted into a string of a finite number of integers, the Delaney symbols, as shown in the documentation of the application 3dt included in the Gavrog project [49]. The advantage of such a coding is that tilings can be classified by simply changing these integers. This is the technique that has been used in this work for the generation of three-dimensional tilings with a given number of kinds of vertex.

3.3 Pattern formation

Pattern formation studies the evolution and the self-organization of patterns found in nature, especially in biology, chemistry and physics (dendrites in solidification, optics).

The analytical study is often conducted via the use of partial differential equations, the most famous of which is the Swift-Hohenberg equation. The general form is shown in Equation 3.8:

$$\frac{\partial u}{\partial t} = au - (\nabla^2 + 1)^2 u + P(u) \tag{3.8}$$

where $u = u(X, t)$, $P(u)$ is a a polynomial in u and X has as many coordinates as the dimension of the problem. Thank to Michael Cross' java applet [50], the outcome of such equation in a two-torus can be examined live and the parameters can be modified interactively. Figure 3.9 shows the values for the function $u(x, y, t)$ at the stationary state where $\frac{\partial u}{\partial t} = 0$:

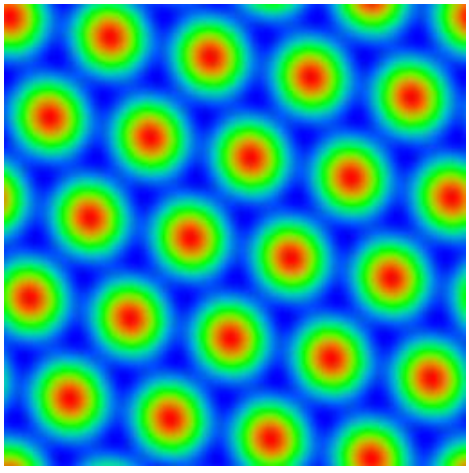

Figure 3.9: The Swift-Hohenberg equation calculated in a two-torus generates a stationary state with local maxima equally spaced. The regions represent the maxima and the blue ones the minima. The picture is taken from Cross' on line demo [50].

The local maxima, at the centre of the red regions, self assemble into a

triangular pattern, which is a pattern by simplices. This inspired the work described in this thesis on the three-dimensional patterns.

Chapter 4

Methods

Three new methods have been used for the first time in this thesis to solve the Kelvin's problem. Although a solution has not been found, 15 new counter-examples and a large number of low cost periodic partitions have been produced.

The first method uses Delaney symbols for tilings [51, 52, 53]. This approach turned out to be extremely powerful because of its intrinsic completeness. Unfortunately, the computational power necessary to find potential candidate structures is still very high, which in simple terms means that the search will take a large period of time, unless shortcuts in the algorithm are able to identify areas with higher probability of finding interesting structures are provided.

The second method uses an additive technique for topological polyhedra, developed for the first time in this thesis and named by the author Corona algorithm. Since a univocal relationship between 3-connected planar graphs and three-dimensional polyhedra exists, joining graphs corresponds to joining polyhedra. The method does not build periodic structures but finite clusters of polyhedra. Periodicity is detected if repetition of the structure is

noted to be persistent after a given step, a sort of mathematical induction.

The third method uses a partial differential equation taken from pattern forming science. This gave the most interesting results. A number of new counter-examples to Kelvin's conjecture have been found in this work using this method.

4.1 Method I: Nets and tilings

The formal definition of nets is necessary for the systematic description of the structure of foamed materials. There is still noticeable disagreement between the morphology of proposed models [4, 6] and that emerging from experimental observation [7]. An accurate examination of the nets found in periodic models having low area-to-volume ratio (cost) could give helpful clues about the bubble polyhedral composition and spatial orientation in real foams.

A net is a graph composed of a set of vertices and a set of edges, each connecting two vertices. If the graph representing the net is periodic, then it can be described using a finite number of elements. This is useful also in crystallography, where the identification of a net and the computation of its symmetry is the key factor for the enumeration of different structures. Methods able to compare periodic nets and compute their symmetry group have been developed quite recently [54].

A tiling is a subdivision of a space into closed regions called tiles. If the tiling is periodic, the number of tiles needed to represent the whole tiling is finite and a periodic unit can be identified in it. A tiling always carries a net with itself, since the subdivision into closed regions includes edges and vertices, all structured as in the graph described in the previous paragraph.

Periodic tilings can be fully described by mathematical symbols, called Delaney symbols, from their inventor.

4.1.1 Delaney symbols

This approach has been proved to be a valuable tool when dealing with storage, classification and manipulation of tilings. Periodic tilings are represented in a concise and efficient data structure that can be handled by a

machine. Algorithms have been developed for classification purposes, leading to a complete enumeration of prescribed classes of tilings [48].

An ongoing research work in collaboration with Olaf Delgado-Friedrichs is producing all the possible periodic euclidean simple tilings by tiles with 12 to 16 faces each, containing only quadrilaterals, pentagons and/or hexagons [55]. The search is conducted on a symmetry basis, where tilings with a given number of kinds of vertex are generated first, then the minimum cost allowed by their topological structure is numerically calculated. All the tilings with up to 10 kind of vertices have been generated, their Delaney symbols stored into a database, and their cost evaluated with the Surface Evolver. The number of tilings found is shown in Table 4.1.

k	1	2	3	4	5	6	7	8	9	10
$z < 14$	0	0	2	1	2	2	2	6	10	14
$z \geq 14$	1	2	7	18	43	105	154	441	722	1094
time (s)	2	7	40	200	10^3	$6 \cdot 10^3$	$3 \cdot 10^4$	$3 \cdot 10^5$	10^6	10^7

Table 4.1: Number of tilings and execution times for vertex transitivity up to 10.

As of August 2009, none of these structures showed lower cost than **sod** apart from the already known Weaire-Phelan structure (**mep**) as shown in Figure 4.1.

This chart displays the values of the cost for the tilings with the lowest cost among those having the same number of kinds of vertex (vertex transitivity). Comparing Figure 4.1 with Table 4.1, it can be noted that with one kind of vertex (k=1) only one tiling is present. This tiling is **sod**, and its cost is 5.306. For k=2 there are in total 2 tilings, each made of one 14-sided polyhedron that tiles space isohedrally. These have been described by Delgado-Friedrichs and O'Keeffe [56]. The cost shown in Figure 4.1 only

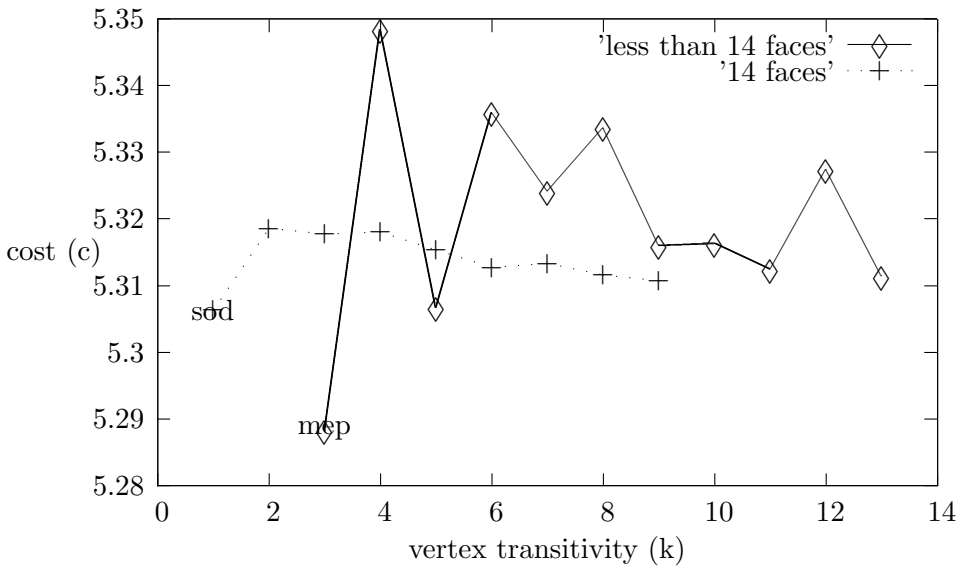

Figure 4.1: This chart shows the cost c against vertex transitivity k. Among the tilings having the same vertex transitivity, only those who showed the least cost are displayed.

refers to the lowest between the two costs, which is just below 5.32. For k=3 there are 9 possible tilings, 2 of which have an average number of faces below 14 ($z < 14$). Figure 4.1 shows 2 values in this case, one for the tiling with the lowest cost among those having an average number of faces per tile below 14 (continuous line, $z < 14$), and one for those with 14 or more (dotted line, $z \geq 14$).

The search is computationally expensive, as shown by the calculation times listed in Table 4.1. At the time of the writing of this thesis, all the possible 2,626 simple tilings with up to 10 kinds of vertex have been determined with this method, requiring four months on three supercomputers, keeping busy a total of 65 cores. The cost of the tilings with $z < 14$ has been determined up to k=10, whilst for $z \geq 14$ only up to k=9. The code is still running and it has already produced new tilings with low cost for k=11,

12 and 13, whose energies have been graphed in Figure 4.1. The tiling with the lowest energy, $k13$, is shown in Figure 4.2.

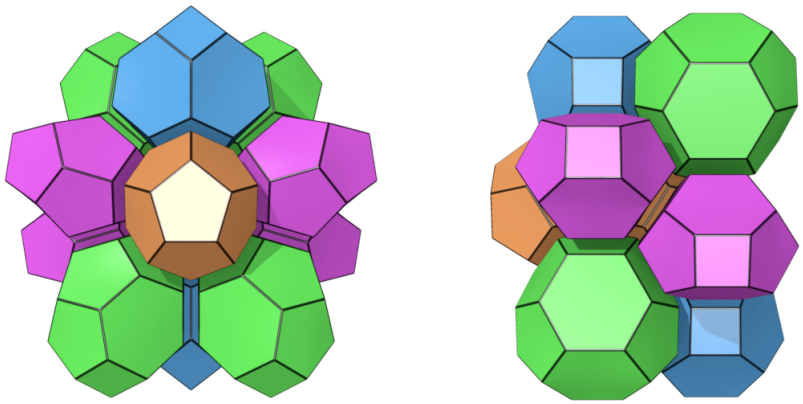

Figure 4.2: A new tiling with 13 kinds of vertex, with energy just above that of the truncated octahedron.

It is worth to note that this method has an enormous potential in finding new structures because of its intrinsic completeness, regardless of the computational time needed. According to Moore's law (co-founder of Intel Corporation), processing speed is growing at an exponential rate, doubling approximately every two years.

4.2 Method II: The Corona algorithm

Isohedral simple tilings with ≤ 16 faces containing only quadrilaterals, pentagons and hexagons have recently been determined [56]. The cost associated with these tilings has been calculated using Surface Evolver [45]. The results have been compared in this work to those of the TCP structures and the result was that tilings by polyhedra with 14 faces had lower cost than those with more than 14 faces.

It has been proved that the lower bound for the average number of faces per cell in an equal-pressure minimal foam is 13.397 [57]. Pentagonal faces are by far the most common kind of face found in foams [7, 9]. These two facts combined suggested the construction of a combinatorial algorithm in which the variance of the number of faces of the polyhedra belonging to the tiling was minimized. Hence, only polyhedra with 13 and 14 faces were selected. Additionally, only polyhedra with high content of pentagons (more than 70%) were selected.

The result was that only polyhedra containing pentagons, hexagons and at most one quadrilateral were suitable. The software *plantri* [58] has been used to generate the possible topologies with these requirements, which resulted to be only three. Each tile has been named with three numbers, [Q-P-H], Q representing the number of quadrilaterals, P that of pentagons, H that of hexagons. The three polyhedra were: [1-10-2], [0-12-2] and [1-10-3]. These are the only possible 13 and 14-faced simple polyhedra with pentagonal, hexagonal and at most one quadrangular face.

An algorithm for the generation of finite clusters of polyhedra has been developed in this work. Using only the three polyhedra defined above, the algorithm begins with an instance of a single quadrilateral face. This will constitute the first element belonging to the tiling. There are three different

ways to add two polyhedra to the starting quadrilateral:

1. Using two [1-10-2]s;
2. Using one [1-10-2] and one [1-10-3];
3. Using two [1-10-3]s.

Because of their symmetry, two [1-10-2]s can be joined in two different ways. A [1-10-2] can be joined to a [1-10-3] in only one way (the other three are symmetrically equivalent to the first case). Finally, two [1-10-3]s can be joined in three different ways. The previous list of pairs of polyhedra is then rewritten as follows:

1. Two [1-10-2]s + (mirrored);
2. Two [1-10-2]s − (mirrored and rotated by π);
3. One [1-10-2] and one [1-10-3];
4. Two [1-10-3]s + (mirrored);
5. Two [1-10-3]s 0 (mirrored and rotated by $\pi/2$);
6. Two [1-10-3]s − (mirrored and rotated by π).

Mirror plane and rotation axis are related to the starting quadrilateral. The six pairs of tiles generated constitute the first step of the algorithm. These pairs of polyhedra are the only way to start a tiling using the given set of three topologically different tiles and having a quadrilateral as starting element. It will now be shown that pair 1 does not admit a tiling, and then that any of the three tiles in the set can be added to pair 2.

Pair 1 is constituted by a couple of [1-10-2]s, each polyhedron being the mirrored image of the other through the starting quadrilateral. This double

(polyhedral) bubble configuration gives rise to four slots for the next polyhedron to be added. Two of these slots are made of two adjacent hexagons, the other two of two adjacent pentagons. Since the set of polyhedra available is limited to the three previously mentioned, the slots with adjacent hexagons can be only filled with a [1-10-3]. This will place a quadrilateral on the adjacent slot. The only configuration possible is then given by adding two [1-10-3]s to the initial couple of [1-10-2]s in such a way that the quadrilaterals do not face the same slot. The potential tiling is now constituted of 4 polyhedra. But the free slots show three adjacent pentagons and a quadrilateral in such an arrangement that cannot be found in any of the polyhedra in the set. Thus, no tiling is possible for this pair.

Pair 2 has got two [1-10-2]s joined on their quadrilateral, mirrored and rotated by $\pi/2$ along the axis normal to the quadrilateral face. Again, there are 4 couples of polygons available to accept a polyhedron each. In this case they are all related by symmetry, so we can work with only one. The couple is made of a pentagon and a hexagon. This means that each of the tiles in the set can fit in: [0-12-2], [1-10-2] and [1-10-3]. Due to its symmetry, there is only one way to place a [0-12-2]. Instead, [1-10-2] has 3 different arrangement. [1-10-3] even more, 7. Thus, there are in total 10 different ways to add a third tile to pair 2.

Pair 3 is composed of one [1-10-2] and one [1-10-3]. The four slots available show these polygon couples (h=hexagon, p=pentagon): h-h, p-h, h-p, p-p. On a h-h we need a [1-10-3], so the third tile is uniquely defined. But it can be placed in two different ways: with the quadrilateral facing p-h or p-p. In the first case the fourth tile can be either a [1-10-2] or a [1-10-3]. In the second case the choice is forced on a [1-10-3]. If we continue on this last path, we notice that only [1-10-3]s can be added. The structure generated is

a semi-helix (it goes to infinity in only one direction). If the first [1-10-2] in the semi-helix is replaced by a [1-10-3], the semi-helix becomes a full helix by [1-10-3]. If this helix is straightened to have a null helix angle, the column obtained can be packed to fill space [59], generating a new simple tiling with unusual properties.

4.2.1 A monotypic, non-isohedral simple tiling

A monotypic simple tiling by a 14-face polyhedron that does not admit an isohedral tiling is now described. The tiling is triclinic and contains four distinct, but combinatorially equivalent, kinds of tile.

A polyhedron has a graph that is planar and three-connected (i.e. at least three vertices and their incident edges have to be deleted to separate the graph into two disjoint parts). In a simple polyhedron, two faces meet at each edge and three at each vertex. In a simple tiling of three-dimensional Euclidean space, the tiles are simple polyhedra and two meet at each face, three at each edge and four at each vertex.

An isohedral tiling is one in which any two tiles are related by an isometry of the symmetry group of the tiling. A monotypic tiling is one in which all tiles are combinatorially equivalent (have the same graph). An isohedral tiling is monotypic but not necessarily vice versa.

Simple tilings are of considerable interest as idealized models of foams and other physical systems [60], their nets (the skeleton of vertices and edges) are of interest in crystal chemistry as the framework types of real and hypothetical zeolites [61], and they present a number of interesting problems. The most celebrated of these is the Kelvin problem [5], which asks for the lowest-energy (smallest surface area) tiling for tiles of a given volume. Among other things, this has prompted numerous studies of isohedral simple

tilings. A recent study is that of Delgado-Friedrichs & OKeeffe [56] who showed that: (a) there are no isohedral simple tilings by tiles with less than 14 faces; (b) all 14-face tiles of isohedral simple tilings have only faces of 4, 5 or 6 sides (4-6 polyhedra); (c) of the 59 different 4-6 polyhedra with 14 faces there are 10 different isohedral tilers that produce 23 distinct isohedral tilings. These results have been confirmed by Komarov et al. [62], who also give a full account of earlier work.

The question of whether a given combinatorial type of polyhedron admits monotypic tilings has also attracted considerable attention. It is known [63] that there are non-tilers, isomorphic copies of which will not tile space in a locally finite and face-to-face fashion; the cuboctahedron is an example. On the other hand, the dual of a k vertex-transitive simple tiling is a k tile-transitive tiling by tetrahedra and necessarily monotypic. In fact, simplicial polyhedra (those with only triangular faces) in general are tilers [64].

In this section, some properties of a new monotypic simple tiling discovered with the use of the Corona algorithm are described. The tile in this structure again has 14 faces but is distinct from the 10 isohedral tilers and is the unique 14-face 4-6 simple polyhedron with one quadrilateral face. It has symmetry m; its Schlegel diagram, which shows the kind of faces of the polyhedron and their relative positions, is shown in Figure 4.3. The combinatorial symmetry of the net of this tiling is $P\bar{1}$ as determined by the program Systre [54].

The unit cell contains eight tiles, each of symmetry 1, that are four pairs of enantiomers . The inversion centers are located in 4-and 6-sided faces. An illustration of a repeat unit made with the program 3dt is shown in Figure 4.4. The structure has 24 kinds of vertex, 48 kinds of edge, 32 kinds of face and 4 kinds of tile (transitivity 24 48 32 4).

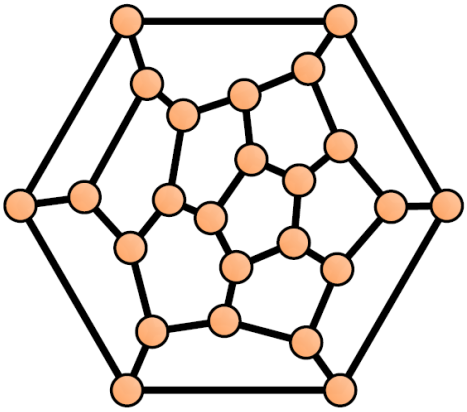

Figure 4.3: The Schlegel diagram of the polyhedron [1-10-3].

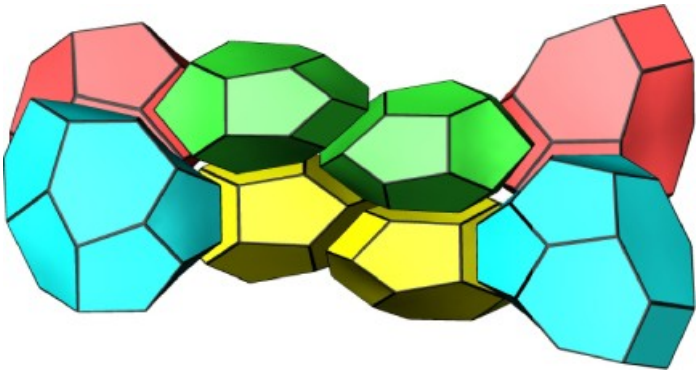

Figure 4.4: The new monotypic, non isohedral, simple tiling, net symbol **rug**.

This is the first example of a monotypic simple tiling by a polyhedron that does not admit an isohedral tiling and it raises some interesting questions. What polyhedra admit monotypic simple tilings other than the known isohedral tilers? In particular, do any of the other 14-face 4-6 polyhedra admit monotypic tilings? Do polyhedra with less than 14 faces admit a monotypic simple tiling? It is known only that the average face size in a simple tiling must be ¡6 and 9/2 [65] so the average number of faces per tile is 8. For an example of a simple tiling with average face size approaching that lower limit [60].

Intrinsically triclinic structures rarely arise in such studies. For example, of the many hundreds of known 3-periodic packings of one kind of sphere, there is exactly one that is triclinic [66]. The net of this structure is the only triclinic entry in the RCSR database [44] of over 1000 nets, and there are no triclinic examples among the thousands of nets in the EPINET database [67].

Crystallographic data for an embedding with edge lengths all equal to 1 are: $a = 5.770, b = 5.806, c = 16.834, \alpha = 94.81, \beta = 94.39, \gamma = 90.62$. The centroids of the polyhedra are at (0.4110, 0.0920, 0.8775; 0.0325, 0.5904, 0.8782; 0.4086, 0.4674, 0.6215; 0.0899, 0.9099, 0.3794). The coordinates of the vertices of the net of the structure have been entered in the RCSR database with the net symbol **rug**.

The computer programs 3dt and Systre, both essential to this work, are by Olaf Delgado Friedrichs [49].

4.3 Method III: Pattern formation

Pattern formation studies the mechanisms of self-organization of lower dimensional (cellular or linear for two-dimensional space) entities in a given n-dimensional space. The mathematical analysis of these patterns is usually conducted by studying the behaviour of a partial differential equation (PDE), typically the Swift-Hohenberg equation [68, 69], which is shown in Equation 4.1.

$$\frac{\partial u}{\partial t} = au - (\nabla^2 + 1)^2 u + bu^2 - cu^3 \tag{4.1}$$

The use of this equation for three-dimensional space partitioning problems is shown in a recent work by the author [1]. The implications of pattern formation and space partitioning in a wide range of disciplines ranging from physics of foams, cellular materials, crystallography, biology (plant cell tissue aggregates), metallurgy (grains in polycrystalline materials), data compression and more, has pushed the author to consider this mathematical tool carefully. The fact that the Swift-Hohenberg equation led to a mathematical discovery on minimal surfaces suggests the existence of some kind of relationship between the cost derived from it and the actual cost of a foam. Seventeen out of more than fifty partitions obtained with this method had lower cost than **sod**. Fifteen of these had never found before.

4.3.1 A new counter-example to Kelvin's conjecture

A new counter-example to Kelvin's conjecture on minimal surfaces [4] has been found in this work [1]. The original conjecture stated that the minimal surface area partition of space into cells of equal volume was a tiling by truncated octahedra with slightly curved faces (K or **sod**). Phelan and Weaire found a counter-example [6] whose periodic unit includes two differ-

ent tiles, a dodecahedron and a polyhedron with 14 faces (A15 or **mep**). Successively, Sullivan showed the existence of a whole domain of partitions [8] by polyhedra having only pentagonal and hexagonal faces that included A15.

This thesis presents a new partition with lower surface area than K containing quadrilateral, pentagonal and hexagonal faces, the first of this kind. These and other new partitions have been generated via the Voronoi diagram of spatially periodic sets of points obtained as local maxima of the stationary solution of the 3D Swift-Hohenberg [68] partial differential equation in a triply periodic boundary, with pseudorandom initial conditions.

The geometrical problem that seems to have its solution in real foams of partitioning space into cells of equal volume with the least interfacial area has not yet been solved. The solution to the two-dimensional problem, also known as the honeycomb conjecture, has been given a formal proof by Hales [38]. For the three-dimensional problem, a conjectured solution has been proposed by Phelan and Weaire [6]. The proof of the existence of a solution for the general n-dimensional case has been recently given by Morgan [41].

A possible solution to the three-dimensional problem was given more than a century ago by William Thomson, better known as Lord Kelvin, who was also the first to formally stated it [4]. Kelvin conjectured that the partition made by a packing of identical truncated octahedra with slightly curved faces (K), had the minimum surface area among all the possible equal volume partitions of space. The truncated octahedron is a polyhedron with 14 faces, 8 of which are hexagons and the remaining 6 of which are quadrilaterals as shown in Figure 4.5. In the partition considered by Kelvin all the edges were curved. The quadrilateral faces were flat, and the hexagonal ones were slightly curved, further reducing the total interfacial area

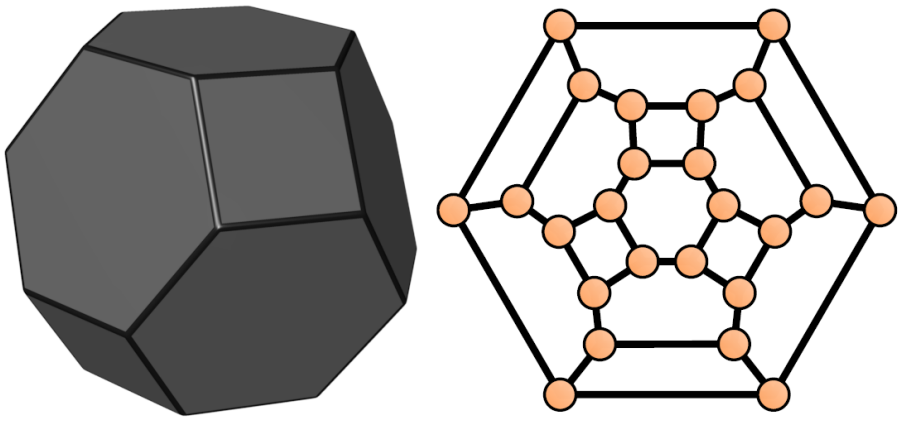

Figure 4.5: A truncated octahedron an its Schlegel diagram. This polyhedron is space-filling.

of the partition when compared to the flat-faced version of the truncated octahedron.

The solution proposed by Kelvin was believed to be optimal until 1993, when Robert Phelan and Denis Weaire, using Ken Brakke's program Surface Evolver [45], showed the existence of a partition (WP) having less area than that by truncated octahedra [6]. The partition, also known as the Weaire-Phelan structure, has two different cell shapes, namely a cubicly deformed pentagonal dodecahedron and 14-hedron with 12 pentagonal and 2 hexagonal faces as in Figure 4.6.

Shortly after the discovery, John Sullivan described a class of mathematical foams known as tetrahedrally close-packed structures, which included WP. Many of these structures have been known for a long time as Frank-Kasper phases [46, 47]. All the structures belonging to this domain are made of polyhedral cells having only pentagonal and hexagonal faces. He constructed infinite families of periodic structures as convex combinations of a finite set of basic structures [8, 70].

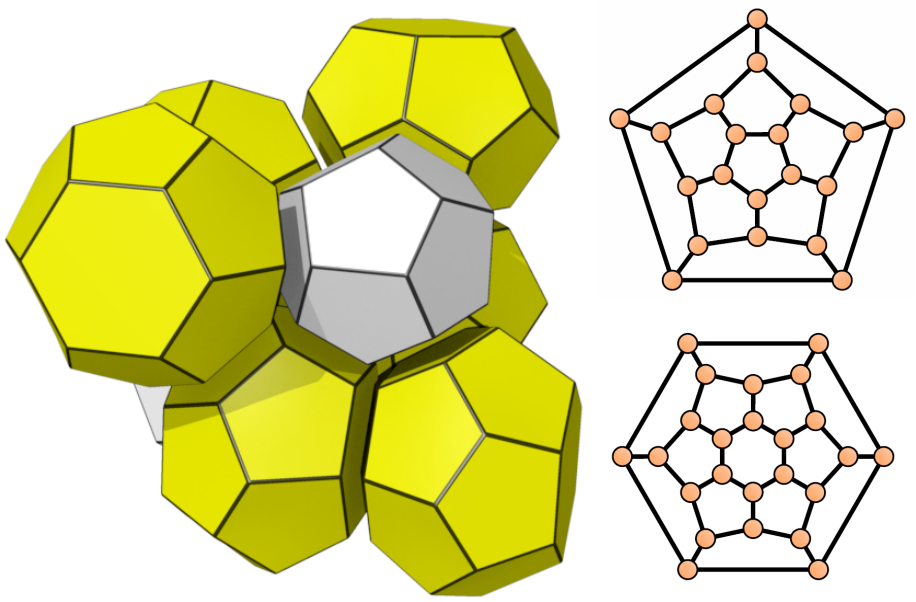

Figure 4.6: The periodic unit of the Weaire-Phelan structure contains 8 polyhedra, two [0-12-0] and six [0-12-2]. The Schlegel diagrams are shown on the right. Tiles are represented slightly detached one from the other for a better visualization. The pictures only display the topological information of the structure.

This showed that not only WP had less area than K, but infinitely many other structures (the terms structure, partition, foam and tiling are used as synonyms here as the problem interests a large number of different fields [60, 71, 72, 73]) could be constructed with such a property. The polyhedral cells used in these structures are of four distinct kinds having 12, 14, 15 and 16 faces. All contain 12 pentagons plus respectively 0, 2, 3 and 4 hexagons. These are the only combinatorially possible simple polyhedra containing only pentagons and/or hexagons where the hexagons are not adjacent, as shown by the program plantri [58]. A simple polyhedron is a polyhedron in which each vertex belongs to exactly three edges. A tiling by polyhedra is simple if every face contained in it is shared by two adjacent tiles, every edge by three incident faces, and every vertex by four incident edges. Since

faces can be in general non-planar, polyhedra should also have at least three faces meeting at each vertex.

Since the only faces that occur in the partitions found have from 4 to 6 sides, a nomenclature for polyhedra based on this fact consisting of three numbers has been considered. Each polyhedron is assigned three numbers [Q-P-H] that represent the number of quadrilaterals (Q), pentagons (P) and hexagons (H). This naming system, called simplified signature, although not always univocal in defining the topology as with the Schlegel diagram [74], presents the advantage of a much more concise form of identification of the polyhedron, very similar to the signature used in the software application 3dt [49], and for this reason it will be used to describe the polyhedral composition of the structures found in this work.

One method of generating foams is by Voronoi partitions in three dimensions. All that is needed is a set of points in a parallelepiped. If the opposite faces are connected each other, a three-torus is the result and the set of points can be thought as periodic and filling the whole three-dimensional space. The Voronoi diagram of these points produces a periodic partition of the space. Generation methods that start from random sets of points in a three-torus have already been used with interesting results [10].

In this thesis a method based on a partial differential equation that shows a pattern forming behaviour, Equation 4.1, also known as the Swift-Hohenberg equation [68, 69] is proposed. A Matlab script provided by David Lloyd previously used for the study of two-dimensional localized hexagonal patterns [75] has been modified for the three-dimensional case. This allowed to find numerical solutions to the Equation 4.1 on a periodic cube of prescribed size L using the Fast Fourier Transform. The coefficients a and b in Equation 4.1 affect the final pattern. The values needed for homogeneously

distributed and isolated maxima to appear in the stationary state were found to be respectively close to 0.001 and 1.0 and for this reason these have been adopted. The unit cell was chosen to be cubic for simplicity. A version of the code that computes Equation 4.1 in a cuboid as also been written and a more general implementation working in a parallelepiped might help. Solutions with non-cubic symmetry arise in a cubic region only if a multiple of their unit cell has arbitrary close to cubic symmetry. This is always the case, the only problem being the fact that the structure might be very large. The mesh grid adopted for the numerical solution consisted of 40x40x40 scalars.

The code is reported below, comment lines start with a % symbol:

```
% Equation parameters
a = 0.001; b = 1.0; c = 1.0;

% Mesh and domain size and time step
N = 40; L= 7; dt= 2;
dx=2*pi/N;x=dx*(1:N)';x=L*(x-pi)/pi;
[xx,yy,zz]=meshgrid(x,x,x);

% Initial data
u = rand (N,N,N);

% Viewing parameters
d = 0.8; eps = 0.00001; rotate3d;

% Compute eigenvalues of linear operator
kk = [0:N/2 -N/2+1:-1]*(pi/L);                  % wave numbers
[kkx,kky,kkz]=meshgrid(kk,kk,kk);
```

```
LU = - (-(kkx.^2 + kky.^2 + kkz.^2)+1).^2 + a; % Linear Operator
EXP = exp(LU*dt);                              % Exact linear bit
ETD = (exp(LU*dt)-1)./LU;                      % ETD1 coeffs
uT = fftn(u);
u2 = rand (N,N,N);

% Main loop
while max(max(max(u2-u)))>eps
    f = s*u.^2 - u.^3 ;                        % nonlinear rhs

    % exponential timestep in fourier space
    fT = fftn(f); uT = uT.*EXP + fT.*ETD;
    u2 = u;
    u = real(ifftn(uT));
end

% Isosurface plot
pa = patch(isosurface(xx,yy,zz,u,d*max(max(max(u)))+
(1-d)*min(min(min(u)))));
set(pa,'FaceColor','r','EdgeColor','none','FaceAlpha',.5);
view(3); camlight; axis vis3d; axis ([-L,L,-L,L,-L,L]);
axis square; grid on; drawnow;

% Pseudotorus
v=zeros(N+2,N+2,N+2);
for k=1:1:N
    for j=1:1:N
```

```
        for i=1:1:N
            v(1,j+1,k+1)=u(N,j,k);
            v(N+2,j+1,k+1)=u(1,j,k);
            v(i+1,1,k+1)=u(i,N,k);
            v(i+1,N+2,k+1)=u(i,1,k);
            v(i+1,j+1,1)=u(i,j,N);
            v(i+1,j+1,N+2)=u(i,j,1);
            v(i+1,j+1,k+1)=u(i,j,k);
        end
    end
end

% Maxima coords extraction
l=1;
for k=1:1:N
    for j=1:1:N
        for i=1:1:N
            if ((v(i+1,j+1,k+1)>v(i,j+1,k+1))&&
            (v(i+1,j+1,k+1)>v(i+2,j+1,k+1))&&
            (v(i+1,j+1,k+1)>v(i+1,j,k+1))&&
            (v(i+1,j+1,k+1)>v(i+1,j+2,k+1))&&
            (v(i+1,j+1,k+1)>v(i+1,j+1,k))&&
            (v(i+1,j+1,k+1)>v(i+1,j+1,k+2)))
                vv(l,1)=j; vv(l,2)=i; vv(l,3)=k; l=l+1;
            end
        end
    end
```

```
end
```

The coefficients a, b and c were the parameters in Equation 4.1, a being the coefficient of the linear, b the quadratic and c the cubic part. N was the resolution of the grid in each of the three spatial directions. L was the domain size, which is the side length of the periodic cube. dt is the time step. x represents the discretized spatial variable, ranging from $-L$ to L. This was used to generate a vector array for volume discretization and successive computation of the function $u = u(x, y, z)$, which has been initialized with random values ($u = rand(N, N, N)$). d has been introduced for visualization purposes. It allows the user to select a value between 0 and 1, which correspond to the absolute minimum and maximum of the function u. The parameter *eps* was set to terminate the execution of the program when variation on u were negligible.

The numerical solution of the PDE 4.1 was performed with a spectral method that uses the discrete Fourier transform ($fftn$). The eigenvalues were computed and the linear and nonlinear parts of the equation written for the exponential time step in Fourier space (EXP and ETD). The main loop repeatedly computes the transform and the inverse transform until the variations in the function u are negligible. This corresponds to the stationary state where the condition $\frac{\partial u}{\partial t} = 0$ is required.

For the purpose of extraction of the coordinates of the maxima a pseudotorus was generated which consisted in a cubic shell of values surrounding the mesh constructed for the function u. The value of u in space was compared to neighbour values and the maxima were stored in the array vv for use in the Voronoi constructor.

The graphical output is shown in Figures 4.7, 4.8 and 4.9. The blob-like objects are surfaces at 80% between the minimum and the maximum of the

function u ($d = 0.8$). The patterns shown in Figures 4.8 and 4.9 are new. Figure 4.9(b) shows the pattern that led to the counter-example to Kelvin's conjecture.

Local maxima for the function $u(x, y, z, t)$ lie inside the sphere-shaped isolevel surfaces shown in the pictures.

The normalised energy associated with Equation 4.1 is given by:

$$E = \frac{1}{8L^3} \int -\frac{au^2}{2} + \frac{[(\nabla^2 + 1)u]^2}{2} - \frac{bu^3}{3} + \frac{u^4}{4} dzdydx \qquad (4.2)$$

This has been used to determine whether a correlation with the cost of a foam was present or not. No link has been found yet, but it is believed that a relationship between this energy and other forms of it like the chemical bond energy of the crystal lattice might exist.

The solution for the function $u = u(x, y, z, t)$ has been found to converge from pseudorandom initial conditions to a stationary state. The three-dimensional coordinates of the local maxima of the function $u = u(x, y, z, t)$ in this final state have been extracted. The method has been run a finite number of times, and the results have been compared for congruence. Successively L has been incremented and the coordinates at the stationary state have been recorded again. It has been found that for large values of L the patterns formed appear locally but not globally ordered. For certain values of the parameter L the system converges to a state where the maxima are arranged on parallel lines in space, all having the same orientation, in a hexagonal packing fashion. The partition obtained from such an arrangement is a cylindrical hexagonal honeycomb.

Another issue is that many of the more simple patterns appear for different values of L. These values are the multiples of the fundamental lattice distance for a given pattern. Thus more complex patterns might be hidden by the simpler ones when looking for a solution for a given size L.

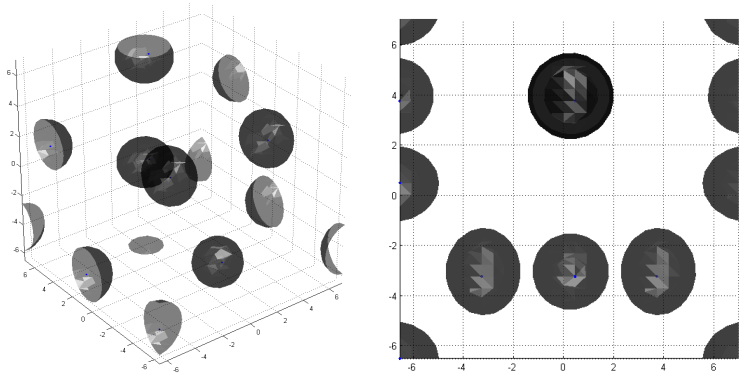

(a)

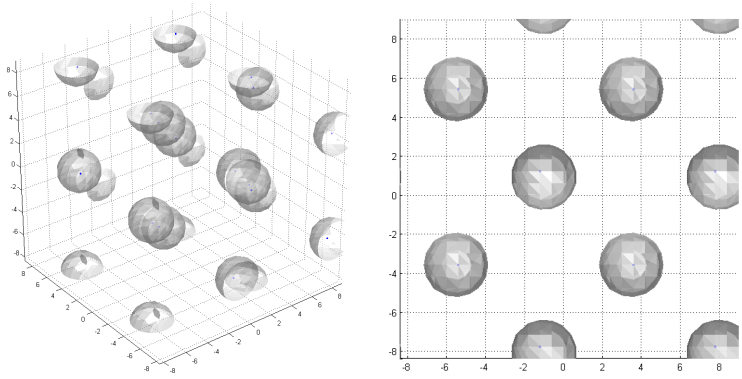

(b)

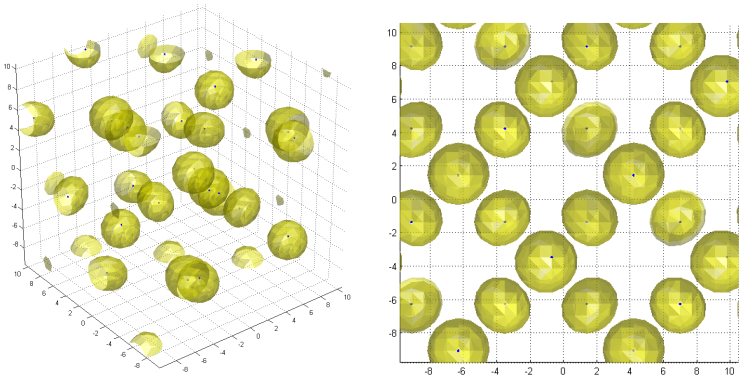

(c)

Figure 4.7: The most frequent periodic patterns that appear for L=7.3 is A15 (a), for L=9 is BCC (b), and for L=10.5 is C15 (c), with respectively 8, 16 and 24 points.

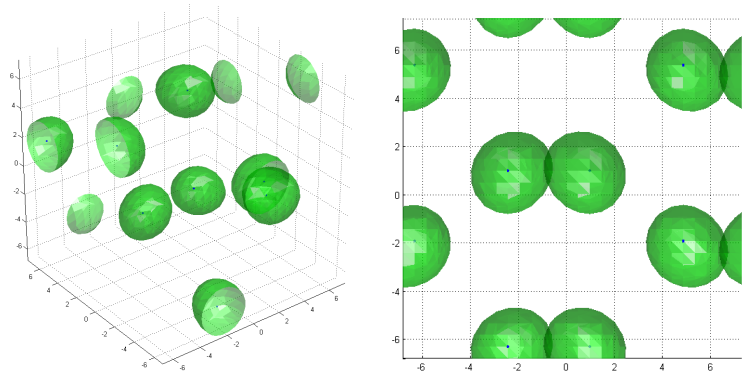

(a)

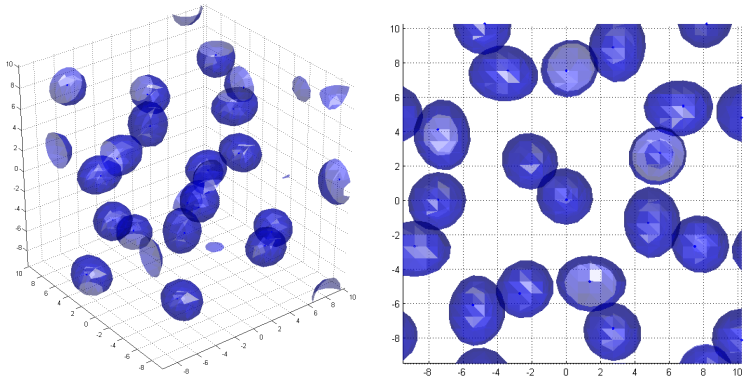

(b)

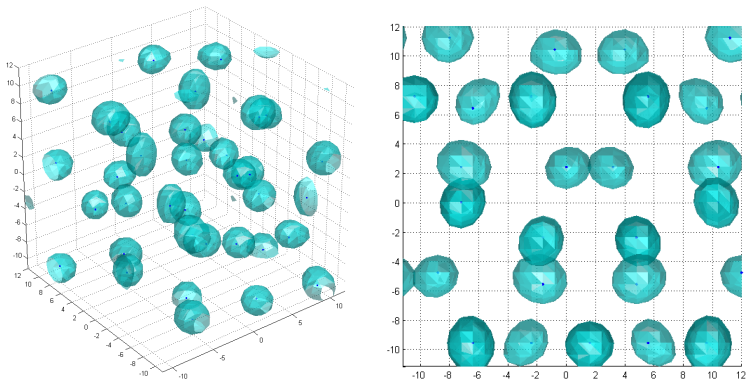

(c)

Figure 4.8: The new periodic patterns that appear for L=7.2 is P8 (a), for L=9.8 is P20 (b) and for L=12 is P36 (c). Note that the discovery of the P8 pattern has been particularly difficult since it was occulted by the more frequent A15 pattern, whose L values (6.7 to 7.9) completely hide those at which P8 arises (7.0 to 7.6).

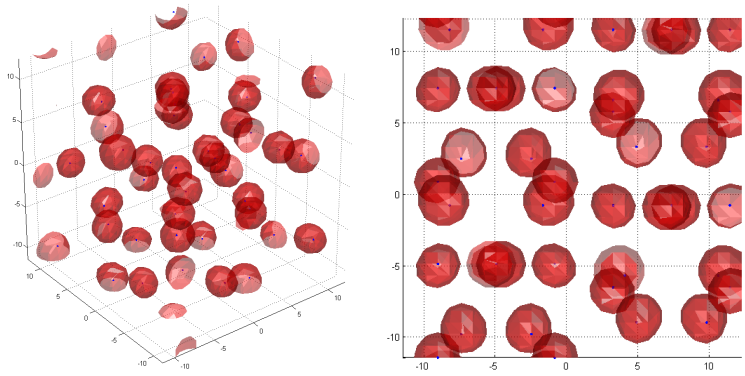

(a)

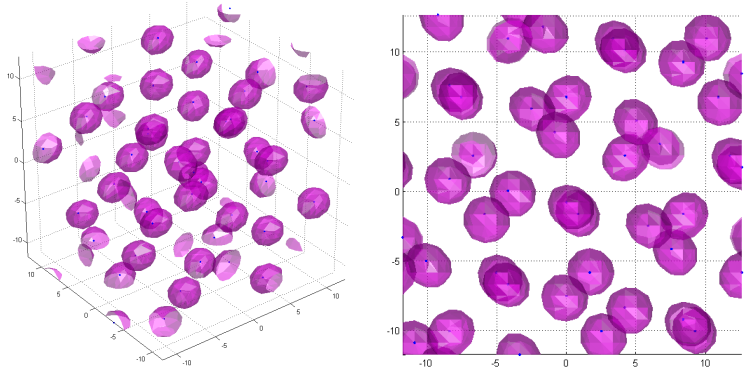

(b)

Figure 4.9: The new periodic patterns that appear for L=12.3 is P40 (or K11) (a) and for L=12.7 is P42 (b). The surface represents locations where the energy functional is at 80% of its maximum. The letter P stands for *points* and the following number indicates the number of points in the pattern. The Voronoi diagram of the pattern P42 is a non-simple tiling by polyhedra with 13 and 14 faces. Some of the simple modifications of this tiling have lower cost than Kelvin's partition of space. The figures on the right are projections along the z-axis.

In general, since the average distances between the local maxima are roughly constant, increasing the size of the cubic region in which the equation is calculated increases the number of the local maxima within the same region. This allows structures with different level of complexity to be found simply acting on the size of the periodic boundary L.

The patterns obtained from such a setup were BCC, FCC, P8, WP, P20, C15 [76, 8], P36, K11, P42. The values of L for which the patterns were found are: 4.5 for BCC, 5.7 for FCC, 7.2 for P8, 7.3 for WP, 9.8 for P20, 10.5 for C15, 12 for P36, 12.3 for K11 and 12.7 for P42. More patterns are present at L=13.9 (P56), 14.0 (P60), 15.0 (P76) and 16.7 (P136). Since the system allows the solution to be stretched, the patterns were also found for values close to those given above. The values listed here correspond to the lowest PDE energy (see Equation 4.2). Any given pattern appears also for values that are integer multiples of these listed. Additionally, some of the patterns arise for more than only one value, such as FCC that also shows up at 7.4 and 9.6. Symbols starting with the letter P identify structures that have not been found in the literature. The number following the letter P specifies the number of points found in the cubic region at the stationary state. K11 contains 40 points. This pattern is described in a separate article [55], since the tiling having these points as Voronoi centers has been found for the first time using a different method.

Using Sullivan's vcs software [77] the Voronoi partition for each pattern of points was created. This software uses the gift-wrapping algorithm for the determination of the Voronoi vertices and for this reason is not stable when more than four Voronoi cells meet at a point. Since some of the new partitions found were non-simple, a small random quantity has been added to the coordinates of the points to avoid algorithm instabilities.

The partitions have been imported into Surface Evolver, where the added errors have been eliminated by deletion of the edges shorter than a given value. A number of additional simple foams has been created directly in Surface Evolver by *popping* vertices of non-simple ones. The outcome of this operation is not a unique structure since there are $3^m + 4^n$ different combinations, if m is the number of 8-connected vertices and n that of 6-connected vertices in the original non-simple foam. However, this number can be drastically reduced due to symmetry considerations.

The periodic graphs of the nets constituted by the edges of the partitions have been analyzed by Systre [54] so that the primitive net could be identified and the number of tiles in the partition therefore reduced to its minimum possible. This helped in the case of P42, where the 42 tiles have been reduced to 14, as shown in Figure 4.10.

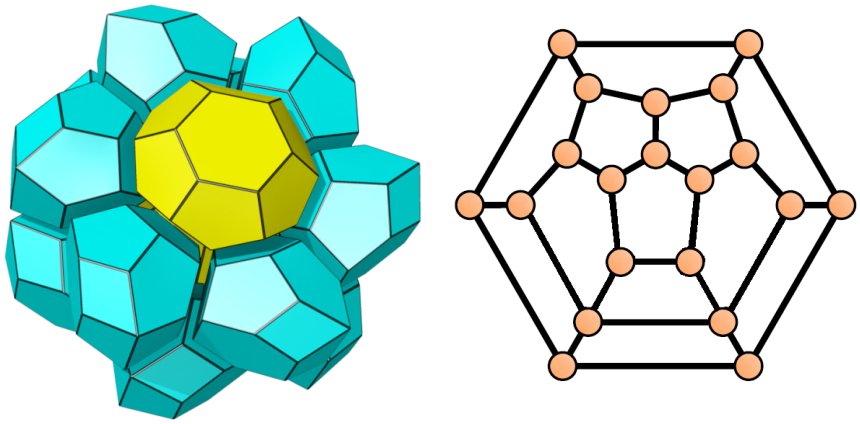

Figure 4.10: The unit cell of the new partition P42 contains 14 polyhedra of 2 different kinds. Twelve non-simple [4-8-1] and two [0-12-2]. The Schlegel diagram of the non-simple [4-8-1] is shown.

Fifteen out of the 81 combinatorially possible simple partitions derived from the P42 non-simple case are topologically distinct configurations. Each of these showed less surface area than K. The partitions contain only poly-

hedra with 13, 14 and 15 faces each, specifically those named below plus a [3-6-4] and a [2-8-5]. Their costs range from 5.303 to 5.306. Figure 4.11 shows a picture of the tiling of the unit cell of the structure with the lowest cost, which has been named P42a.

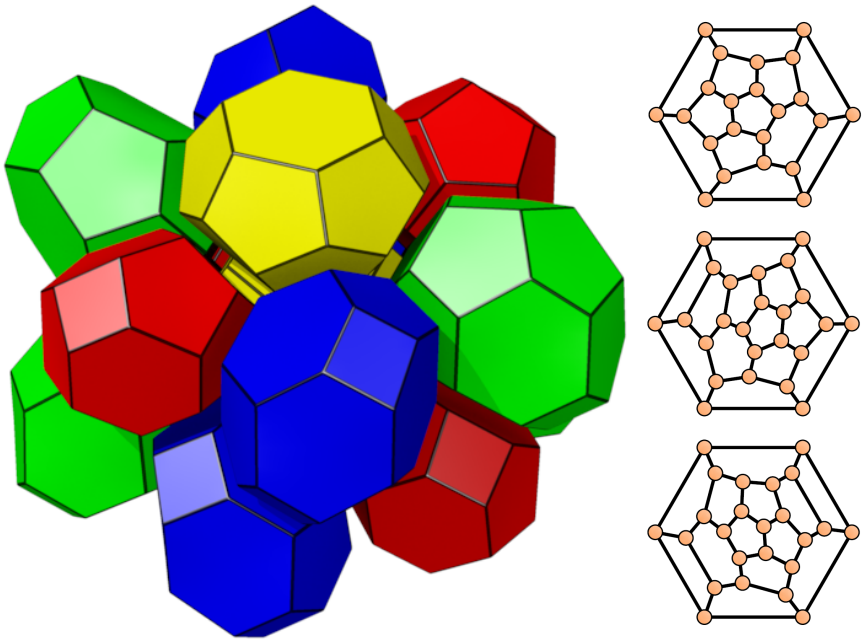

Figure 4.11: The unit cell of the new partition P42a contains 14 polyhedra of 4 different kinds. Four [1-10-2] (red), four [1-10-3] (green), four [2-8-4] (blue) and two [0-12-2] (yellow). Tiles of the same colour are related by point inversion or glides (a glide is a reflection plus a translation). The Schlegel diagrams of the first three are shown. From the top: [1-10-2], [1-10-3] and [2-8-4].

The content of quadrilaterals, pentagons and hexagons in the new partition P42a closely matches (Table 4.2) the values experimentally found in real foams first by the camera lucida drawings of the botanist Edwin Matzke in 1964 [11] and successively by the 3D Nuclear Magnetic Resonance images of Katsumi Kose in 1996 [9].

The fundamental unit is made of ten 14-hedra and four 13-hedra. The

	polygon count				percentage		
	quad	pent	hex	tot	quad	pent	hex
Kose	10	76	23	109	9	70	21
Matzke	866	5503	1817	8221	11	67	22
K	3	-	4	7	43	-	57
WP	-	48	6	54	-	89	11
P42a	8	68	20	96	8	71	21

Table 4.2: Polygonal composition experimentally found in real foams by Kose and Matzke compared to the distribution in some of the lowest cost periodic partitions known. Note the similarities with the P42a structure.

polyhedral composition of P42a matches very closely that observed by Matzke [11]. The three most common cells in this partition [1-10-2], [1-0-3] and [2-8-4] are the first three entries in Matzke's experiments. The [0-12-2] cell is at the fifth place in Matzke's list, followed by the pentagonal dodecahedron [0-12-0], not present in P42a. The average number of faces is 13.71, very close to the values of 13.70 found by Matzke [11], 13.63 by Kose [9], the theoretical optimal value of 13.56 given by Coxeter for random close-packing [78], not far from the value of the currently conjectured solution to the Kelvin problem of 13.5 [6] and above the lower bound for equal-pressure foams of 13.40 given by Kusner [57]. The lower bound for the cost corresponding to this last value is 5.254 as shown by Glicksman and Rios [79].

The space group for each of the foams produced were determined by 3dt, which is part of the Gavrog Project [49], and refers to the structure with the highest degree of symmetry having the same topology. The minimum cost is obtained by constraining the structure to have tiles of the same volume. It is relevant to note that the configuration of minimum cost does not always

coincide with the most symmetrical one. Note that P42a is characterized by a very low symmetry when compared to K and WP. Table 4.3 reports the data for comparison.

	simplified signature	sp. gr.	c	z
K	[6-0-8]	$Im\overline{3}m$	5.306	14
WP	[0-12-0]+3[0-12-2]	$Pm\overline{3}n$	5.288	13.5
P42a	2[2-8-4]+2[1-10-2]+2[1-10-3]+[0-12-2]	$C12/c1$	5.303	13.71
P42	6[4-8-1]+[0-12-2]	$P6/mcc$	5.307	13.14

Table 4.3: Simplified signature, space group of the most symmetrical configuration, minimum cost c of the equal-volume configuration and average number of faces per cell z.

The Surface Evolver code used for the calculation of foams properties and parameters (including their cost) has been provided by Sullivan. The code for the directional popping has been provided by Brakke. The code for the relaxation of the periods has been written by the author. This step consisted in numerical iterations in which lengths and angles of the vectors defining the periodic unit, along with the coordinates of all the vertices defining the structure where varied one at a time and the surface area further minimized.

The periods of the unit cell and the coordinates of the centers of the Voronoi cells for the partition P42 are reported in Table 4.4.

A graphical illustration for the set is shown in Figure 4.12, where the third dimension has been represented by varying the size of the dots. It is easy to see that the fundamental periodic unit of the pattern consists of two rings of six points stacked one on the top of the other with a relative rotation of $\pi/6$ and two points at the centre of these rings lying on intermediate planes.

	Periods			Points ($k \in \mathbb{N}, 1 \leqslant k \leqslant 12$)		
ρ	$\frac{5}{2}\cos(\frac{\pi}{12})$	$\frac{5}{2}\cos(\frac{\pi}{12})$	0	0	0	$\frac{\sqrt{3}}{2}$
θ	0	$\frac{\pi}{3}$	0	0	0	$(2k-1)\frac{\pi}{12}$
z	0	0	2	0	1	$1+\frac{(-1)^k}{2}$

Table 4.4: Parameters for the periodic point set for the Voronoi generation of the partition P42, given in the cylindrical system.

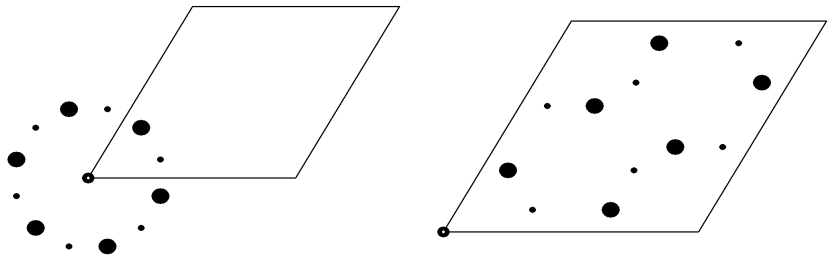

Figure 4.12: The 14 points in the P42 pattern and how they relate to the periodic unit cell. The radius of the dots expresses the third dimension otherwise not representable on paper. There are four different sizes: one point in the origin at $z = 0$ (in white), six points at $z = 0.5$, one point at $z = 1$ (this coincides with that at $z = 0$ in this views) and six points at $z = 1.5$.

The method described, opportunely tuned, can also be used to find new clues about the honeycomb problem considered by Tóth [80].

The pictures of the tilings have been generated with 3dt [49]. The Schlegel graphs (apart from that in Figure 4.10 that has been partially edited by hand) have been produced with Olaf Delgado-Friedrichs' code in

Thomas Harmuth's 3-regular planar graphs generator built in the software CaGe [81].

The point set P8 produces a new space-filling polyhedron with 13 faces, a [6-6-1]. Space group is $Pa\overline{3}$ (see Figure 4.13).

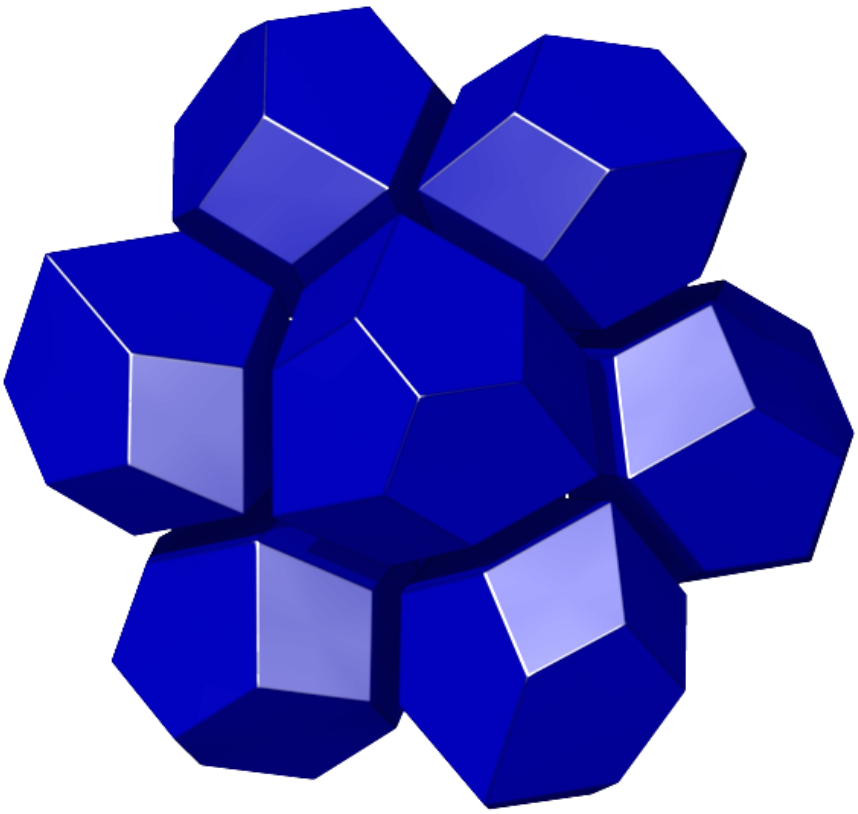

Figure 4.13: The new partitions P8 is made of a single polyhedron having 13 faces, a [6-6-1]. Space group is $Pa\overline{3}$.

The tilings for the sets P20 and P36 are shown in Figure 4.14. Space groups are $P4332$ and $Pca21$ respectively.

The stress concentration under static load of periodic foam structures,

including that derived from the tiling P42a, have been compared with the geometries produced in Chapter 5. The numerical results are described in the Chapter 7.

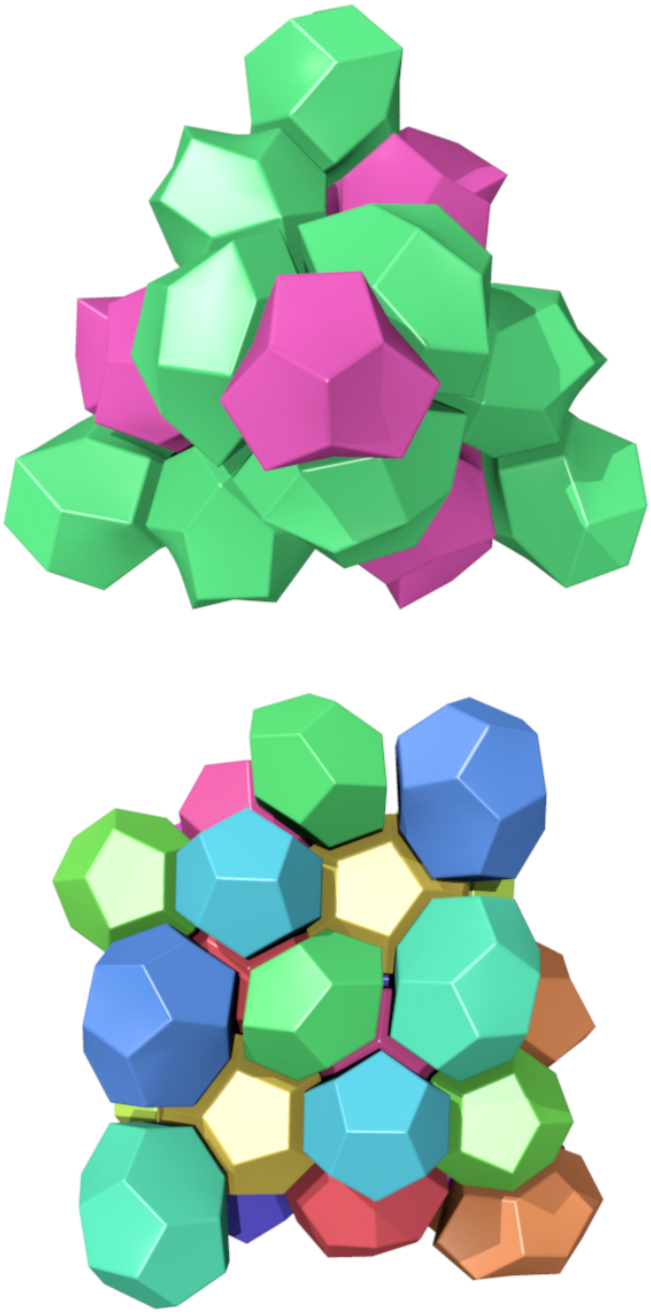

Figure 4.14: The partitions P20 and P36. Space groups are $P4332$ and $Pca21$ respectively.

Summary

- An extensive search on periodic simple tilings approximating the structure of foams has been conducted [55].
- An algorithm for corona of polyhedra chosen among a given set has been developed. It is believed that its implementation on a computer would give rise to new structured arrangements of polyhedra, such linear (helices) or fully three-dimensional (tilings) [2].
- The first monotypic, non-isohedral simple tiling has been discovered [59].
- A partial differential equation known in pattern formation has been used for the first time with success for the solution of a problem in geometric measure theory [1].
- A new family of counter-examples to Kelvin's conjecture on minimal surfaces has been discovered, showing a link with experimental evidence and a possible explanation to the intrinsic disorder in foams. One of the members of this family is also the first example of simple tiling containing only polyhedra with 13 and 14 faces [1].
- A new space-filling polyhedron with 13 faces has been discovered (the Voronoi diagram of the P8 pattern [1]).

Chapter 5

Periodic Nodal Surfaces

The use of mathematical surfaces in defining the morphology of porous materials allows simple models to be analyzed in a virtual environment without the need of any physical testing, this way reducing costs for equipment, eliminating the inevitable errors due to the heterogeneity of the feature of the source specimens, both relative to their material properties and morphology. Additionally, measurement errors that always arise from experimental setups can this way be avoided. A further advantage is that such models can be easily and rapidly generated, modified and exchanged between scientists and engineers, who can then feedback their results to the rest of the scientific community. Defining a standard is much more simple and, for the same effort spent, more reliable and consistent than in the physical world.

The main disadvantage is that models are not able to fully simulate the real object behaviour. The investigation of different properties requires the generation of different models for the same system. Models are created to solve individual problems related in general to a much larger and complex system. Even the apparently simple problem of understanding the mechanical response of porous materials in terms of stress distribution under load

would require different models, often on different scales, for an appropriate investigation. It will become clear that the geometrical models developed in this work could be used to predict both structural and fluid dynamical properties of highly porous materials with interconnected porosity. The fluid permeability of triply periodic minimal surfaces, which is a family of surfaces strictly related to the PNS, has been recently evaluated by Jung and Torquato [82]. In this study the structural behaviour of materials bounded by PNS has been considered, and a correlation between their geometry and the stress concentration in the solid phase resulting from compressive load has been established.

In this study, in order to generate the geometry of the scaffold, two different parametric methods have been investigated, lattice generation by a three-dimensional modelling application and surface definition by implicit triply periodic trigonometric functions. The first approach consists of the design of the lattice with the aid of a parametric modeler. The geometry obtained is shown in Figure 5.1.

The implicit function method - the second method used in this work - uses a set of triply periodic level surfaces [83], in a way that has been recently used also in nano design [84]. These surfaces are not only periodic, but also approximating a set of minimal surfaces. A more extensive description of minimal surfaces is given later in this chapter. At this stage, it is sufficient to know that if a surface is minimal, the area included in any closed curve lying on the surface is the minimum possible. The surface also divides the three-dimensional space into two equal volumes.

The set of triply periodic minimal surfaces chosen in this work for their ability to produce skeletal graphs of different interconnectivity order is composed of: the primitive surface, the diamond surface and the gyroid surface

(Figure 5.2), having interconnectivity order respectively equal to 6, 4 and 3.

In this section the structures of porous materials will be described from a topological point of view. In order to achieve this, the surface of separation that defines the internal arrangement of the porosity will be considered. The boundary surface between the solid and the void part of the structure will be designed via a mathematical model on the basis of the functions and constraints defined in the material. An advantage of using mathematical expressions to define the surface is that a desired number of parameters can be assigned to the model so that a subsequent shape optimization study can be carried out with relative ease.

The surface has been modelled with the aid of a routine written by Michael Carley which uses the GNU Triangulated Surface Library [85]. Finally, the geometry has been tested via Finite Element Analysis (FEA) to

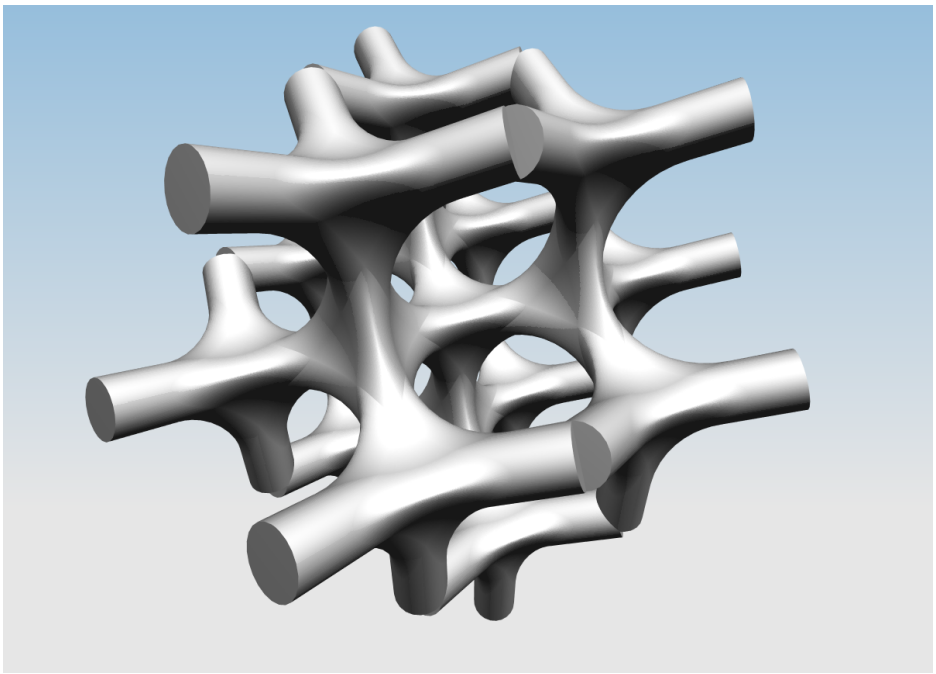

Figure 5.1: Lattice generated by a three-dimensional modelling application.

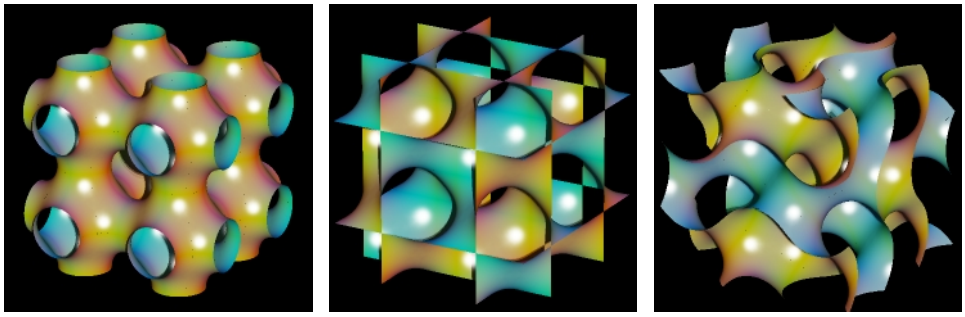

Figure 5.2: P (primitive), D (diamond) and G (gyroid) triply periodic minimal surfaces divide the space into two equal parts. These and more pictures are available on the Scientific Graphics Project website [83].

determine the effective stress distribution under load (Chapter 6).

5.1 Surfaces

The number of possible continuous surfaces that satisfy the requirement of dividing the space into two parts of given volumes is obviously infinite. The periodicity constraint narrows down this number without losing in generality. Several methods have been and are being adopted to model periodic surfaces [84] for geometries with the prescribed functions and constraints. Two of them have been developed in the present study, and they will be described below, in increasing order of versatility and potential number of applications.

The first method consists in using a solid modelling software application. With a 3-D modelling program it is relatively easy to build a structure starting from elemental objects such as cylinders, join them together and provide them with a smooth surface fillet, to obtain a parametric cell. A 3D periodic array will complete the exercise. Although this method seems rapid and intuitive, the information stored on a computer increases quickly when handling NURBS (Non Uniform Rational B-Spline) and there are limits

to the surface continuity at the junctions between struts and node fillets. This inevitably leads to processor and memory overload, often resulting in unmanageable graphical data handling.

NURBS are mathematical curves obtained by the junction of more polynomial curves. They are widely used in computer graphics because of their high versatility in representing shapes and the ease with which curvature continuity can be imposed to the geometry.

The second method is to generate the structures purely by mathematical expressions. This study considers an extension of the minimal surfaces discovered in 1890 by the German mathematician Hermann Schwarz [19] and in 1970 by Alan Schoen [20], in a similar way to that considered by several authors in recent years in different areas [84, 22]. This method is quite versatile because the geometries produced, defined by just one mathematical expression, are easily modifiable. A further advantage is that randomness can be introduced into the lattice, so that its distortion provides isotropic properties to the macroscopic porous matter. The only drawback is that a change in the parameters will result in an apparently unpredictable change in the shape. An accurate study of the behaviour of the function parameters used will allow the designer to understand their effects and relate them to more tangible physical quantities such as distances and angles.

5.1.1 Minimal surfaces

Minimal surfaces are those that minimize the area for a given closed contour. Mathematically they are defined as surfaces with zero mean curvature anywhere. From a structural point of view the minimization of the surface area produces smooth surfaces and therefore the solid created by filling one side of the surface shows low stress concentration under applied load. In such a

geometry the stresses would tend to flow into the structure completely filling the volume available in an homogeneous way. At the same time, and for the same reason, there are no valleys or cavities in the surface so that stress concentration would be minimized. The minimality condition makes the surface "straight", having the minimal area for any given closed curve lying on it. An immediate consequence is that ideally the yield point (or fracture, in case of brittle materials) is reached for a higher load than in samples made of exactly the same materials and having the same volume fraction of solid but with different geometry (for example a 3D grid of intersecting cylinders).

The mean curvature of a surface S at a point P on itself is expressed by $k = k_1 + k_2$ where k_1 and k_2 are the principal curvatures of S in P. This means that if k_1 is positive, k_2 is negative and vice versa, making each point of the surface a saddle point. Unfortunately, a minimal surface also partitions the space into two symmetric zones, which in turns means that only 50% volume porous material can be designed. To obviate this fact, a different and more versatile (all the partitions possible) family of curves which closely approximates the minimal surfaces has been taken into account, the level surfaces approximation of minimal surfaces. This work extends the method shown by David Hoffman in the Scientific Graphics Project [83].

5.1.2 Level surfaces

Level surfaces are expressed by the equality:

$$f(x, y, z) = 0 \tag{5.1}$$

where f is a function declared in the implicit form. Using a combination

of trigonometric functions is possible to generate a wide range of periodic shapes, in the form:

$$\sum_{i=1}^{3} \prod_{j=1}^{n} cos(x_i) + k = 0 \tag{5.2}$$

where symmetry is guaranteed by the rotational interchangeability of each spatial variable x_i.

Three different surfaces have been chosen that satisfy the constraints given above and show promising structural properties: the gyroid, the diamond and the primitive surface as shown in Figure 5.3. The promising properties are provided by the fact that these level surfaces approximate the relative minimal ones.

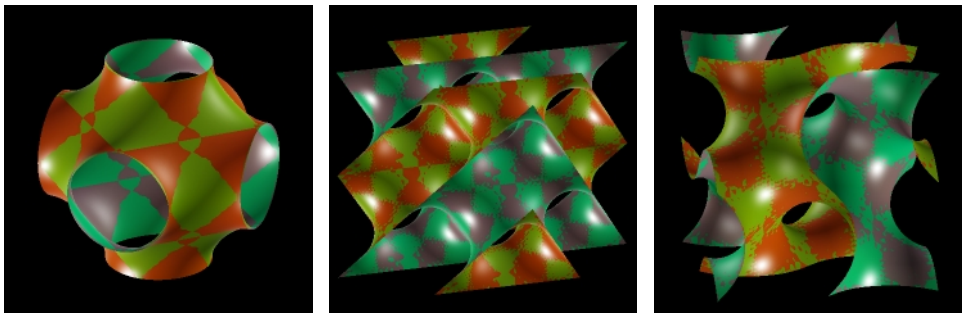

Figure 5.3: P, D and G minimal surfaces (red) and level surfaces (green) cross each other many times, and the crossings appear to lie roughly on planes [83].

5.2 Modelling methods

In this study, two different parametric methods have been used, lattice generation by a 3D modelling application and surface definition by implicit functions.

The first method consists of the design of the cell lattice with the aid of the parametric modeller Unigraphics NX (UGS, Plano, Texas), as shown

in figure 5.4. The parameters chosen were interconnectivity order, which is the number of struts (or channels) departing from one node (4 in the case shown in Figure 5.1), length of the strut l, neck diameter of the strut d and curvature radius between struts r as in Figure 5.4. This shows a smooth surface covering the diamond lattice (carbon atoms can be imagined at the nodes). Figure 5.5 could result very useful for the intuitive understanding of these parameters, especially the interconnectivity order and the idea of node, which is the region where three or more struts meet.

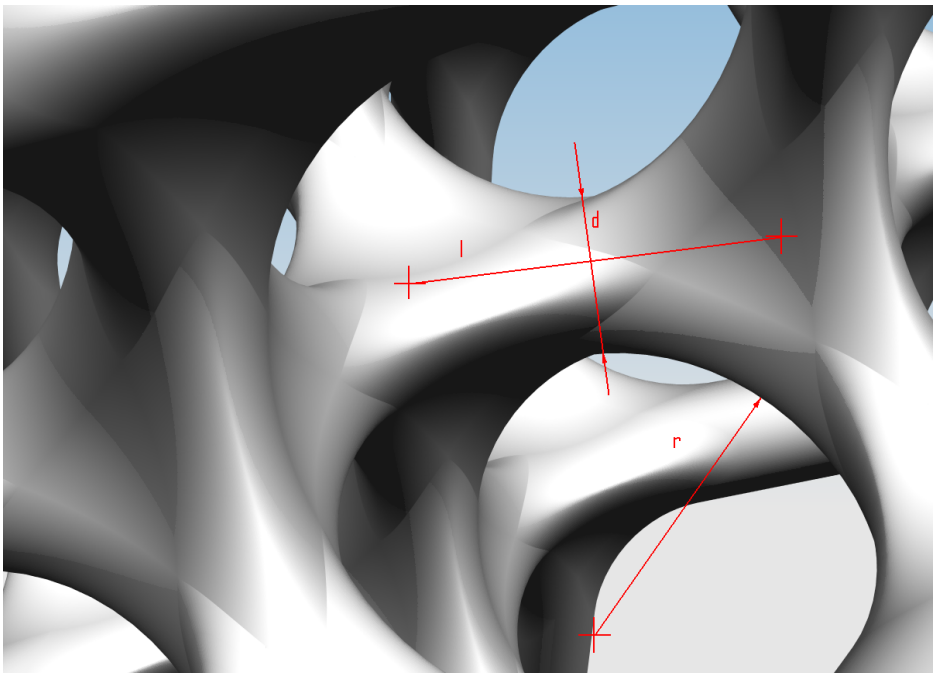

Figure 5.4: Parameter set chosen for the lattice generated by a three-dimensional modelling application. Length of strut l, neck diameter d and curvature radius r are indicated.

The second method, the implicit function method, uses a set of triply periodic level surfaces that has extended starting from the functions proposed in the Scientific Graphics Project (Figure 5.5) [83].

The boundary surface between the solid and the void region of the structure has been designed via a mathematical model on the basis of the func-

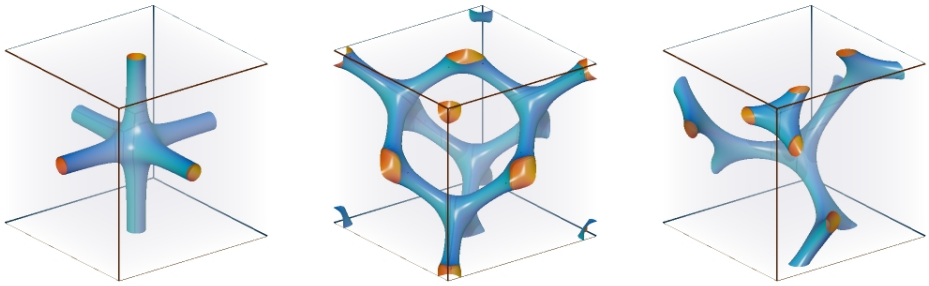

Figure 5.5: Modifications of the P (primitive), D (diamond) and G (gyroid) triply periodic minimal surfaces to their skeletal nets as shown on the Scientific Graphics Project website [83].

tions and constraints defined in the material. A three-dimensional implicit function is defined as $f(x, y, z) = 0$ whose graphic representation is a surface in the space. For example the equation:

$$x^2 + y^2 + z^2 - 1 = 0 \tag{5.3}$$

represents a sphere with radius 1. An advantage of using mathematical expressions to define the surface is that a desired number of parameters can be assigned to the model so that a subsequent shape optimization study can be carried on with relative ease. A code written in C using the GNU Triangulated Surface Library has produced a wide range of shapes with different porosity.

Equation 5.4 has been used to generate the porous structures illustrated in Figure 5.6. Is it easy to show that the parameter k_i is proportional (not linearly) to the solid volume fraction.

The calculation time for this kind and size of surface is between 0.4 and 2 s, mainly depending on the size and the desired resolution of the output samples. The machine used for these operations is run by a Pentium 4 processor, 2.4 GHz with 1 GB RAM.

$$\cos x + \cos y + \cos z + k_i((\cos x \cos y + \cos y \cos z + \cos z \cos x) + 2.8) < 0$$

$$i = 1, 2, 3 \qquad k_1 = -0.51,\ k_2 = 0\ ,\ k_3 = 0.51 \quad (5.4)$$

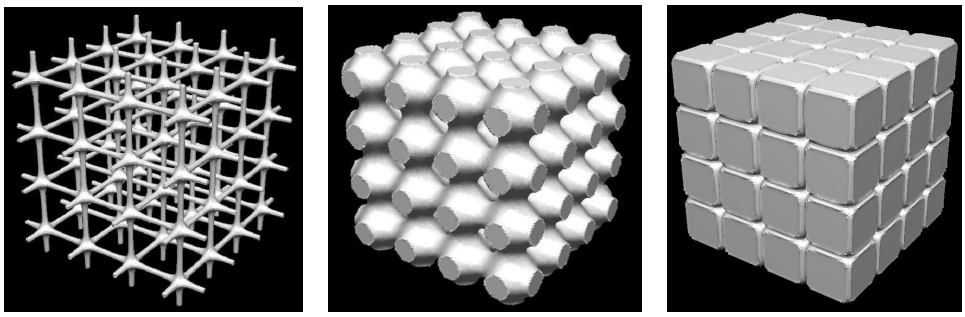

Figure 5.6: Modified level P surface showing how porous materials with low (left, 10%), medium (centre, 50%) and high (right, 90%) volume fraction can be represented using the same mathematical parametric expression.

By tuning the parameters of the model it is possible to generate functionally graded materials with a porous inner core and a dense outer layer, imitating for example the transition in bone structure from cortical (compact) to cancellous (porous). Equation 5.5 produces the geometry shown in Figure 5.7.

This is a modified G level surface with variable porosity along one preferential direction. The linear term kx has been added to the trigonometric terms providing the gyroid in order to vary the porosity. The parameter k gives the porosity gradient.

The isolevel section (level surface) of the 3D modelling software application K3DSurf [24] has been used for the generation of the structures shown in Figure 5.8.

The use of the viewer provided the opportunity to produce complex structures in a finite volume via implicit functions and inequalities. Equation 5.7 generates the bone wedge shown in Figure 5.9.

$$\cos x \sin y + \cos y \sin z + \cos z \sin x + kx < 0 \qquad k \in \mathbb{R} \tag{5.5}$$

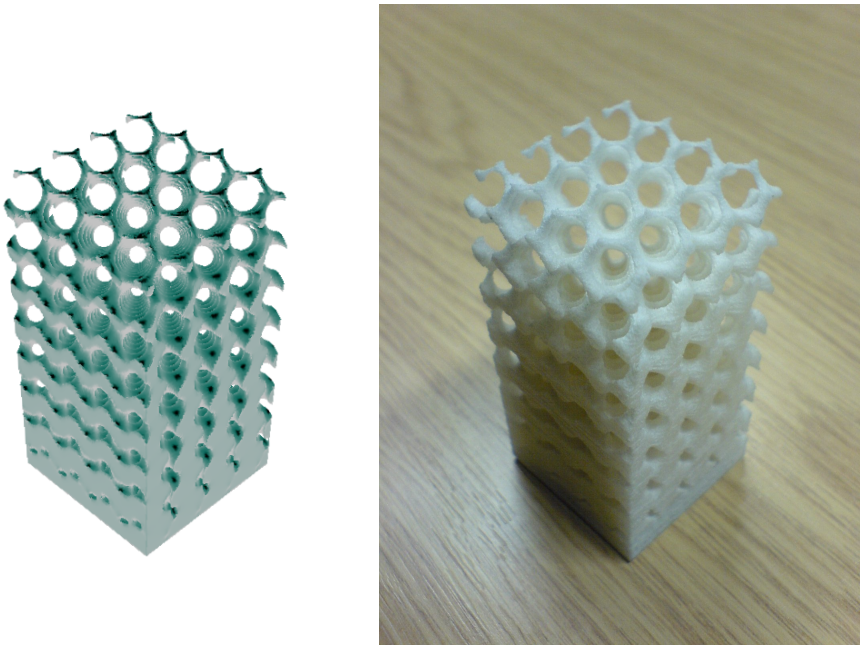

Figure 5.7: The graphical output of the 3D modeller K3DSurf (left) and its physical realization on a 3DSystems Selective Laser Sintering machine (right). This is a modified G level surface that defines the boundary of a porous sample with a porosity gradient. Solid volume fraction (the complementary size of porosity) varies from zero (top) to one (bottom).

The boundaries are produced by the first three inequalities, namely a cylinder and two inclined planes. The main inequality is a modified level G surface whose principal directions have been made coincide with cylindrical coordinates (radial and tangential). Also, the porosity has been imposed to grow logarithmically with th radius to simulate trabecular bone distribution in long bones.

The radius of the outer cylinder is R and the two cutting planes are $x + z = 0$ and $x - z = 0$.

This new approach to 3D modelling is particularly useful when dealing

$$\cos x \sin y + \cos y \sin z + \cos z \sin x +$$
$$0.08(\cos(2x)\cos(2y) + \cos(2y)\cos(2z) + \cos(2z)\cos(2x)) + 1.4 < 0 \quad (5.6)$$

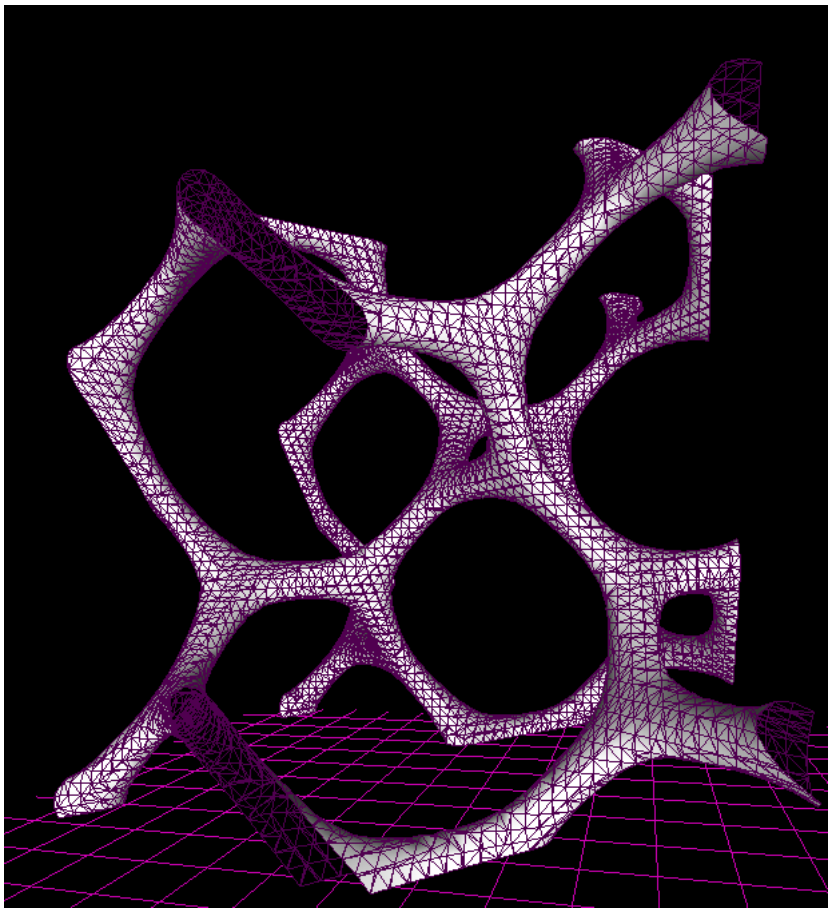

Figure 5.8: A modified G surface generated via a 3D viewer.

with microstructure of materials, because of its capability of representing small features like struts and pores with little memory allocation. Additionally, the highest degree of continuity is implicitly guaranteed at any point on the surface because these functions are of class C^∞, which means that they are differentiable an infinite number of times.

In the next chapter, a different geometrical class of porous materials has

$$
\begin{aligned}
&(x^2+y^2<R^2)\&(x+z>0)\&(x-z>0)\\
&\cos(a\log r)\sin(a\theta)+\cos(a\theta)\sin z+\cos z\sin(a\log r)+\\
&+k_1(cos(2r)cos(2a\theta)+cos(2a\theta)cos(2z)+cos(2z)cos(2r)+\\
&+2(k_2-(x^2+y^2)/R^2)<0\\
&r=\sqrt{x^2+y^2},\ \theta=\arctan(y/x),\ a\in\mathbb{N},\ k_i\in\mathbb{R} \qquad (5.7)
\end{aligned}
$$

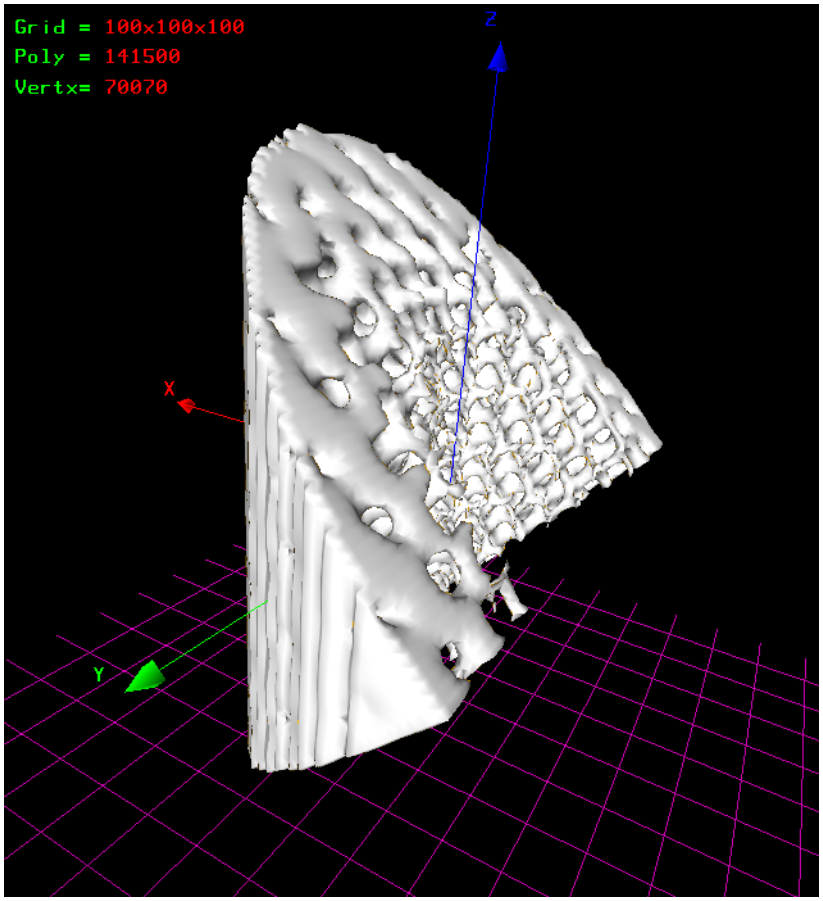

Figure 5.9: A bone wedge generated via mathematical functions. The first three terms generate a cylindrical wedge, the first inequality being a cylinder, the second and the third ones a plane. A radial, logarithmically growing, gyroidal porosity is shaped by the main inequality.

been assessed. The vast majority of porous material nowadays produced by the manufacturing industry is created through techniques that either directly introduce a foaming agent or a surfactant into a solidifying liquid, either copy the geometry of the structures produced with this method to create samples made out of other materials (replica technique), typically by spraying or dipping.

These materials are referred to as foams. Due to their wide use in engineering applications, the prediction of their properties based on their geometry would be quite handy. Additionally, an idealized model for foams could be directly comparable to the models described in the present chapter.

Summary

- Minimal surfaces and their approximation by Periodic Nodal Surfaces have been identified as potential candidates for porous matter modelling
- A general formula for the generation of a family of modified surfaces has been proposed (Equation 5.2)
- An example of the design of porous materials to hard tissue replacement in orthopaedics has been shown

Chapter 6

Numerical Simulations

The geometries generated with the two methods described in the previous chapters have been converted into solid parts having the same volume fraction, which has been fixed in 0.1, and tested with a Finite Element Analysis software. The solid volume fraction of foamed materials typically range from 0.03 to 0.12 (ERG Duocel foams). Since the aim considered at this stage consisted in evaluating the influence of network topology on the stress concentration under static load, a constant value has been chosen. The study aims to test PNS models and establish whether they present lower stress concentration than foam-like geometries when a static axial load is applied, assuming the material as linear elastic.

6.1 PNS models

The unit nodes of the PNS models (see Chapter 5) shown in Figure 6.1 have been isolated and two struts departing from the same node have been applied a load on the direction of the line joining the node centres.

The geometries shown in Figure 6.1 have been generated with a version of the application K3DSurf [24] that has been personally provided by its

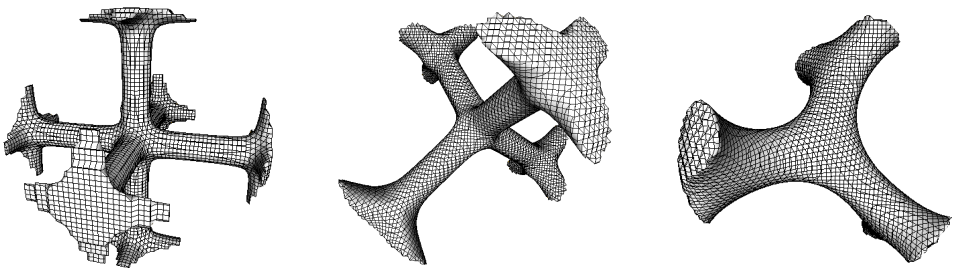

Figure 6.1: The nodes of the three structures, obtained as the intersection of a solid sphere of radius equal to the distance between two neighbour nodes, with a solid bounded by the isolevel surfaces P, D and G.

developer, Taha Abderrahman. Implicit functions and boundaries are given by Equations 6.1 and 6.2 for the P surface, Equations 6.3 and 6.4 for D and Equations 6.5 and 6.6 for G.

$$\begin{aligned} \cos x + \cos y + \cos z + & \\ +0.553(\cos x \cos y + \cos y \cos z + \cos z \cos x) &< 1.34 \qquad (6.1) \\ (x-\pi)^2 + (y-\pi)^2 + (z-\pi)^2 &< (2\pi)^2 \qquad (6.2) \\ \sin x \sin y \sin z + \sin x \cos y \cos z + & \\ + \cos x \sin y \cos z + \cos x \cos y \sin z + & \\ +0.1(\cos(4x) + \cos(4y) + \cos(4z)) &< 1.07 \qquad (6.3) \\ (x-\frac{\pi}{4})^2 + (y-\frac{\pi}{4})^2 + (z-\frac{\pi}{4})^2 &< \pi^2 \qquad (6.4) \\ \cos x \sin y + \cos y \sin z + \cos z \sin x + & \\ -0.02(\cos(2x)\cos(2y) + & \\ + \cos(2y)\cos(2z) + & \\ + \cos(2z)\cos(2x)) &< 1.17 \qquad (6.5) \\ (x-\frac{\pi}{4})^2 + (y-\frac{\pi}{4})^2 + (z-\frac{\pi}{4})^2 &< \pi^2 \qquad (6.6) \end{aligned}$$

The graphical application is able to export the surface mesh into the

Wavefront Object format (obj), which consists of a list of vertices and facets. An example is probably the best way to understand how the information is structured in such a file format. A cube, with its 8 vertices and 6 quadrilateral faces, would look like this:

```
v 0.0 0.0 0.0
v 0.0 0.0 1.0
v 0.0 1.0 0.0
v 0.0 1.0 1.0
v 1.0 0.0 0.0
v 1.0 0.0 1.0
v 1.0 1.0 0.0
v 1.0 1.0 1.0
f 1 3 7 5
f 1 5 6 2
f 1 2 4 3
f 3 4 8 7
f 2 6 8 4
f 5 7 8 6
```

where the letter v indicates the presence of a vertex, followed by three real numbers that represent the three-dimensional coordinates and f of a facet, in this case followed by a finite set of integers, each referring to the n-th vertex in the list of vertices. Note that vertex order gives facet orientation.

The exported surface were triangulated meshes. The resolution of the grid was 30x30x30 voxels, where each voxel contained one vertex of the mesh. This produced obj files of respectively 73, 116 and 71 KB in size. The exported obj files have been converted into the 3DStudio format (3ds) using the multi-translator tool ivcon [86] and finally into the IGES format, which

is readable by all the most common industrial FEA platforms. This last step needed the application exoTKAD [87], which uses the OpenCASCADE libraries [88].

The translation operation is a step that might be affected by data loss. Different computer graphics file formats that handle three-dimensional data structure the information in different ways. For this reason standards have been developed that can cope with many formats this way allowing the exchange of 3D data between different applications. One of these is the IGES standard [89], that has been used in this work. The standard is organized in geometrical entities, each of which defines the topology of the elements considered, and their features, listed as attributes of the entities.

6.2 Foam models

The models that showed the lowest value of the cost, described in Section 3.1 and 4 have been converted into a format suitable to be fed into a FEA application. These models are related to the structures A15, ZA15 (a structure belonging to the TCP range) and P42a. The input files for the mechanical tests have been generated with a Surface Evolver script provided by Brakke able to cut cubic finite samples out of a given periodic, infinte foam. Figure 6.2 shows one of these, ZA15.

As previously stated, the A15 foam model, also known as the Weaire-Phelan structure, is the current conjectured solution to the Kelvin problem and - as such - the best approximation of the geometry of real foams by a crystalline structures. The model consists belongs to the TCP structures.

The ZA15 foam model also belongs to the TCP structures. Its unit cell is made of 15 polyhedral cells. It can be thought of as the union of an A15 foam (8 cells) and a Z foam (7 cells).

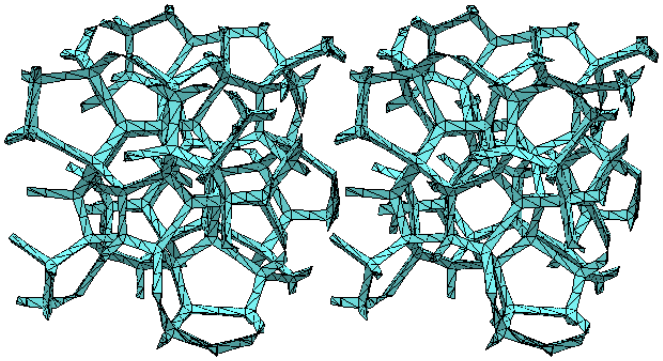

Figure 6.2: A crossed-eye stereo image of a cubic sample of the foam generated by the partition ZA15.

The new P42a foam model has been discovered within this work using a novel method able to find tetrahedrally close packed structures. The method is based on the partial differential equation named after Swift and Hohenberg [1]. The periodic unit of P42a consists of 14 polyhedral cells, all having either 13 or 14 faces each. Its cost is just below 5.304. As a reminder, the cost of the partition related to the b.c.c. lattice, mentioned in a famous manuscript by Lord Kelvin [4], is about 5.306, then conjectured to be minimal.

The models for the new partition P42a can be downloaded from the web in Surface Evolver, D-symbols and OFF formats [90]. Conversion to different file formats is available upon request.

6.3 Stress analysis

The geometry of the samples has been imported into FEA software for a bending test. For each geometry, two neighbouring struts have been extracted from the periodic net. A compressive load in the direction of the line joining the centres of the free ends has been applied, as shown in Figure 6.3.

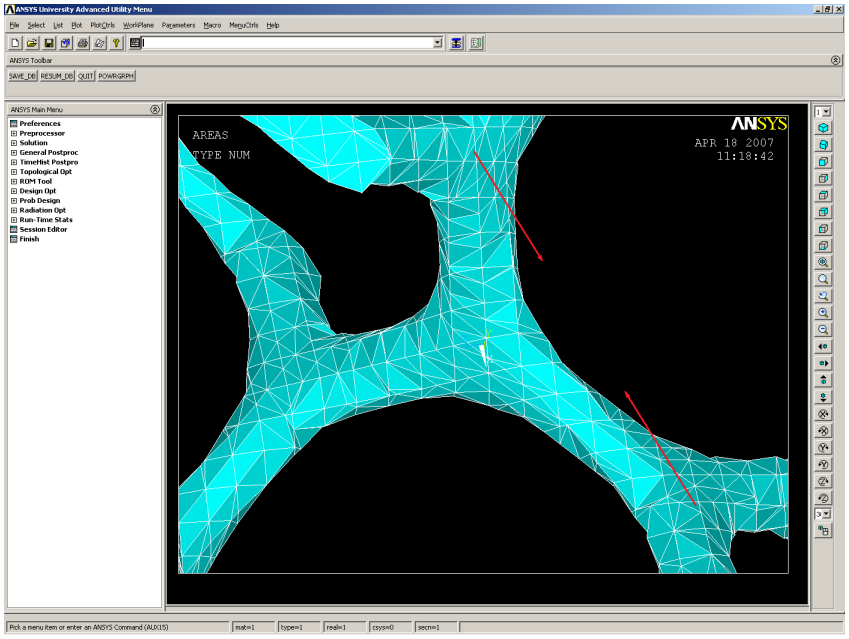

Figure 6.3: A tetrahedral mesh of the G structure. The sample shown does not contain any closed rings.

Tetrahedral volume meshes have been generated using the element provided by the software Ansys called SOLID72. The study has been limited to the flexural behaviour of two contiguous struts, isolated from the rest of the net, for each of the geometries proposed, with the purpose of demonstrating the existence of a link between the number of struts meeting at a node and the spatial rate of stress at their junctions. Note that the samples considered are finite and do not contain closed rings.

The cross-sectional area along the struts in the PNS structures has been varied by adjusting the parameters of Equations 6.1 and by keeping the volume fraction constant. The initial values of these parameters have been chosen so that the resulting computer generated image of the structure was reasonably solid. Then, a numerical has been run and the results stored in a file. Parameters have been varied and new analyses taken until a local

minimum was found.

Numerical values for the material properties and applied load were chosen in an arbitrary way, since the interest was directed on the relative, not absolute, behaviour. Elastic modulus and Poisson's ratio were chosen equal to $100GPa$ and 0.3. The force applied was $1kN$.

The rate of stress r at the common node has finally been recorded. This has been measured as the derivative of the Von-Mises stress respect to length on the surface of the inner part of the node. The results are shown in Table 6.1.

	P	D	G	A15	ZA15	P42a
r (Pa/m)	42.8	38.1	30.9	39.3	41.3	41.1

Table 6.1: Rate of stress at the central node (on the surface, inner side).

As expected, the foam-like models have a similar values to the D structure, since both have four struts per node and an average angle between the struts of $\arccos(-1/3)$.

The lowest rate of stress is achieved by the gyroidal sample. This makes this kind of structure particularly suitable for porous components used in load bearing applications and where mass dictates the rules for the choice of the material.

Summary

- A parametric study on the PNS has been carried out. Manual iterations led to a local minimum for a specific target.
- The rate of stress under load at the junction of neighbouring struts in two families of models of highly porous structures has been measured.
- A comparison betwwen the rate of stress at the junction of isolated nodes of the PNS and the foam-like structures with identical solid volume fraction indicated the surface G as the ideal model.

Chapter 7

Results

This work led to four main results, three theoretical discoveries and one practical invention.

The first result is about the mathematical optimization problem of dividing the space in regions of equal volume with the least interfacial area. Geometry is the key to the understanding of the mechanical behaviour of cellular solids. It should not come as a surprise the fact that soap bubbles have elements in common with uniformly spread patterns of points in space.

The second result is an unusual tiling by a polyhedron with 14 faces that has been obtained from a combinatorial algorithm presented for the first time in this work.

The third result is a new space-filling polyhedron with 13 faces. It has been found using the Swift-Hohenberg equation. Six were the documented space-filling polyhedra with 13 faces before this study [91].

The fourth result offers a new design approach for the surface of orthopaedic joints and implants. A patent, describing one of the possible applications, has been filed in the UK (patent application no. 0809721.4, AI 13634 GB). The interface body-implant is one the most common causes

of misalignment and poor fixation. This invention increases the porosity of the interface of the implant allowing bone in-growth and biointegration.

7.1 Discovery: Soap bubbles and cell aggregates

The Kelvin problem has not been solved but a new family of counter-examples has been found with one of the methods proposed in this thesis. The counter-example with the lowest cost among the structures in this family is shown in Figure 7.1.

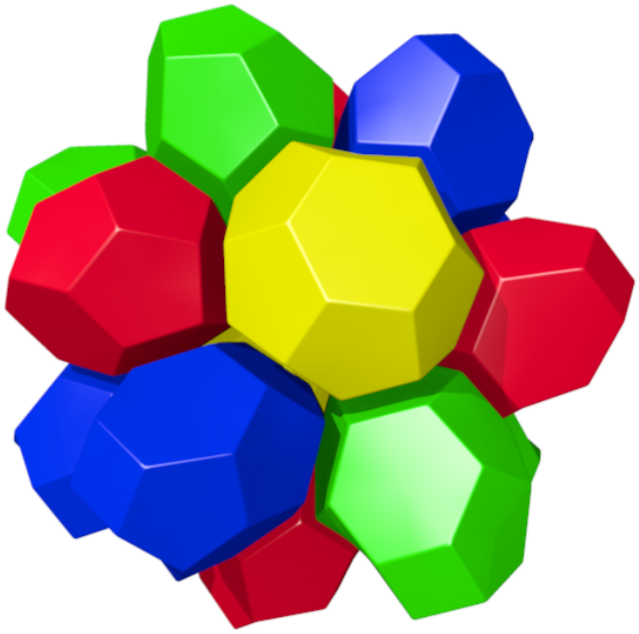

Figure 7.1: The new tiling P42a. The net carried by this tiling is a good approximation of a foam, since its cost is low and it contains a ratio of polyhedra close to that found in real foams. The image has been generated with 3dt [49].

After the discovery of new anisotropic patterns associated to configurations of minimality, the interest has moved to the understanding of the links between the Swift-Hohenberg equation and the solution to the Kelvin

problem. The PDE energy has been computed for many patterns but no numerical correlation has been found between this and the cost of the partition derived by the Voronoi diagram of such patterns. An analytical study is planned in the near future. At the moment the only outstanding fact is that both are converging towards a tiling by regular simplicia (triangles in the plane, tetrahedra in the space), the first by evolving to a pattern with the relative minima located at the vertices of *almost* regular simplicia (the regular tetrahedron does not tile the space), the second by requiring the bubbles to be tetrahedrally packed (its dual structure is a tiling by simplicia).

The concentration of quadrilaterals, pentagons and hexagons in the new partition P42a closely matches (Table 4.2) that of real foams found by Matzke [7].

Figure 7.2 shows a crossed-eye stereo image produced with the Surface Evolver of the minimal surface of P42a's periodic unit.

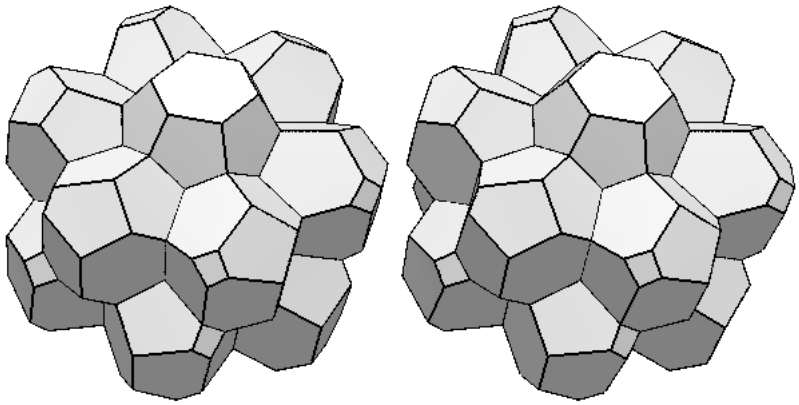

Figure 7.2: A crossed-eye stereo image of the partition P42a as it appears in the Surface Evolver at the end of the optimization iterations and periods relaxation, showing its slightly curved faces.

Figure 7.3 shows a model built using a plastic flexible pipe and tetrahedral plastic joints by Cochranes of Oxford$^{\mathrm{TM}}$.

Figure 7.3: A plastic model of half of the unit cell of P42a. Photo courtesy of Tim Holsgrove.

7.2 Discovery: A new simple tiling with unusual properites

A new tiling has been discovered using a novel combinatorial algorithm developed for the first time in this thesis. The polyhedron belonging to the tiling comes in four different geometries, called enantiomers. It has 14 faces: 1 quadrilateral, 10 pentagons and 3 hexagons. It tiles the space within the triclinic system, the only entry of this type on the Reticular Chemistry Structure Resource. Space group is $P\bar{1}$. A picture of its periodic unit shows the spatial arrangement of the single tiles composing its periodic unit in Figure 7.4. The image has been generated with 3dt [49].

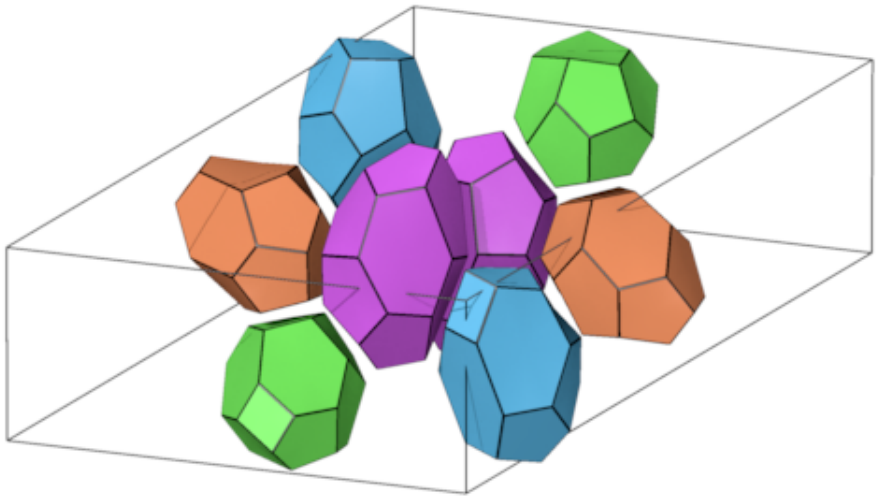

Figure 7.4: The periodic unit of the tiling **rug**, made of chiral copies of the same polyhedron [1-10-3]. The four pairs of enantiomers have different colours. The image has been generated with 3dt [49].

7.3 Discovery: A new space-filling polyhedron

A new space-filling polyhedron has been discovered using the Swift-Hohenberg partial differential equation for pattern formation. It is a non-simple polyhedron with 13 faces having 6 quadrilaterals, 6 pentagons and 1 hexagon. It tiles the space with the symmetry group $Pa\overline{3}$. It is the first space-filling 13-hedron that tiles space with cubic symmetry. The previously known examples belongs to the tetragonal system [91]. Its periodic unit is shown in Figure 7.5. The image has been generated with 3dt [49].

7.4 Invention: Improvement in joints and implants

Mathematical surfaces derived from the trigonometric implicit functions, approximating the PNS, have been used to produce the three-dimensional file of an acetabular cup, one of the components of a hip replacement system.

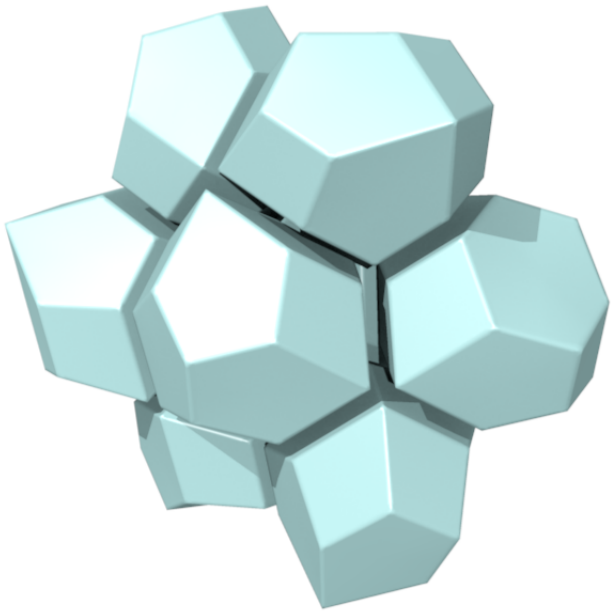

Figure 7.5: The periodic unit of the tiling by [6-6-1] polyhedra, derived by the Voronoi diagram of the pattern P8 obtained with the three-dimensional Swift-Hohenberg equation used in pattern formation. The image has been generated with 3dt [49].

A common problem with implants is their fixation to the structure of bone. Loosening of the implant at the interface is likely to invalidate or drastically reduce the functions for which the implant was made for. It is the main cause of revision surgery. Many are the techniques nowadays used to increase bone fixation and reduce the chances of an early revision. In this work the surface feature of the implant has been modelled so bone is allowed to grow into it. The upper surface of the cup has been modelled with the gyroidal motif, with gradually varying porosity, ranging from 0 (solid) to 1 (external surface) as shown in Figure 7.6. The surface can be easily modelled with different motifs. The reason the gyroidal motif was chosen is that stress concentration is minimized among the structures studied in this work (see Table 6.1).

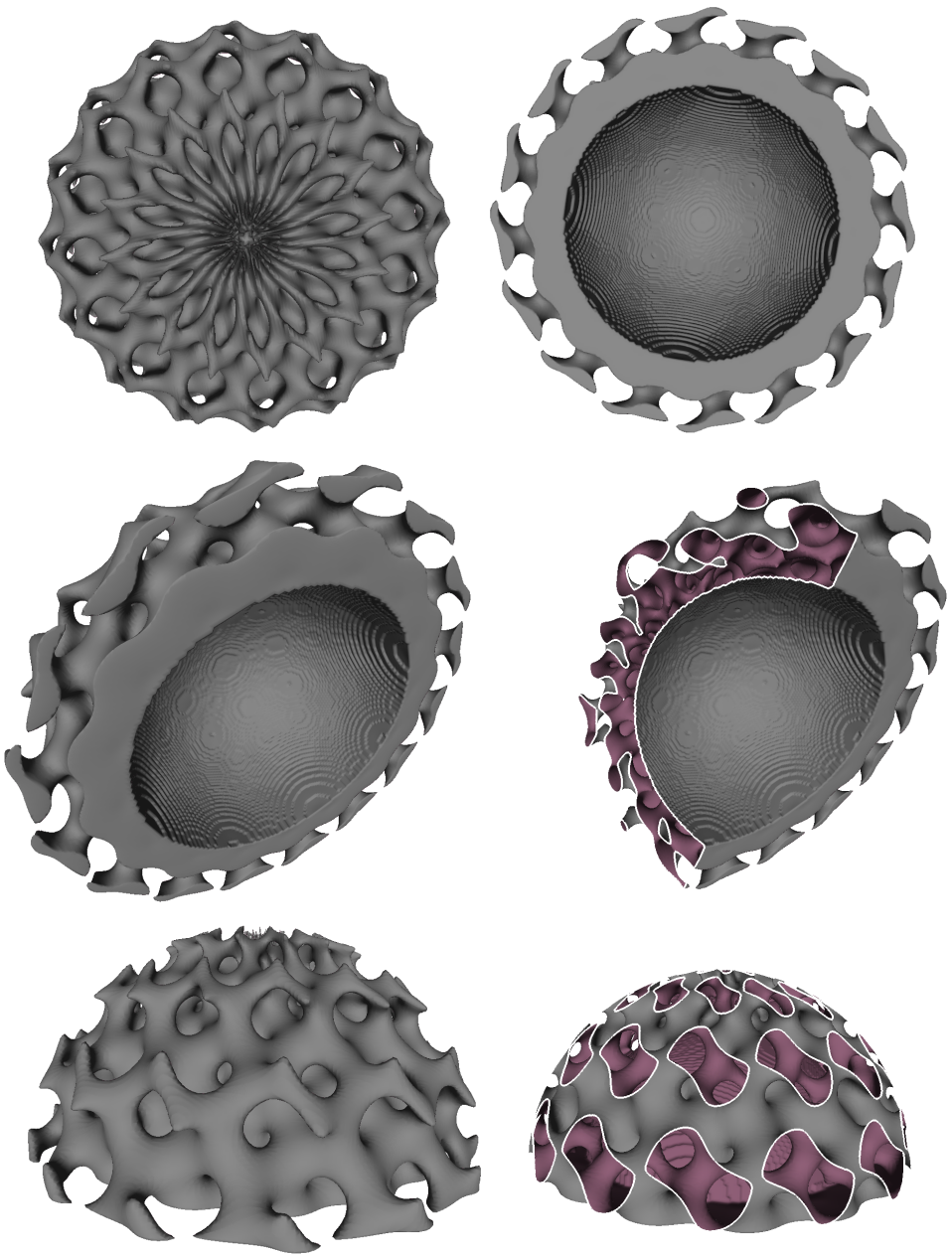

Figure 7.6: The acetabular cup, showing an exaggerated gyroidal surface feature with porosity gradient.

The parameters and the function used to describe the gyroidal surface are shown in Equation 7.1 and 7.2.

$$\begin{aligned} r &= \sqrt{x^2+y^2+z^2} \\ \theta &= \arctan\frac{y}{x} \\ \phi &= \arctan\frac{z}{\sqrt{x^2+y^2+z^2}} \end{aligned} \tag{7.1}$$

$$\begin{aligned} z &> 0 \\ x^2+y^2+z^2 &> r_i^2 \\ \cos r\sin n\theta + \cos n\theta \sin n\phi + \cos n\phi \sin r + ar - b &< 0 \end{aligned} \tag{7.2}$$

The gyroidal motif was chosen because of its smoothly distributed stress field under static load as shown in Table 6.1. The porosity gradient in the radial direction allows bone to grow into the feature of the implant for a rigid and long-lasting bone fixation.

The invention has been recently filed as a UK patent, application no. 0809721.4, AI 13624 GB [92].

Chapter 8

Future work

The double outcome of the work conducted in this thesis addresses new lines for further development of the methods employed, both for the modelling of highly porous structures and the algorithms for the solution to the Kelvin problem.

Regarding the modelling, future work should consider the coupled structural and fluid dynamic case. Fluid permeability is strictly connected with the structural problem, since the vast majority of engineering applications that utilise highly porous materials with low solid volume fraction require them to be also permeable to fluids. The only study available considers the flow through periodic minimal surfaces [82], which represent the 0.5 volume fraction case.

More is planned for the the second aim of this work, the solution to the Kelvin problem and the problems associate with it, like the covering problem [93]. Now that a proof for the existence of minimal partitions has been given [43], the search for methods able to produce structures that might show less surface area than the Weaire-Phelan structure is making even more sense.

The main aim of the future activity is to continue the search for space

partitions with lower surface area than the Weaire-Phelan structure. Three are the methods that have been proposed within this thesis. They have not been exhausted yet and they need to be continued and improved in a future work. The methods will allow the identification of possible candidates for surface-minimizing foams (the surface free energy of an interface is, in first approximation, proportional to the surface area).

The first method consists of a complete search for 3D simple tilings with increasing complexity (and decreasing symmetry) based on the Delaney symbols and the combinatorial tiling theory [48]. The search began in March 2008 and is now running on three supercomputer facilities. The work planned for this project consists of improvements (shortcuts) to the current algorithm and in managing the I/O file stream on the supercomputer facilities, since these are at the moment the major bottlenecks in the whole process.

The second method is based on the combinatorial matching rules for simple polyhedra with 13 and 14 faces having at most one quadrilateral face [2]. The algorithm has already been used to find a monotypic simple tiling [59], but it needs to be implemented on a machine. The plan is to define the data structure needed for this method, set the steps for the algorithm and write the necessary code. Substantial difficulties have been encountered in the very first stage of this procedure, the definition of the ideal data structure for the polyhedra and for the available slots in the cluster of polyhedra. The future developer of the algorithm is advised not to underestimate this problem, as it might result in increased computational complexity, which eventually will make the algorithm inefficient for any practical use.

The third method is by construction of the Voronoi diagram of point sets obtained with the 3D Swift-Hohenberg equation in a three-torus and

pseudorandom initial conditions. This approach has produced the most interesting results [1]. It starts from random initial conditions and for this reason a large number of runs is necessary in order to evaluate the output. An implementation of a script that automatizes the process of pattern production and data extraction would be of valuable help. This software, if necessary, will run on a parallel architecture machine and the results will be directly fed into the downstream softwares, the Voronoi generator [77] and the surface area minimizer [45].

The extension of the investigation to cases of higher dimensions is another target of possible future projects. All of the algorithms mentioned above can be used to approach the n-dimensional problem, in most cases by simply adding an extra coordinate to the algorithm.

8.1 Intellectual merit

A solution to the problem would be a result in geometric measure theory. Both unicity and crystalline order of the solution are open problems. The discovery of new structures will provide clues that might prove useful in the construction of the formal proof to the Kelvin's problem.

The question about order of the solution has fascinated scientists and engineers for years, since physical foams made of large aggregates of bubbles of equal volume do not show any kind of order and any effort spent in producing experimentally dry Weaire-Phelan foams has not given a positive outcome so far [33].

The generation of a geometrical reference model for foams would be particularly useful in the process of understanding their mechanical behaviour, e.g., for the understanding of cellular solids, because it would represent the topological standard for use in numerical simulation such as finite element

analysis both structural and thermo-fluid dynamical.

Also, the solution to Kelvin's problem has applications in data compression (optimal quantizers) [94, 95, 31], biology (cell aggregates) [42], crystallography [60], spatial arrangement of sensors [30], condensed matter physics [28] and the physics of amorphous solids [71].

Glossary

dry foam A foam with less than 1% liquid, 4

enantiomer A crystal or three-dimensional form that is not superposable on its mirror image, 92

enantiomer A mirror object that can not be superposed on its source, as in the left and the right hand. Same as chiral, or point inverted image, 41

FGM Functionally Graded Material: Materials that can be characterized by the variation in composition and structure gradually over volume, resulting in corresponding changes in the properties of the material, 2

k tile-transitive Containing k symmetrically distinct tiles, 41

k vertex-transitive Containing k symmetrically distinct vertices, 41

Kelvin Problem In geometric measure theory, the problem of dividing space into equal volume cells with minimum partitional area, 1

manifold In mathematics, more specifically in differential geometry and topology, a manifold is a mathematical space that on a small enough scale resembles the Euclidean space of a certain dimension, called the dimension of the manifold, 13

monodisperse Same as monosized, made of subunits or particles having the same size, 1

pattern formation The science that studies the orderly outcomes of self-organization and the common principles behind similar patterns, 1

PNS Periodic Nodal Surfaces: a family of surfaces at which a standing wave has minimal amplitude. Their mathematical expressions are implicit functions of sinusoidal terms, 1

polyhedron A geometric solid with faces, edges and vertices, 1

polytope A generalized term referring to an n-dimensional geometrical entity made of (n-1)-dimensional subunits. Examples inlcude polygons and polyhedra, 1

SFF techniques A collection of techniques for manufacturing solid objects by the sequential delivery of energy and/or material to specified points in space to produce that solid. SFF is sometimes referred to as rapid prototyping, rapid manufacturing, layered manufacturing and additive fabrication, 1

sphere covering In geometry, the problem concerning the arrangement of the minimum number of overlapping identical spheres able to cover a space, 1

sphere packing In geometry, the problem concerning the arrangement of non-overlapping identical spheres in a space, 1

Swift-Hohenberg eq. A partial differential equation derived from the equation for thermal convection, mainly used for its pattern forming behaviour, 3

TCP structures A family of simple tilings by a set of polyhedra having 12, 14, 15 and 16 faces each, containing pentagonal and hexagonal faces only, 1

tessellation See tiling, 1

tiling An n-dimensional assembly of tiles that fills the space with no gaps. Also called tessellation, 1

torus A doughnut, or anything that is homeomorphic to (has the same topology of) a torus. A two-torus is a periodic square, where points on the left side coincide with points on the right side (and top with bottom), 29

TPMS Triply Periodic Minimal Surfaces: a family of three-dimensional surfaces having zero mean curvature and showing periodicity in the three directions of space, 7

triclinic In crystallography, the triclinic crystal system is one of the 7 lattice point groups and the lowest symmetry system, 40

List of Figures

References

[1] R. Gabbrielli. A new counter-example to Kelvin's conjecture on minimal surfaces. *Phil. Mag. Lett.*, 89:483–491, 2009.

[2] R. Gabbrielli. An algorithm for equal-volume minimal surface area partitions of three-space. Available at `http://people.bath.ac.uk/rg247/corona.pdf`.

[3] H. G. von Schnering and R. Nesper. Nodal surfaces of fourier series: Fundamental invariants of structured matter. *Zeitschrift für Physik B*, 83:407–412, 1991.

[4] W. Thomson. On the division of space with minimum partitional area. *Phil. Mag.*, 24:503, 1887.

[5] D. Weaire. *The Kelvin Problem: foam structures of minimal surface area.* CRC, first edition, 1997.

[6] D. Weaire and R. Phelan. A counter-example to kelvin's conjecture on minimal surfaces. *Phil. Mag. Lett.*, 69:107–110, 1994.

[7] E. B. Matzke. The three-dimensional shape of bubbles in foam - an analysis of the role of surface forces in three-dimensional cell shape determination. *Am. J. Bot.*, 33:58–80, 1946.

[8] J. Sullivan. The geometry of bubbles and foams, 1998.

[9] K. Kose. 3D NMR imaging of foam structures. *Journal of Magnetic Resonance*, A118:195–201, 1996.

[10] A.M Kraynik, D. A. Reinelt, and F. van Swol. Structure of random monodisperse foam. *Phys. Rev. E*, 67, 2003.

[11] E. B. Matzke. The three-dimensional shape of bubbles in foams. *Proceedings of the National Academy of Sciences of the United States of America*, 31:281–289, 1945.

[12] H. Fountain. A problem of bubbles frames an olymic design. *The New York Times*, August, 5:F4, 2008.

[13] N. Mills. *Polymer foams handbook*. Butterworth-Heinemann, first edition, 2007.

[14] M. F. Ashby, N. A. Fleck, et al. *Metal foams*. Elsevier, first edition, 2000.

[15] M. Scheffler and P. Colombo. *Cellular ceramics*. Wiley-VCH, first edition, 2005.

[16] A. Kelly. Why engineer porous materials? *Phil. Trans. R. Soc. A*, 364:5–14, 2006.

[17] D. L. Bourell, H. L. Marcus, et al. Selective laser sintering of metals and ceramics. *International Journal of Powder Metallurgy*, 28:369–381, 1992.

[18] M. F. Ashby. The properties of foams and lattices. *Phil. Trans. R. Soc. A*, 364:15–30, 2006.

[19] H. A. Schwarz. *Gesammelte Mathematische Abhandlungen*. Springer-Verlag, Berlin (Reprinted by Chelsea Publishing Company, 1972, 1890.

[20] A. H. Schoen. Infinite periodic minimal-surfaces without self-intersections. *NASA Technical Note*, D-5541:1–70, 1970.

[21] R. Gabbrielli, I. G. Turner, and C. R. Bowen. Development of modelling methods for materials to be used as bone substitutes. *Key Eng. Mat.*, 361:903–906, 2008.

[22] S. Rajagopalan and R. A. Robb. Schwarz meets schwann: design and fabrication of biomorphic and durataxic tissue engineering scaffolds. *Medical Image Analysis*, 10:693–712, 2006.

[23] Oed online, mar 2008.

[24] Available at `http://k3dsurf.sourceforge.net`, apr 2007.

[25] L.J. Gibson and M.F. Ashby. *Cellular solids, structure and properites.* Cambridge University Press, second edition, 1997.

[26] G. C. Barker. All kinds of bubbles. *Science*, 289:398, 2000.

[27] P. Ziherl and Kamien R. D. Maximizing entropy by minimizing area: towards a new principle of self-organization. *J. Phys. Chem. B*, 105:10147, 2001.

[28] G. M. Grason. The packing of soft materials: Molecular asymmetry, geometric frustration and optimal lattices in block copolymer melts. *Physics Reports*, 433:1–64, 2006.

[29] D. Weaire, S. J. Cox, et al. Foams in microgravity. *J. Phys. IV France*, 11:213, 2001.

[30] S. M. Nazrul Alam and J. Haas Zygmunt. Coverage and connectivity in three-dimensional underwater sensor networks. *Wirel. Commun. Mob. Comput.*, 8:995–1009, 2008.

[31] R. P. Barnes and N. J. A. Sloane. The optimal lattice quantizer in three dimensions. *SIAM J. Algebr. Disc. Meth.*, 4:30–41, 1983.

[32] W. Y. Jang, A. M. Kraynik, et al. On the microstructure of open-cell foams and its effect on elastic properties. *Int. J. Solids Struct.*, 2008.

[33] A. ven der Net, W. Drenckhan, D. Weaire, and S. Hutzler. The crystal structure of bubbles in the wet foam limit. *The Royal Society of Chemistry, Soft Matter*, 2:129–134, 2006.

[34] J. E. Taylor. The structure of singularities in soap-bubble-like and soap-film-like minimal surfaces. *Ann. Math.*, 103:489–539, 1976.

[35] R. Kusner and J. Sullivan. Comparing the weaire-phelan equal-volume foam to kelvin's foam. *Forma*, 11:233—242, 1996.

[36] Wolfram mathworld. Available at `http://mathworld.wolfram.com`, mar 2009.

[37] Pappus d'Alexandrie. *La collection mathématique.* Albert Blanchard, 1982.

[38] T. C. Hales. The honeycomb conjecture. *Discr. Comput. Geom.*, 25:1–22, 2001.

[39] D. Weaire. Kelvin's foam structure: a commentary. *Phil. Mag. Lett.*, 88:91–102, 2008.

[40] F. J. Almgren. *Plateau's problem: an invitation to varifold geometry.* W. A. Benjamin, Inc., first edition, 1966.

[41] F. Morgan. *Geometric measure theory: a beginner's guide.* Academic Press, third edition, 2000.

[42] R. E. Williams. Space-filling polyhedron: its relation to aggregates of soap bubbles, plant cells, and metal crystallites. *Science*, 161:276–277, 1968.

[43] F. Morgan. Existence of least-perimeter partitions. *Phil. Mag. Lett.*, 88:647–650, 2008.

[44] Available at `http://rcsr.anu.edu.au/`, mar 2008.

[45] K. A. Brakke. The surface evolver. *Exp. Math.*, 1:141, 1992.

[46] F. C. Frank and J. S. Kasper. Complex alloy structures regarded as sphere packings. I. Definitions and basic principles. *Acta Cryst.*, 11:184–190, 1958.

[47] F. C. Frank and J. S. Kasper. Complex alloy structures regarded as sphere packings. II. Analysis and classification of representative structures. *Acta Cryst.*, 12:483–499, 1959.

[48] O. Delgado-Friedrichs. Data structures and algorithms for tilings i. *Theoretical Computer Science*, 303:431–445, 2003.

[49] O. Delgado-Friedrichs. The gavrog project. Available at `http://gavrog.sourceforge.net`, 2008.

[50] Available at `http://crossgroup.caltech.edu/Patterns/Demo4\_2.html`, October 2008.

[51] H. Heesch. *Reguläres Parkettierungsproblem*. Westdeutscher Verlag, 1968.

[52] B. N. Delone, N. P. Dolbilin, et al. Combinatorial and metric theory of planigons. *Proc. of Steklov Inst. of Math.*, 4:111–141, 1980.

[53] B. Grünbaum and Shepard G. C. A hierarchy of classification methods for patterns. *Zeitschrift f. Kristallographie*, 154:163–187, 1981.

[54] O. Delgado-Friedrichs and M. O'Keeffe. Identification of and symmetry computation for crystal nets. *Acta Cryst.*, A59:351–360, 2003.

[55] O. Delgado-Friedrichs, R. Gabbrielli, M. O'Keeffe, and D. M. Proserpio. An algorithm for the solution to the Kelvin problem. Results available at: `http://people.bath.ac.uk/rg247/javaview/start.html`, 2008.

[56] O. Delgado-Friedrichs and M. O'Keeffe. Isohedral simple tilings: binodal and by tiles with ≤ 16 faces. *Acta Cryst. A*, 61:358–362, 2005.

[57] R. Kusner. The number of faces in a minimal foam. *Proceedings: Mathematical and Physical Sciences*, 439:683–686, 1992.

[58] G. Brinkmann and McKay B. D. Fast generation of planar graphs. *MATCH Commun. Math. Comput. Chem.*, 58:323–357, 2007.

[59] R. Gabbrielli. A new simple tiling, with unusual properties, by a polyhedron with 14 faces. *Acta Cryst.*, A64:430–431, 2008.

[60] M. O'Keeffe. *Foams and emulsions*, chapter 24, pages 403–422. Springer, 1999.

[61] O. Delgado-Friedrichs, Dress A. W. M., et al. Systematic enumeration of crystalline networks. *Nature*, 400:644, 1999.

[62] V. Yu. Komarov, Solodovnikov, et al. Phase formation and structure of high-pressure gas hydrates and modeling of tetrahedral frameworks with uniform polyhedral cavities. *Crystallogr. Rev.*, 13:257–297, 2007.

[63] E. Schulte. The existence of non-tiles and non-facets in three-dimensions. *J. Combinatorial Thoery A*, 38:75–81, 1985.

[64] B. Grünbaum, P. Mani-Levitska, et al. Tiling three-dimensional space with polyhedral tiles of a given isomorphism type. *J. London Math. Soc.*, 29:181–191, 1984.

[65] F. Luo and R. Stong. Combinatorics of triangulations of three-manifolds. *Trans. Am. Math. Soc.*, 337:891–906, 1993.

[66] W. Fischer and E. Koch. Homogeneous sphere packings with triclinic symmetry. *Acta Cryst. A*, 58:509–513, 2002.

[67] The epinet project. Available at `http://epinet.anu.edu.au/`, 2008.

[68] J. Swift and P. C. Hohenberg. Hydrodynamic fluctuations at the convective instability. *Phys. Rev. A*, 15:319–328, 1977.

[69] M. C. Cross and P. C. Hohenberg. Pattern-formation outside of equilibrium. *Reviews of modern physics*, 65:851–1112, 1993.

[70] J. M. Sullivan. *Foams and emulsions*, chapter 23, pages 379–402. Springer, 1999.

[71] R. Zallen. *The Physics of Amorphous Solids*, chapter 2, pages 51–59. Wiley-VCH, 1998.

[72] J. H. Conway and S. Torquato. Packing, tiling and covering with tetrahedra. *Proc. Natl. Acad. Sci. U S A*, 103:10612–10617, 2006.

[73] D. P. Shoemaker and C. B. Shoemaker. Comment on "filling three-dimensional space with tetrahedra: A geometric and crystallographic problem". *Phys. Rev. B*, 38:6319–6321, 1988.

[74] V. Schlegel. Theorie der homogen zusammengesetzten raumgebilde. *Nova Acta Acad. Leop. Carol.*, 44:343–459, 1883.

[75] D. J. B. Lloyd, B. Sandstede, D. Avitabile, and A. R. Champneys. Localised patterns in the 2d swift-hohenberg equation. *SIAM Journal on Applied Dynamical Systems*, 7(3):1049–1100, 2008.

[76] D. P. Shoemaker and C. B. Shoemaker. Concerning the relative numbers of atomic coordination types in tetrahedrally close packed metal structures. *Acta Cryst.*, B42, 1986.

[77] J. M. Sullivan. Vcs. Available at `http://torus.math.uiuc.edu/jms/software`, 1988.

[78] H. S. M. Coxeter. Close-packing and froth. *Ill. J. Math.*, 2:746–758, 1958.

[79] M. E. Glicksman and P. R. Rios. Minimal network partitions using average n-hedra. *Phil. Mag.*, 87:189–208, 2007.

[80] L. F. Tóth. What the bees know and what they do not know. *Bull. Amer. Math. Soc.*, 70:468–481, 1964.

[81] T. Harmuth. Cgf. Available at `http://www.math.uni-bielefeld.de/~CaGe`, 2004.

[82] Y. Jung and S. Torquato. Fluid permeabilities of triply periodic minimal surfaces. *Phys. Rev. E*, 72:056319, 2005.

[83] D. Hoffman. Scientific graphics project. Available at `http://www.msri.org/about/sgp/jim`, 2007.

[84] Y. Wang. Periodic surface modeling for computer aided nano designs. *Journal of Materials Chemistry*, 39:179–189, 2007.

[85] Available at `http://gts.sourceforge.net`, mar 2008.

[86] Available at `http://sourceforge.net/projects/ivcon-tl`, jan 2009.

[87] Available at `http://www.exotk.org/download.html`, jan 2009.

[88] Available at `http://www.opencascade.org`, jan 2009.

[89] Available at `http://ts.nist.gov/standards/iges`, jan 2009.

[90] Available at `http://people.bath.ac.uk/rg247`, jan 2009.

[91] M. Goldberg. Convex polyhedral space-fillers of more than twelve faces. *Geometriae Dedicata*, 8:491–500, 1979.

[92] C. R. Bowen, R. Gabbrielli, and I. G. Turner. Improvements in or related to joints and/or implants.

[93] J.H. Conway and N.J.A. Sloane. *Sphere Packings, Lattices and Groups*. Springer-Verlag, 1988.

[94] A. Gersho. Asymptotically optimal block quantization. *IEEE Trans. Inf. Th.*, 25:373, 1979.

[95] N. Kashyap and D. L. Neuhoff. On quantization with the Weaire-Phelan partition. *IEEE Trans. Inf. Th.*, 47:2538, 2001.

Appendices

Appendix A

Research Publications

The author has published one conference paper and two articles in referred journals. Below is given a background and a brief description of the findings for each publication, in chronological order.

A.1 Development of modelling methods for materials used as bone substitutes

The idea of investigating the geometrical structure of idealized, highly porous materials has been given to the author by a natural material found in vertebrates, osseous tissue. This mineralized connective tissue is thought to optimize strength and stiffness to mass ratios in order to facilitate animal locomotion. The guidance of the author's supervisors combined with his interest in the emerging technologies for the rapid manufacture of geometrically complex parts yielded his first publication, the content of which was presented at the Bioceramics20 conference in Nantes in September 2007 and a month later at the European Society for Biomaterials conference in Brighton.

The paper describes a family of triply periodic surfaces generated by implicit functions of finite sequences of trigonometric terms. The application to porous materials, functionally graded materials and bone substitutes is substantiated with SFF polymeric samples.

A.2 A new simple tiling, with unusual properties, by a polyhedron with 14 faces

On a parallel path, the author has always considered the geometry of a class of materials that have been and are often used as the starting point in the manufacture of bone substitutes. This is the class of foamed materials. A problem related to the geometry of the ground state of foams widened the author's interests to more theoretical issues in chemistry and crystallography, physics and condensed matter, combinatorics, symmetry and complexity and the nature of order/disorder in materials. A new combinatorial approach for the tiling of polytopes generated a new structure that aroused the interest of people working in the area of crystallography and led to a second publication.

The article, published as a short communication, describes a polyhedron with 14 faces that fills the space with no gaps. Many are the tiles of this type that have been already discovered, but the unique feature of this tiling is given by its tiles. Although sharing the same Schlegel diagram (i.e. having the same face adjacency map), tiles can not be be superpose each other (i.e. they are chiral, like the left and the right hand).

A.3 A new counter-example to Kelvin's conjecture on minimal surfaces

The third publication, the idea of which was suggested to the author by an interactive applet showing the numerical solution of a partial differential equation, represents the most appreciated result of the author's work worldwide. This is a new - and the first known - method able to actively search for solutions to the celebrated Kelvin problem, which asks for the partition of space in equal volume cells with minimal area. The problem relates to the geometry of cell aggregates, foams and soap bubbles but the connections with wave theory, metal crystallites, photonics and data compression, as well as the more theoretical ones like sphere coverings, n-dimensional quantization and tilings, can not be ignored. A series of invited lectures in the US, Australia, Italy, UK and the Netherlands followed the discovery and is still growing at the time of the writing of this thesis.

The article describes an application of pattern formation to optimal geometry. A well-known partial differential equation has been numerically computed in three-dimensional space with periodic boundary conditions. Starting from random initial conditions, the equation converges to a stationary state. The coordinates of the local maxima have then been extracted and used for the generation of periodic Voronoi partitions. The surface area of the partitions has then been numerically minimized and compared with that of the previously known structures, showing the existence of a new counter-example to Kelvin's conjecture.

Citation data are for the articles are listed below:

- *Development of modelling methods for materials used as bone substitutes*, with Irene Turner and Chris Bowen, Key Eng. Mat. 361-363, 2008, pp 903-906.

- *A new simple tiling, with unusual properties, by a polyhedron with 14 faces*, with Mike O'Keeffe, Acta Cryst., A64, 2008, pp 430-431.

- *A new counter-example to Kelvin's conjecture on minimal surfaces*, Phil. Mag. Lett., 89, 2009, Issue 8.

Key Engineering Materials Vols. 361-363 (2008) pp. 903-906
online at http://www.scientific.net

Development of Modelling Methods for Materials to be Used as Bone Substitutes

R. Gabbrielli[1, a], I. G. Turner[1,b] and C. R. Bowen[1,c]

[1]Centre for Orthopaedic Biomechanics, Department of Mechanical Engineering, University of Bath, BA2 7AY, UK

[a]r.gabbrielli@bath.ac.uk, [b]i.g.turner@bath.ac.uk, [c]c.r.bowen@bath.ac.uk

Keywords: Scaffolds, porosity, triply periodic surfaces, lattices, bone substitutes.

Abstract. The demand in the medical industry for load bearing materials is ever increasing. The techniques currently used for the manufacture of such materials are not optimized in terms of porosity and mechanical strength. This study adopts a microstructural shape design approach to the production of open porous materials, which utilizes spatial periodicity as a simple way to generate the models. A set of triply periodic surfaces expressed via trigonometric functions in the implicit form are presented. A geometric description of the topology of the microstructure is necessary when macroscopic properties such as mechanical strength, stiffness and isotropy are required to be optimised for a given value of volume fraction. A distinction between the families of structures produced is made on the basis of topology. The models generated have been used successfully to manufacture both a range of structures with different volume fractions of pores and samples of functional gradient material using rapid prototyping.

Introduction

The need for new materials which have a high porosity and low weight but also a relatively high strength and tailored stiffness, has pushed research towards a more in depth analysis of the microstructure of porous materials. The numerous applications that, today, require a good balance of mechanical properties and porosity encompass the aerospace, automotive, biomedical materials, chemical and renewable energy industries. The wide range of properties available in the form of porous materials justifies the market demand and the interest in further developing their properties. In the medical sector, porous materials are highly desired as a substitute for osseous tissue, as some of their properties resemble those of bone, being lightweight, strong and having a totally interconnected porosity [1-4]. The demand from the medical industry for a material of this kind is continuously growing, and the manufacturing processes for foaming metals, polymers and ceramics which are continuously evolving. There is also increasing interest in the production of functional gradient materials which more closely resemble the naturally occurring structures found in bone [5-7]. A limitation of the materials currently used for biomedical applications is their lack of interconnected porosity and their limited load bearing capacity. The aim of this study is to adopt a microstructural shape design approach to the manufacture of open porous materials, which utilizes spatial periodicity as a simple way to generate the models. The intention is to minimize stress concentrations in open porous materials via structural design of interconnected three-dimensional lattices hence optimising properties such as strength. The optimised models and geometries which are finally developed can be subsequently produced in material form by the use of rapid prototyping techniques.

Model development

Consider a finite volume of porous matter. Interconnected voids inside the continuous matter can be defined via a surface. In mathematical terms, let S be a surface defined by:

$$S : F(X) = 0 \quad X \in R^3 \qquad \text{Eq. 1}$$

where X is a point of coordinates x, y and z.

The surface S represents the border between the matter and the voids. A trigonometric polynomial has been used for the definition of the function *F(X)*, which can be written as a sum of *d* terms as shown in Eq. 2:

$$1 + \sum_{c=1}^{d} a_c \sin^i x \cdot \sin^j y \cdot \sin^k z \cdot \cos^l x \cdot \cos^m y \cdot \cos^n z \quad i, j, k, l, m, n = 0, 1 \qquad \text{Eq. 2}$$

This gives rise to triply periodic level surfaces: the primitive (P) surface, the diamond (D) surface and the gyroid (G) surface, having interconnectivity orders respectively equal to 6, 4 and 3.

$$\begin{aligned} P: \quad & a_1(\cos x + \cos y + \cos z) + a_2(\cos x \cos y + \cos y \cos z + \cos z \cos x) + 1 = 0 \\ D: \quad & a_3(\sin x \sin y \sin z + \sin x \cos y \cos z + \cos x \sin y \cos z + \cos x \cos y \sin z) + \\ & + a_4[\cos(4x) + \cos(4y) + \cos(4z)] + 1 = 0 \\ G: \quad & a_5(\cos x \sin y + \cos y \sin z + \cos z \sin y) + \\ & + a_6[\cos(2x)\cos(2y) + \cos(2y)\cos(2z) + \cos(2z)\cos(2x)] + 1 = 0 \end{aligned} \qquad \text{Eq. 3}$$

From a topological point of view, the interconnectivity order states how many struts depart from each node of the lattice.

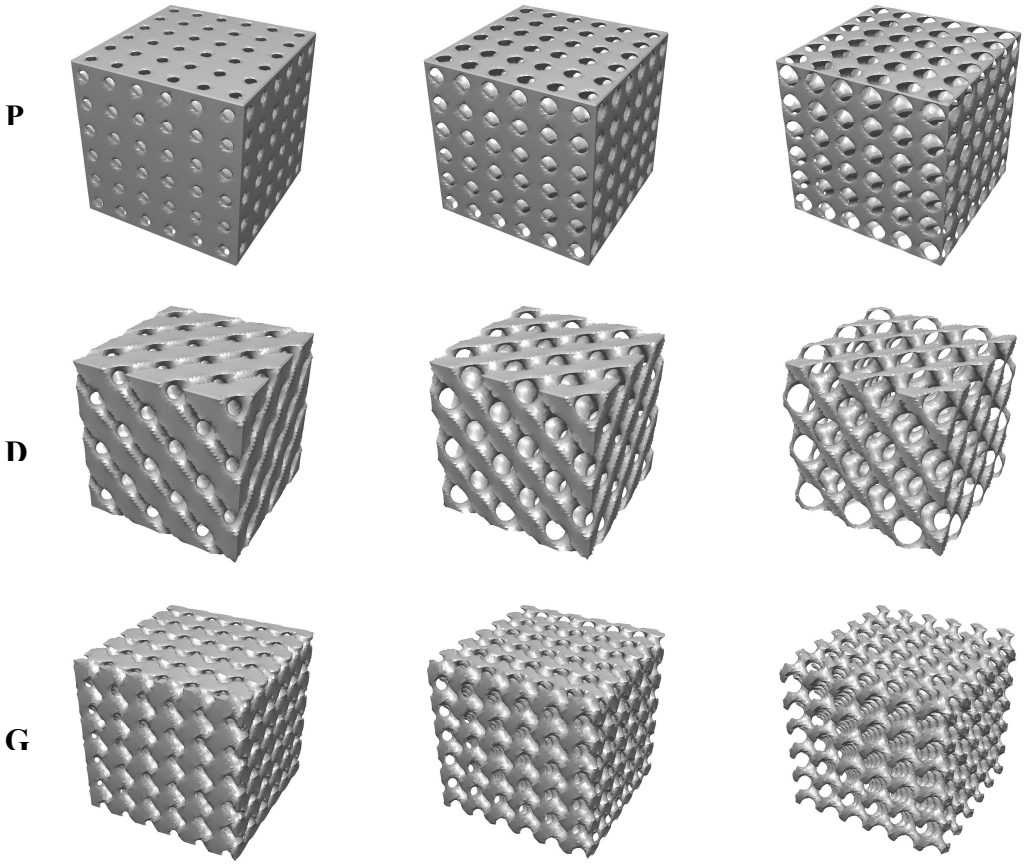

Fig.1: The P, D and G surfaces with different values of volume fraction (from left to right: 0.7, 0.5 and 0.3).

A particular advantage of using mathematical expressions to define the surface is that a desired number of parameters can be assigned to the model so that a subsequent shape optimization study can be carried out with relative ease. Subsequently, the generation of models with a range of pore volume fractions and interconnectivities is possible.

The surface has been modelled with the aid of a routine written in the computer language C which uses the GNU Triangulated Surface Library [8]. The shapes obtained are illustrated in Fig. 1 which shows P, D and G surfaces with different values of volume fraction.

Different values for volume fraction have been assigned to the scaffold geometries, demonstrating how cortical and cancellous bone (respectively ~0.7 and ~0.2 volume fraction) can be represented using the same mathematical expression, where just a few coefficients vary. The calculation time for this type and size of surface is between 0.4 and 2 s, and primarily depends on the number of cells per unit volume and the desired resolution of the output. The machine used for these operations is run by a Pentium 4 processor, 2.4 GHz with 1 GB RAM.

By adding a linear term to Eq. 1 it is possible to generate functionally graded materials with a porous inner core and a dense outer layer, imitating the transition seen in bone from the outer dense cortical to the inner porous cancellous structure. Fig. 2 shows examples of functionally graded structures produced in this way.

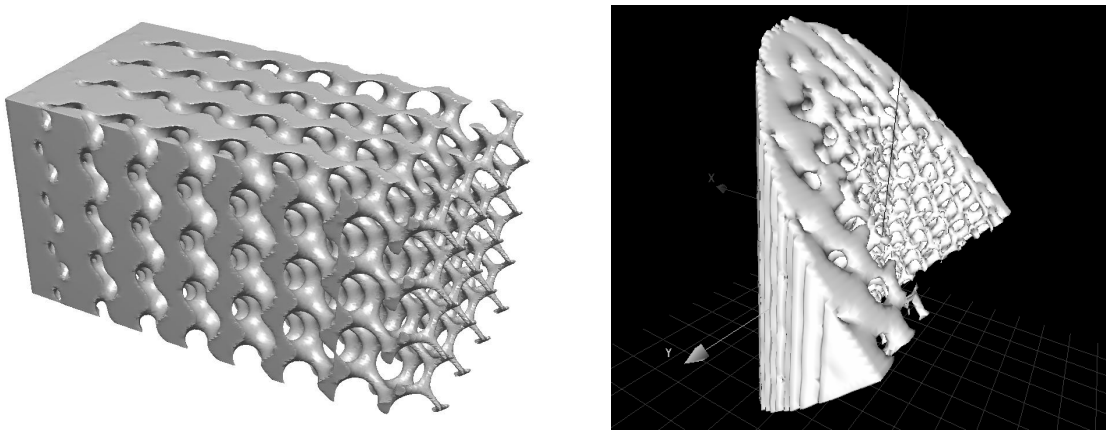

(a) (b)

Fig. 2: (a) Variable porosity structure resembling functional gradient material. (b) Representation of a bone wedge generated via mathematical function.

The use of the viewer K3DSurf [9] provided the opportunity to produce complex structures in a finite volume via implicit functions and inequalities. A more complex function with a radial variation of the porosity can be used to generate the bone wedge shown in Fig. 2(b). This new approach to 3-D modelling is particularly useful when dealing with the microstructure of materials, because of its ability to represent small features such as struts and pores with little computer memory allocation. Additionally, the highest degree of continuity is implicitly guaranteed over the entirety of the defined surface.

Manufacturing

The modelling outputs in Fig. 1 and Fig. 2(a) were used to generate the geometries using rapid prototyping techniques. The specimens shown in Fig. 4(a) have been manufactured using a 3DSystem SLS Vanguard Rapid Prototyping machine. In addition, a model of the functional gradient scaffold using a G surface has also been produced via SLS on a DTM Sinterstation 2500, Fig. 4(b). All the scaffolds are made from polyamide PA12, although in the longer term it is intended to pursue the direct formation of these structures in ceramic [10].

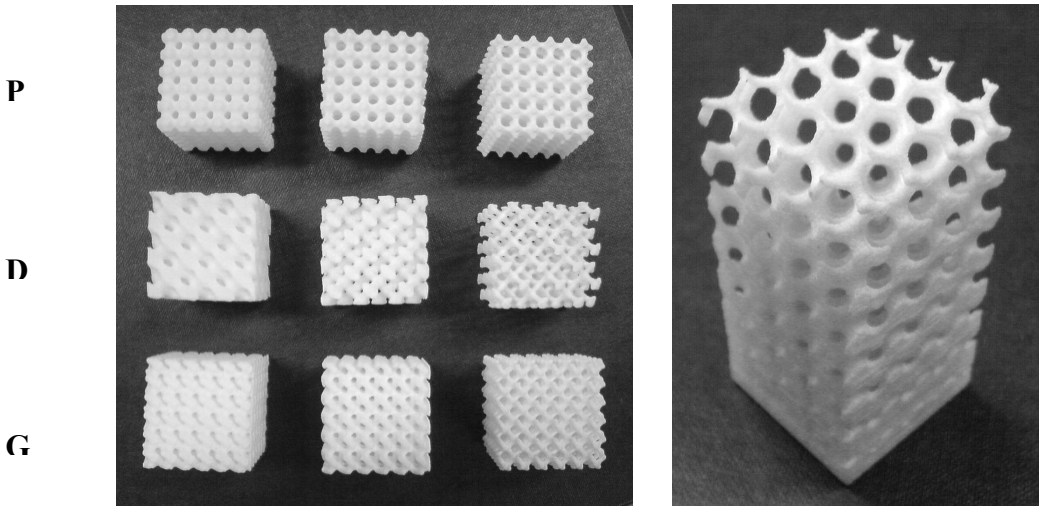

(a) (b)

Fig. 4: The samples in (a) are 30x30x30 mm, the one in (b) is 30x30x60 mm.

Conclusions

A range of materials with different volume fractions have been successfully modelled and subsequently manufactured using rapid prototyping. The techniques have been further developed to produce models and prototype functional gradient samples with a similar bimodal structure to that found in natural bone. In order to optimize the mechanical properties of such structures, the load bearing capacity of such materials needs to be further investigated. However this success in developing simple, yet effective, modelling methods for the generation of materials with a diversity of microstructural features indicates the potential use of the technique to manufacture tailor made structures that could be used in dental and orthopaedic applications.

Acknowledgments

We would like to thank M. Carley for the code used for the generation of the geometries.

References

[1] A. Tampieri, G. Celotti, S. Sprio, A. Delcegliano and S. Franzese: Biomaterials, Vol. 22 (2001), p. 1365

[2] J. Werner, B. Linner-krcmar, W. Friess, and P. Greil: Biomaterials, Vol. 23 (2002), p. 4285

[3] E. Roncari and C. Galassi: J. Mater. Sci. Lett., Vol. 19 (2000), p. 33

[4] K.A. Hing, S.M. Best and W.Bonfield: J. Mater. Sci.: Mater. Med., Vol. 10 (1999), p. 135

[5] L. Vaz, A.B. Lopes and M. Almeida: J. Mater. Sci.: Mater. Med., Vol. 10 (1999), p. 239

[6] I.H. Arita, V.M. Castano and D.S. Wilkinson: J. Mater. Sci.: Mater. Med., Vol. 6 (1995), p. 19

[7] G. Carotenuto, G. Spagnuolo, L. Ambrosio and L. Nicolais: J. Mater. Sci.: Mater. Med., Vol. 10 (1999), p. 671

[8] Information on http://gts.sourceforge.net, June 2007.

[9] Information and application used on http://k3dsurf.sourceforge.net/, June 2007.

[10] B. Leukers, H. Gulkan, S.H. Irsen, S. Milz, C. Tille, M. Schieker, H. Seitz: J. Mater. Sci. : Mater. Med., Vol. 16 (2005), p. 1121

Acta Crystallographica Section A
Foundations of Crystallography
ISSN 0108-7673

Received 23 January 2008
Accepted 15 February 2008

A new simple tiling, with unusual properties, by a polyhedron with 14 faces

Ruggero Gabbrielli[a]* and Michael O'Keeffe[b]*

[a]Department of Mechanical Engineering, University of Bath, Bath BA2 7AY, UK, and [b]Department of Chemistry and Biochemistry, Arizona State University, Tempe, AZ 85287, USA. Correspondence e-mail: r.gabbrielli@bath.ac.uk, mokeeffe@asu.edu

A monotypic simple tiling by a 14-face polyhedron that does not admit an isohedral tiling is described. The tiling is triclinic and contains four distinct, but combinatorially equivalent, kinds of tile.

A polyhedron has a graph that is planar and three-connected (*i.e.* at least three vertices and their incident edges have to be deleted to separate the graph into two disjoint parts). In a *simple polyhedron*, two faces meet at each edge and three at each vertex. In a *simple tiling* of three-dimensional Euclidean space, the tiles are simple polyhedra and two meet at each face, three at each edge and four at each vertex. An *isohedral* tiling is one in which any two tiles are related by an isometry of the symmetry group of the tiling. A *monotypic* tiling is one in which all tiles are combinatorially equivalent (have the same graph). An isohedral tiling is monotypic but not necessarily *vice versa*.

Simple tilings are of considerable interest as idealized models of foams and other physical systems (Sadoc & Rivier, 1999), their nets (the skeleton of vertices and edges) are of interest in crystal chemistry as the framework types of real and hypothetical zeolites (Delgado-Friedrichs *et al.*, 1999), and they present a number of interesting problems. The most celebrated of these is the Kelvin problem (Weaire, 1996), which asks for the lowest-energy (smallest surface area) tiling for tiles of a given volume. Among other things, this has prompted numerous studies of isohedral simple tilings. A recent study is that of Delgado-Friedrichs & O'Keeffe (2005) who showed that: (*a*) there are no isohedral simple tilings by tiles with less than 14 faces; (*b*) all 14-face tiles of isohedral simple tilings have only faces of 4, 5 or 6 sides (4-6 polyhedra); (*c*) of the 59 different 4-6 polyhedra with 14 faces there are 10 different isohedral tilers that produce 23 distinct isohedral tilings. These results have been confirmed by Komarov *et al.* (2007), who also give a full account of earlier work.

The question of whether a given combinatorial type of polyhedron admits monotypic tilings has also attracted considerable attention. It is known (Schulte, 1985) that there are *non-tilers*, isomorphic copies of which will not tile space in a locally finite and face-to-face fashion; the cuboctahedron is an example. On the other hand, the dual of a *k* vertex-transitive simple tiling is a *k* tile-transitive tiling by tetrahedra and necessarily monotypic.[1] In fact, simplicial polyhedra (those with only triangular faces) in general are tilers (Grünbaum *et al.*, 1984).

In this report, we describe some properties of a new monotypic simple tiling discovered by one of us (RG). The tile in this structure again has 14 faces but is distinct from the 10 isohedral tilers and is the unique 14-face 4-6 simple polyhedron with one quadrilateral face. It has symmetry *m*; its Schlegel diagram is shown in Fig. 1. The combinatorial symmetry of the net of this tiling is $P\bar{1}$ as determined by the program *Systre* [the method is described by Delgado-Friedrichs & O'Keeffe (2003)]. The unit cell contains eight tiles, each of symmetry 1, that are four pairs of enantiomers. The inversion centers are located in 4- and 6-sided faces. An illustration of a repeat unit made with the program *3dt* is shown in Fig. 2. The structure has 24 kinds of vertex, 48 kinds of edge, 32 kinds of face and 4 kinds of tile (transitivity 24 48 32 4).

As far as we know, this is the first example of a monotypic simple tiling by a polyhedron that does not admit an isohedral tiling and it raises some interesting questions. What polyhedra admit monotypic simple tilings other than the known isohedral tilers? In particular, do any of the other 14-face 4-6 polyhedra admit monotypic tilings? Do polyhedra with less than 14 faces admit a monotypic simple tiling? It

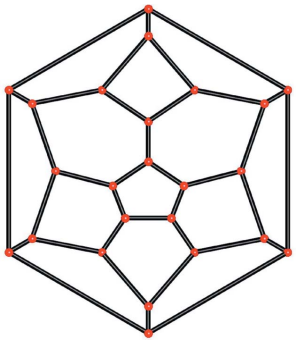

Figure 1
The Schlegel diagram of the polyhedron.

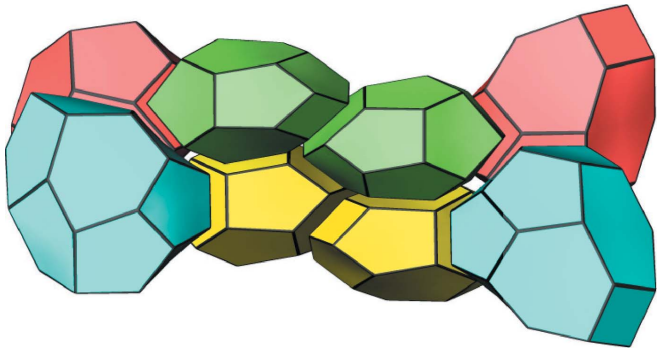

Figure 2
A repeat unit of the tiling. Tiles of the same color are related by inversion.

[1] By *k* tile (vertex) transitive, we mean that there are *k* kinds of tile (vertex) in which all tiles (vertices) of one kind are related by symmetry but there is no symmetry operation relating tiles (vertices) of different kinds.

is known only that the average face size in a simple tiling must be <6 and ≥9/2 (Luo & Stong, 1993) so the average number of faces per tile is ≥8. For an example of a simple tiling with average face size approaching that lower limit, see O'Keeffe (in Sadoc & Rivier, 1999).

We remark also that intrinsically triclinic structures rarely arise in such studies. For example, of the many hundreds of known 3-periodic packings of one kind of sphere, there is exactly one that is triclinic (Fischer & Koch, 2002). The net of this structure is the only triclinic entry in the RCSR database (http://rcsr.anu.edu.au) of over 1000 nets, and there are no triclinic examples among the thousands of nets in the EPINET database (http://epinet.anu.edu.au).

Crystallographic data for an embedding with edge lengths all equal to 1 are $a = 5.770$, $b = 5.806$, $c = 16.834$, $\alpha = 94.81$ $\beta = 94.39$, $\gamma = 90.62^\circ$. The centroids of the polyhedra are at ±(0.4110, 0.0920, 0.8775; 0.0325, 0.5904, 0.8782; 0.4086, 0.4674, 0.6215; 0.0899, 0.9099, 0.3794). The coordinates of the vertices of the net of the structure are being entered in the RCSR database with the net symbol **rug**.

Research at Bath is supported by a University of Bath research studentship. Work at ASU is supported by the US National Science Foundation (grant No. DMR 0451443). The computer programs *3dt* and *Systre*, both essential to this work, are by Olaf Delgado Friedrichs and available at http://gavrog.org.

References

Delgado-Friedrichs, O., Dress, A. W. M., Huson, D. H., Klinowski, J. & Mackay, A. L. (1999). *Nature (London)*, **400**, 644–647.
Delgado-Friedrichs, O. & O'Keeffe, M. (2003). *Acta Cryst.* A**59**, 351–360.
Delgado-Friedrichs, O. & O'Keeffe, M. (2005). *Acta Cryst.* A**61**, 358–362.
Fischer, W. & Koch, E. (2002). *Acta Cryst.* A**58**, 509–513.
Grünbaum, B., Mani-Levitska, P. & Shephard, G. C. (1984). *J. London Math. Soc.* **29**, 181–191.
Komarov, V. Yu., Solodovnikov, S. F., Grachev, E. V., Kosyakov, V. I., Manakov, A. Yu., Kurnosov, A. V. & Shestakov, V. A. (2007). *Crystallogr. Rev.* **13**, 257–297.
Luo, F. & Stong, R. (1993). *Trans. Am. Math. Soc.* **337**, 891–906.
Sadoc, J. F. & Rivier, N. (1999). Editors. *Foams and Emulsions.* Dordrecht: Kluwer Academic Publishers.
Schulte, E. (1985). *J. Combinatorial Theory A*, **38**, 75–81.
Weaire, D. (1996). Editor. *The Kelvin Problem: Foam Structures of Minimal Surface Area.* London: Taylor and Francis.

Philosophical Magazine Letters
Vol. 89, No. 8, August 2009, 483–491

Taylor & Francis
Taylor & Francis Group

A new counter-example to Kelvin's conjecture on minimal surfaces

Ruggero Gabbrielli*

Department of Mechanical Engineering, University of Bath, BA2 7AY, Bath, UK

(*Received 25 October 2008; final version received 5 May 2009*)

A new counter-example to Kelvin's conjecture on minimal surfaces has been found. The conjecture stated that the minimal surface area partition of space into cells of equal volume was a tiling by truncated octahedra with slightly curved faces (K). Weaire and Phelan found a counter-example whose periodic unit includes two different tiles, a dodecahedron and a polyhedron with 14 faces (WP). Successively, Sullivan showed the existence of an infinite number of partitions by polyhedra having only pentagonal and hexagonal faces that included WP, the so-called tetrahedrally close packed structures (TCP). A part of this domain contains structures with lower surface area than K. Here, we present a new partition with lower surface area than K, the first periodic foam containing in the same structure quadrilateral, pentagonal and hexagonal faces, in ratios that are very close to those experimentally found in real foams by Matzke. This and other new partitions have been generated via topological modifications of the Voronoi diagram of spatially periodic sets of points obtained as local maxima of the stationary solution of the 3D Swift–Hohenberg partial differential equation in a triply periodic boundary, with pseudorandom initial conditions. The motivation for this work is to show the efficacy of the adopted method in producing new counter-examples to Kelvin's conjecture, and ultimately its potential in discovering a periodic partition with lower surface area than the Weaire–Phelan foam. The method seems tailored for the problem examined, especially when compared to methods that imply the minimization of a potential between points, where a criterion for neighboring points needs to be defined. The existence of partitions having a lower surface area than K and an average number of faces greater than the maximum value allowed by the TCP domain of 13.5 suggests the presence of other partitions in this range.

Keywords: tetrahedra packing; bubbles; crystal geometry; foams

The geometrical problem that seems to have its solution in real foams of partitioning space into cells of equal volume with the least interfacial area has not yet been solved. The solution to the two-dimensional problem, also known as the honeycomb conjecture, has been formally proven by Hales [1]. For the three-dimensional problem, a conjectured solution has been proposed by Weaire and Phelan [2]. The proof of the existence of a solution for the general *n*-dimensional case has been recently given by Morgan [3].

*Email: r.gabbrielli@bath.ac.uk

ISSN 0950–0839 print/ISSN 1362–3036 online

DOI: 10.1080/09500830903022651
http://www.informaworld.com

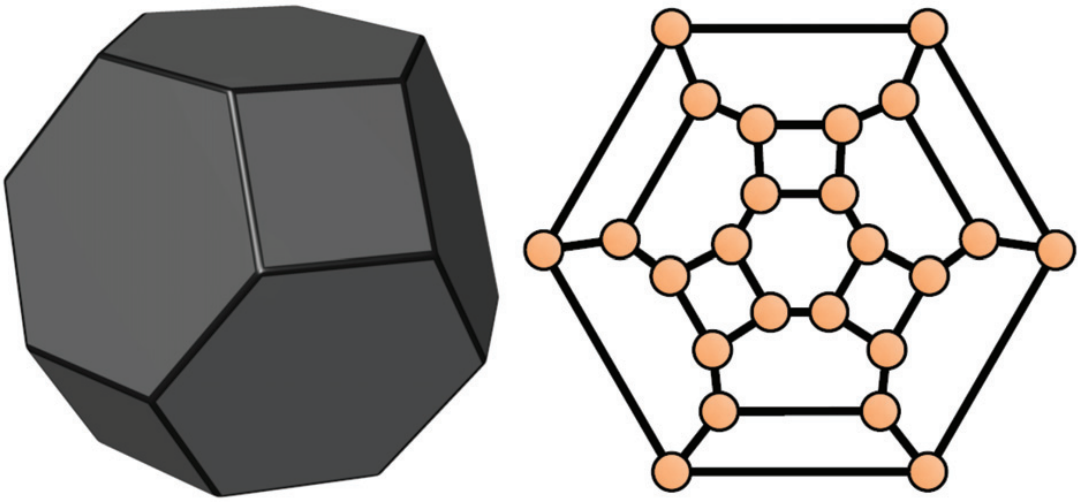

Figure 1. A truncated octahedron and its Schlegel diagram. This polyhedron is space-filling.

A possible solution to the three-dimensional problem was given more than a century ago by William Thomson [4], better known as Lord Kelvin, who was also the first to formally state it. Kelvin conjectured that the partition made by a packing of identical truncated octahedra with slightly curved faces (K), had the minimum surface area among all the possible equal volume partitions of space. The truncated octahedron is a polyhedron with 14 faces, eight of which are hexagons and the remaining six are quadrilaterals, as shown in Figure 1. In the partition considered by Kelvin, all the edges were curved. The quadrilateral faces were flat, and the hexagonal ones were slightly curved, this way further reducing the total interfacial area of the partition when compared to the flat-faced version of the truncated octahedron.

In general, if A is the average interfacial area per cell and V is the volume of each cell in the periodic partition, a dimensionless, scale-invariant quantity can be defined as

$$c = A/V^{2/3}. \tag{1}$$

This quantity, known as the cost of a foam (or partition) [5], has been used throughout this work for comparison purposes between different structures.

The solution proposed by Kelvin was believed to be optimal until 1993, when Robert Phelan and Denis Weaire, using Ken Brakke's [6] program Surface Evolver, showed the existence of a partition (WP) with less area than that by truncated octahedra [2]. The partition, also known as the Weaire–Phelan structure, has two different cell shapes, namely, a cubicly deformed pentagonal dodecahedron and 14-hedron with 12 pentagonal and two hexagonal faces, as in Figure 2.

Shortly after the discovery, John Sullivan described a class of mathematical foams known as tetrahedrally close-packed structures, which included WP. Many of these structures have been known for a long time as Frank–Kasper [7,8] phases. All the structures belonging to this domain are made of polyhedral cells having only pentagonal and hexagonal faces. He constructed infinite families of periodic structures as convex combinations of a finite set of basic structures [9,10].

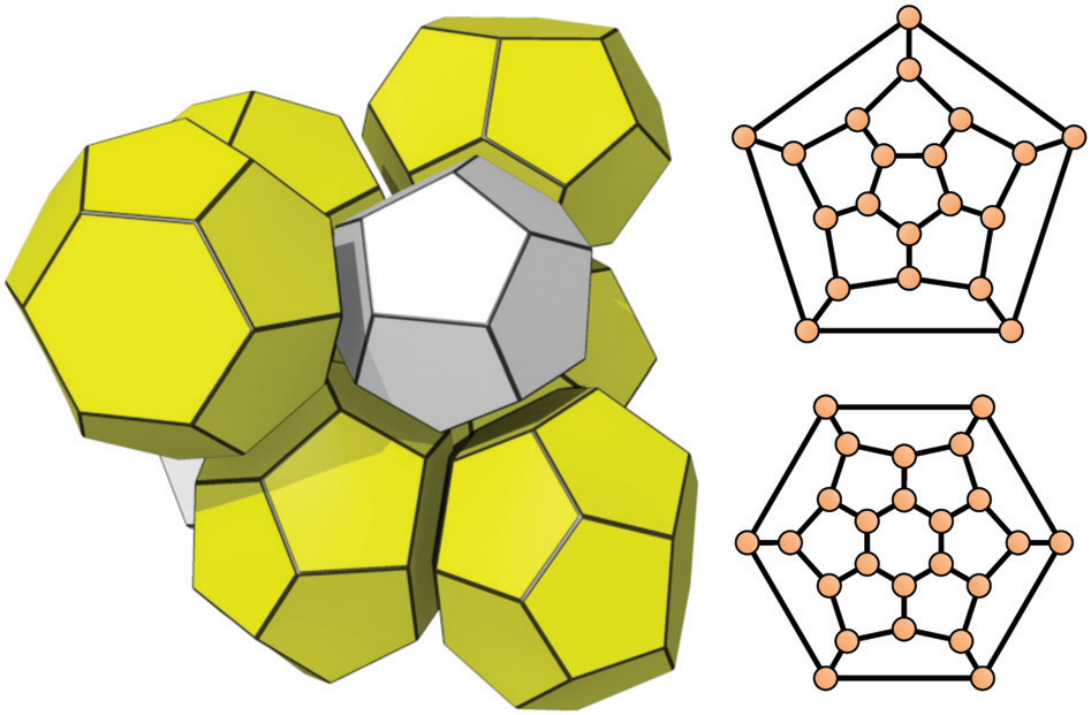

Figure 2. The periodic unit of the Weaire–Phelan structure contains eight polyhedra, two [0-12-0] and six [0-12-2]. The Schlegel diagrams are shown on the right. Tiles are represented slightly detached one from the other for better visualization. The pictures only display the topological information of the structure.

This showed that not only did WP have less area than K, but infinitely many other structures (the terms structure, partition, foam and tiling are used as synonyms here, as the problem interests a large number of different fields [11–14]) could be constructed with such a property. The polyhedral cells used in these structures are of four distinct kinds having 12, 14, 15 and 16 faces. All contain 12 pentagons plus, respectively, zero, two, three and four hexagons. These are the only combinatorially possible simple polyhedra containing only pentagons and/or hexagons where the hexagons are not adjacent, as shown by the program plantri [15]. A simple polyhedron is a polyhedron in which each vertex belongs to exactly three edges. A tiling by polyhedra is simple if every face contained in it is shared by exactly two adjacent tiles, every edge by exactly three incident faces, and every vertex by exactly four incident edges. Since faces can be in general non-planar, polyhedra should also have exactly three faces meeting at each vertex.

Since the only faces that occur in the partitions found to have from four to six sides, a nomenclature for polyhedra based on this fact consisting of three numbers has been considered. Each polyhedron is assigned three numbers [Q-P-H] that represent the number of quadrilaterals (Q), pentagons (P) and hexagons (H). This naming system, called simplified signature, although not always univocal in defining the topology, as with the Schlegel diagram [16], presents the advantage of a much more concise form of identification of the polyhedron, very similar to the signature used in the software application 3dt [17], and for this reason it will be used to describe the polyhedral composition of the structures found in this work.

One method of generating foams is by Voronoi partitions in three dimensions. All that is needed is a set of points in a parallelepiped. If the opposite faces are connected to each other, a three-torus is the result and the set of points can be thought of as periodic and filling the whole three-dimensional space. The Voronoi diagram of these points produces a periodic partition of the space. Generation methods that start from random sets of points in a three-torus have already been used with interesting results [18].

A method is proposed here, based on a partial differential equation that shows a pattern forming behavior, the Swift–Hohenberg equation [19,20]. A Matlab script previously used for the study of two-dimensional hexagonal patterns [21] has been modified for the three-dimensional case. This allowed us to find numerical solutions to the equation

$$\frac{\partial u}{\partial t} = au - (\nabla^2 + 1)^2 u + bu^2 - u^3, \tag{2}$$

on a periodic cube of prescribed size L using the Fast Fourier Transform. The coefficients a and b in Equation (2) affect the final pattern. The values needed for homogeneously distributed and isolated maxima to appear in the stationary state were found to be, respectively, close to 0.001 and 1, and for this reason these have been adopted. The unit cell was chosen to be cubic for simplicity. A version of the code that computes Equation (2) in a cuboid has also been written and a more general implementation working in a parallelepiped might help. Solutions with non-cubic symmetry arise in a cubic region only if a multiple of their unit cell has arbitrary close to cubic symmetry. This is always the case, the only problem being the fact that the structure might be very large. The mesh grid adopted for the numerical solution consisted of $40 \times 40 \times 40$ scalars.

The normalized energy associated with Equation (2) is given by

$$E = \frac{1}{8L^3} \int -\frac{au^2}{2} + \frac{[(\nabla^2 + 1)u]^2}{2} - \frac{bu^3}{3} + \frac{u^4}{4} \, \mathrm{d}z \, \mathrm{d}y \, \mathrm{d}x. \tag{3}$$

This has been used to determine whether a correlation with the cost of a foam was present or not. No link has been found yet, but it is believed that a relationship between this energy and other forms of it like the chemical bond energy of the crystal lattice might exist.

The solution for the function $u = u(x, y, z, t)$ has been found to converge from pseudorandom initial conditions to a stationary state. The three-dimensional coordinates of the local maxima of the function $u = u(x, y, z, t)$ in this final state have been extracted. The method has been run a finite number of times, and the results have been compared for congruence. Successively, L has been incremented and the coordinates at the stationary state have been recorded again. It has been found that for large values of L the patterns formed appear locally but not globally ordered. For certain values of the parameter L the system converges to a state where the maxima are arranged on parallel lines in space, all having the same orientation, in a hexagonal packing fashion. The partition obtained from such an arrangement is a cylindrical hexagonal honeycomb.

Another issue is that many of the simpler patterns appear for different values of L. These values are the multiples of the fundamental lattice distance for a given pattern. Thus more complex patterns might be hidden by the simpler ones when looking for a solution for a given size L.

In general, since the average distances between the local maxima are roughly constant, increasing the size of the cubic region in which the equation is calculated increases the number of the local maxima within the same region. This allows structures with different levels of complexity to be found simply acting on the size of the periodic boundary L.

The patterns obtained from such a setup were BCC, FCC, P8, WP, P20, C15 [9,22], P36, K11 and P42. The values of L for which the patterns were found are 4.5 for BCC, 5.7 for FCC, 7.2 for P8, 7.3 for WP, 9.8 for P20, 10.5 for C15, 12 for P36, 12.2 for K11 and 12.9 for P42. Since the system allows the solution to be stretched, the patterns were also found for values close to those given above. The values listed here correspond to the lowest PDE energy (Equation (3)). Any given pattern also appears for values that are integer multiples of these listed. Additionally, some of the patterns arise for more than only one value, like FCC that also shows up at 7.4 and 9.6. Symbols starting with the letter P identify structures that have not been found in the literature [23]. The number following the letter P specifies the number of points found in the cubic region at the stationary state. K11 contains 40 points. This pattern is described in a separate article [24], since the tiling having these points as Voronoi centers has been found for the first time using a different method.

Using Sullivan's vcs software [25], the Voronoi partition for each pattern of points was created. This software uses the gift-wrapping algorithm for the determination of the Voronoi vertices and for this reason it is not stable when more than four Voronoi cells meet at a point. Since some of the new partitions found were non-simple, a small random quantity has been added to the coordinates of the points to avoid algorithm instabilities.

The partitions have been imported into Surface Evolver, where the added errors have been eliminated by deletion of the edges shorter than a given value. A number of additional simple foams have been created directly in Surface Evolver by *popping* vertices of non-simple ones. The outcome of this operation is not a unique structure since there are $3^m + 4^n$ different combinations, if m is the number of eight-connected vertices and n that of six-connected vertices in the original non-simple foam. However, this number can be drastically reduced due to symmetry considerations.

The periodic graphs of the nets constituted by the edges of the partitions have been analyzed by Systre, which is part of the Gavrog Project [17], so that the primitive net could be identified and the number of tiles in the partition therefore reduced to its minimum possible. This helped in the case of P42, where the 42 tiles have been reduced to 14, as shown in Figure 3.

Fifteen out of the 81 combinatorially possible simple partitions derived from the P42 non-simple case are topologically distinct configurations. Each of these showed less surface area than K. The partitions contain only polyhedra with 13, 14 and 15 faces each, specifically those named below plus a [3-6-4] and a [2-8-5]. Their costs range from 5.303 to 5.306. Figure 4 shows a picture of the tiling of the unit cell of the structure with the lowest cost, which has been named P42a.

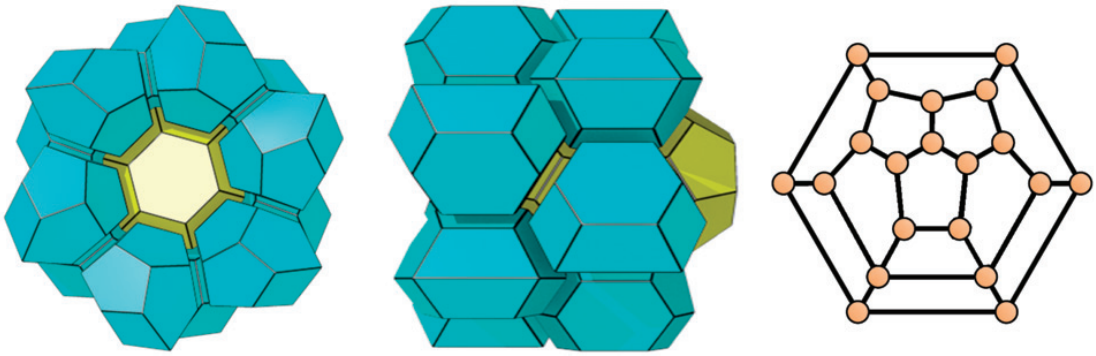

Figure 3. The unit cell of the new partition P42 contains 14 polyhedra of two different kinds. Twelve non-simple [4-8-1] (cyan) and two [0-12-2] (yellow). The Schlegel diagram of the non-simple [4-8-1] is shown.

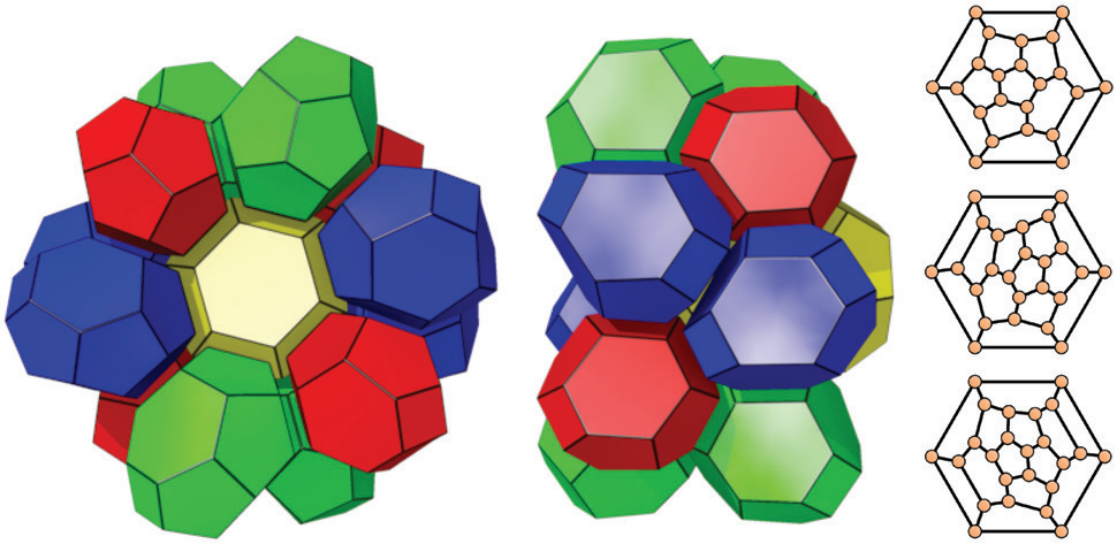

Figure 4. The unit cell of the new partition P42a contains 14 polyhedra of four different kinds. Four [1-10-2] (red), four [1-10-3] (green), four [2-8-4] (blue) and two [0-12-2] (yellow). Tiles of the same color are related by point inversion or glides (a glide is a reflection plus a translation). The Schlegel diagrams of the first three are shown. From the top: [1-10-2], [1-10-3] and [2-8-4].

The content of quadrilaterals, pentagons and hexagons in the new partition P42a closely matches (Table 1) that of real foams found experimentally by the botanist Edwin Matzke [26].

The fundamental unit is made of ten 14-hedra and four 13-hedra. The polyhedral composition of P42a matches very closely that observed by Matzke [27]. The three most common cells in this partition [1-10-2], [1-10-3] and [2-8-4] are the first three entries in Matzke's experiments. The [0-12-2] cell is at the fifth place in Matzke's list, followed by the pentagonal dodecahedron [0-12-0], not present in P42a. The average number of faces is 13.71, very close to the value of 13.70 found by Matzke, the theoretical optimal value of 13.56 given by Coxeter [27] for random close-packing, not far from that of the currently conjectured solution to the Kelvin problem of 13.5 [2] and above the lower bound for equal-pressure foams of 13.40

Table 1. Polygonal composition experimentally found in real foams by Matzke compared to the distribution in some of the lowest cost periodic partitions known. Note the similarities with the P42a structure.

	Polygon count				Percentage		
	Quad	Pent	Hex	Tot	Quad	Pent	Hex
K	3	–	4	7	43	–	57
WP	–	48	6	54	–	89	11
P42a	8	68	20	96	8	71	21
Matzke	866	5503	1817	8221	11	67	22

Table 2. Simplified signature, space group of the most symmetrical configuration, minimum cost c of the equal-volume configuration and average number of faces per cell z.

	Simplified signature	Sp. gr.	c	z
K	[6-0-8]	$Im\bar{3}m$	5.306	14
WP	3[0-12-2] + [0-12-0]	$Pm\bar{3}n$	5.288	13.5
P42a	2[2-8-4] + 2[1-10-3] + 2[1-10-2] + [0-12-2]	$C12/c1$	5.303	13.71
P42	6[4-8-1] + [0-12-2]	$P6/mcc$	5.307	13.14

Table 3. Parameters for the periodic point set for the Voronoi generation of the partition P42, given in the cylindrical system.

	Periods			Points ($k \in \mathbb{N}$, $1 \leqslant k \leqslant 12$)		
ρ	$\frac{5}{2}\cos(\frac{\pi}{12})$	$\frac{5}{2}\cos(\frac{\pi}{12})$	0	0	0	$\frac{\sqrt{3}}{2}$
θ	0	$\frac{\pi}{3}$	0	0	0	$(2k-1)\frac{\pi}{12}$
z	0	0	2	0	1	$1+\frac{(-1)^k}{2}$

given by Kusner [28]. The lower bound for the cost corresponding to this last value is 5.254, as shown by Glicksman and Rios [29].

The space group for each of the foams produced were determined by 3dt, which is part of the Gavrog Project [17] via the method described by Delgado-Friedrichs and O'Keeffe [30], and refers to the structure with the highest degree of symmetry having the same topology. The minimum cost is obtained by constraining the structure to have tiles of the same volume. It is relevant to note that the configuration of minimum cost does not always coincide with the most symmetrical one. Note that P42a is characterized by a very low symmetry when compared to K and WP. Table 2 reports the data for comparison.

The Surface Evolver code used for the calculation of foams properties and parameters (including their cost) has been provided by Sullivan. The code for the directional popping has been provided by Brakke. The code for the relaxation of the

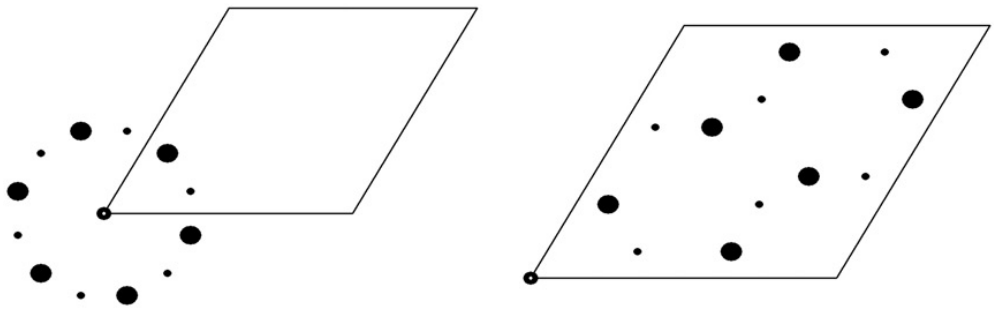

Figure 5. The 14 points in the P42 pattern and how they relate to the periodic unit cell. The radius of the dots expresses the third dimension otherwise not representable on paper. There are four different sizes: one point in the origin at $z=0$ (in white), six points at $z=0.5$, one point at $z=1$ (this coincides with that at $z=0$ in this view) and six points at $z=1.5$.

periods has been written by the author. This step consisted in numerical iterations in which lengths and angles of the vectors defining the periodic unit, along with the coordinates of all the vertices defining the structure, were varied one at a time and the surface area further minimized.

The periods of the unit cell and the coordinates of the centers of the Voronoi cells for the partition P42 are reported in Table 3 and shown in Figure 5.

The method described, opportunely tuned, can also be used to find new clues about the honeycomb problem considered by Tóth [31].

The pictures of the tilings have been generated with 3dt [17]. The Schlegel graphs (apart from that in Figure 3 that has been partially edited by hand) have been produced with Olaf Delgado-Friedrichs' code in Thomas Harmuth's 3-regular planar graphs generator built in the software CaGe [32].

A three-dimensional model of the P42a partition realized with JavaView [33] can be viewed online [34].

Acknowledgements

The author wishes to thank Michael Cross. His java demo [35] of the Swift–Hohenberg equation provided the idea for this work. Thanks are also due to Ken Brakke for the support received on the Surface Evolver, John Sullivan for the scripts used to evaluate foam properties, David Lloyd for the Matlab solver of the two-dimensional case of the Swift–Hohenberg equation and Davide Proserpio and Keri Collins for the many suggestions received on the first draft of this manuscript. Research has been supported by the University of Bath and by a Flexible Award within the EPSRC Bridging the Gaps Project between the Department of Mathematical Sciences and the Department of Mechanical Engineering at the University of Bath.

References

[1] T.C. Hales, Discrete Comput. Geom. 25 (2001) p.1.
[2] D. Weaire and R. Phelan, Phil. Mag. Lett. 69 (1994) p.107.
[3] F. Morgan, Phil. Mag. Lett. 88 (2008) p.647.
[4] W. Thomson, Phil. Mag. 24 (1887) p.503.

[5] R. Kusner and J. Sullivan, Forma 11 (1996) p.233.
[6] K.A. Brakke, Exp. Math. 1 (1992) p.141.
[7] F.C. Frank and J.S. Kasper, Acta Cryst. 11 (1958) p.184.
[8] F.C. Frank and J.S. Kasper, Acta Cryst. 12 (1959) p.483.
[9] J.M. Sullivan, *New tetrahedrally close-packed structures*, in *Proceedings of Eurofoam 2000 (Delft)*, 2000, p.111.
[10] J.M. Sullivan, *The geometry of bubbles and foams*, in *Foams and Emulsions*, N. River and J.F. Sadoc, eds., Kluwer, Dordrecht, 1999, p.379–402.
[11] M. O'Keeffe, *Crystal structures as periodic foams and vice versa*, in *Foams and Emulsions*, N. Rivier and J.F. Sadoc, eds., Kluwer, Dordrecht, 1999, p.403.
[12] R. Zallen, *The Physics of Amorphous Solids*, Vol. 2, Wiley-VCH, New York, 1998, p.51.
[13] J.H. Conway and S. Torquato, Proc. Natl. Acad. Sci. USA 103 (2006) p.10612.
[14] D.P. Shoemaker and C.B. Shoemaker, Phys. Rev. B 38 (1988) p.6319.
[15] G. Brinkmann and B.D. McKay, MATCH Commun. Math. Comput. Chem. 58 (2007) p.323.
[16] V. Schlegel, Nova Acta Acad. Leop. Carol. 44 (1883) p.343.
[17] O. Delgado-Friedrichs, The Gavrog project. Available at http://gavrog.sourceforge.net.
[18] A.M. Kraynik, D.A. Reinelt and F. Swol van, Phys. Rev. E 67 (2003).
[19] J. Swift and P.C. Hohenberg, Phys. Rev. A 15 (1977) p.319.
[20] M.C. Cross and P.C. Hohenberg, Rev. Mod. Phys. 65 (1993) p.851.
[21] D.J.B. Lloyd, D. Avitabile and A.R. Champncys, SIAM J. Appl. Dynam. Syst. 7 (3) (2008) p.1049.
[22] D.P. Shoemaker and C.B. Shoemaker, Acta Cryst. B 42 (1986) p.3.
[23] R. Gabbrielli, Foam geometry and structural design of porous material, PhD dissertation, University of Bath, 2009.
[24] O. Delgado-Friedrichs, R. Gabbrielli, M. O'Keeffe and D.M. Proserpio, An algorithm for the solution to the Kelvin problem, in preparation (2009).
[25] J.M. Sullivan, vcs. Available at http://torus.math.uiuc.edu/jms/software.
[26] E.B. Matzke, Am. J. Bot. 33 (1946) p.58.
[27] H.S.M. Coxeter III, J. Math. 2 (1958) p.746.
[28] R. Kusner, Proc. Math. Phys. Sci. 439 (1992) p.683.
[29] M.E. Glicksman and P.R. Rios, Phil. Mag. 87 (2007) p.189.
[30] O. Delgado-Friedrichs and M. O'Keeffe, Acta Cryst. A59 (2003) p.351.
[31] L.F. Tóth, Bull. Amer. Math. Soc. 70 (1964) p.468.
[32] T. Harmuth, CGF. Available at http://www.math.uni-bielefeld.de/~CaGe.
[33] K. Polthier, JavaView. Available at http://www.javaview.de.
[34] R. Gabbrielli, A comparison between periodic units of models for equal-volume partitions. Available at http://people.bath.ac.uk/rg247/javaview/p42a_comparison.html.
[35] M.C. Cross, Pattern formation in the Swift–Hohenberg equation. Available at http://crossgroupcaltech.edu/Patterns/Demo4_2.html.

Appendix B

Patent

This patent is the outcome of a fruitful collaboration between the University of Bath and a manufacturer of orthopaedic implants. The idea of filing a patent on the geometry of the surface of orthopaedic implants originates from an informal chat at the Bioceramics20 conference in Nantes between the author and Corrado Piconi, inspired by the oral presentation at the venue.

The document describes the application of a set of mathematically defined surfaces to the geometry of the outer layer of joints and implants. Functionally Graded Materials can be modelled according to these principles and their geometry defined simply by representing the boundary between solid and void fractions of material.

- *Improvements in or relating to joints and/or implants*, patent application no. 0809721.4, AI 13624 GB [92].

University of Bath 13634 GB

0809721.4

filed 28 May 2008

Improvements in or relating to joints and/or implants

Abel & Imray
Chartered Patent Attorneys
Westpoint Building
James Street West
Bath
BA1 2DA

Improvements in or relating to joints and/or implants

This invention relates to joints and joint parts for medical and non-medical use and to implants suitable for implanting in a human body in place of bone, and also to methods of making such joints or implants. The invention is more particularly, but not exclusively, directed to joint parts, for example, ball and socket joints, for use in all kinds of applications, including non-medical applications and to load-bearing implants that are able to be implanted without the use of cement and provide a major part of, or the whole of, one part of a joint, for example a component of a hip, knee, ankle, shoulder, elbow or wrist.

The particular requirements of an implant suitable for implanting in a human body vary very much according to the application. Broadly there are two kinds of bone implant. Firstly, there are those that are used in tissue engineering applications to provide a scaffold in which bone tissue may be encouraged to grow; implants of this kind, which may be used for small reconstruction and repair applications, do not themselves have great structural strength and are often in the form of thin sheets or blocks. Secondly, there are those that are used to replace all or part of a joint, or in other load bearing applications. Such implants are often of a particular curved shape and may be required to bear substantial loads; in that respect, their strength is important, but it is

also important that they can be fixed securely in position; such fixing can be carried out by using a suitable cement but it is preferred where possible to provide an implant which can be integrated into existing bone material through natural incursion of biological tissue into one or more portions of the implant. Considerations of the kind just described may lead to implants of composite construction, with a first part having the necessary strength and other properties to enable it to act as part of a joint and a second part formed separately from the first part and being able to be integrated into, and thus fixed securely to, adjacent or surrounding bone material.

Key properties of a load bearing implant are its mechanical strength and its porosity. A common approach when creating an implant is to adopt a trial and error approach to finding an implant with desired porosity and strength characteristics. Thus a first prototype implant may be made and its physical properties tested. Thereafter a modified version of the prototype may be manufactured with an altered structure to effect a change to the porosity and/or strength of the implant. A difficulty that is often encountered in this process is seeking to assess quantitatively the effect on porosity and strength of a given change in the structure. That applies when the structure is of uniform strength and porosity throughout, but it is all the more problematic where it is desired to provide variation in the porosity and/or strength of the implant from one region of the structure to another.

In a paper entitled "Fabrication methods of porous metals for use in orthopaedic applications" by Ryan, Pandit and Apatsidis published in Biomaterials 27 (2006) 2651-2670, a range of methods of making metal implants are reviewed. Those methods include one using rapid prototyping technology to create porous shapes from a multiplicity of cubic elements. Whilst using such rapid prototyping technology as taught in the paper can speed up the production of an implant, it does not make it any easier to adjust the characteristics of the implant in a predictable and systematic manner, for example to effect a preselected increase in the porosity of the implant.

Rapid prototyping techniques are used in a wide variety of applications including many non-medical applications and the disadvantage of not being able easily to predict the characteristics of a product made by such techniques is disadvantageous in those applications too.

It is an object of the invention to provide an improved joint part and an improved method of making a joint part.

It is a further object of the invention to provide an improved implant and to provide an improved method of making an implant.

According to the invention there is provided a joint part having a porous portion that is defined by a multiplicity of solid regions where material is present and a remaining multiplicity of pore regions where material is absent, the locations of at least most of the multiplicity

of solid regions being defined by one or more mathematical functions. The invention further provides a joint including a joint part as defined immediately above.

According to the invention there is also provided a load-bearing implant having a porous portion that is defined by a multiplicity of solid regions where material is present and a remaining multiplicity of pore regions where material is absent, the locations of at least most of the multiplicity of regions where material is present being defined by one or more mathematical functions.

According to the invention there is further provided a method of making a load-bearing implant having a porous portion defined by a multiplicity of solid regions where material is present and a remaining multiplicity of pore regions where material is absent, the method including the step of depositing solid material in the multiplicity of solid regions during a process of solid freeform fabrication in which one or more mathematical functions are used to determine at least most of the multiplicity of regions where material is present.

By defining the solid regions mathematically, it becomes much simpler to vary the nature of the porous portion in a systematic way that will have predictable results in terms of its effect on mechanical strength and porosity. It is only necessary to change the values of one or more constants in the mathematical functions defining the solid regions and an implant with different and varying characteristics of porosity and strength can readily be

produced. Where reference is made to determining regions where material is present, it should be understood that this may involve determining all the regions where material is absent (the negative image) or it may involve (as in a preferred embodiment of the invention described below) determining the boundary surface of the solid regions.

Preferably, the method of the invention further includes the step of modifying one or more of the mathematical functions to vary the porosity and/or strength of the porous portion, calculating the porosity and/or strength of the modified porous portion and making the joint part or implant with the modified porous portion, the method including the step of depositing solid material during a process of solid freeform fabrication in which the one or more modified mathematical functions are used to determine at least most of the multiplicity of regions where material is present.

It is within the scope of the invention for some portion(s) of the joint part or implant to be defined in a non-mathematical way, but in a preferred embodiment of the invention all the solid regions of the implant are defined mathematically.

Where reference is made herein to solid freeform fabrication, it should be understood that there are many known methods of this kind and that the invention is not limited to any particular kind of such fabrication, nor indeed is it concerned with which method is adopted. Any appropriate method may be employed. Typically, in a solid

freeform fabrication (SSF), material is laid down in a multiplicity of thin layers each layer being laid in a respective pattern and fixed to the layer below. In that way a three dimensional shape of any desired kind, including re-entrant surfaces and the like can be formed. Machines which provide for solid freeform fabrication are sometimes referred to as rapid prototyping machines, but it should be understood that in the present invention the products produced may not only be prototypes but also final products.

Preferably the one or more mathematical functions define a periodic nodal surface as a boundary surface between solid and pore regions. Suitable periodic nodal surfaces are triply periodic surfaces, namely the primitive (P) surface, the diamond (D) surface and the gyroid (G) surface having interconnectivity orders equal to 6, 4 and 3 respectively. From a topological point of view, the interconnectivity order refers to how many struts depart from each node of the lattice. In an example of the invention defined below, a set of inequalities for defining a gyroidal (G) structure is given as one example of an appropriate mathematical function.

The joint part or implant may be made of a metal material and this may most commonly be the case, but the invention may be employed with any of a wide variety of materials. For example, it has recently become feasible to deposit ceramic materials using a solid freeform fabrication technique and the implant of the invention may

thus be formed of ceramic material. As well it is possible to deposit polymeric materials using a solid freeform fabrication technique and the implant of the invention may thus be formed also of polymeric material.

The joint part or implant may consist exclusively of the porous portion or it may also include a solid portion. The latter is more usual. The "solid" portion may have some level of porosity, provided the level is substantially less than the porosity of the porous portion, but preferably the solid portion has no porosity. The porous portion preferably has a porosity, which may be no porosity, in the region bordering the solid region substantially equal to the porosity of the solid region and increases in porosity away from the solid portion. The increase in porosity is preferably gradual and more preferably without any discontinuity. It is a particular advantage of the present invention that it can become a straightforward matter to avoid discontinuities in physical properties of the porous portion and thereby enable regions of especially high stress to be avoided.

The solid portion preferably has a curved bearing surface. For example, the solid portion may define a cup, which may provide part or all of the socket of a ball and socket joint; in this case the cup may have a concave load bearing cup portion which is solid and may have a porous portion extending outwardly from the cup portion to a peripheral outer surface. Similarly, the solid portion may define a ball, which may provide part or all of the ball of

a ball and socket joint; in this case the ball may have a convex load bearing ball portion which is solid and may have a porous portion extending away from the ball portion.

By way of example, for a femoral head, the ball head of the ball and socket joint needs to be as highly polished and smooth as possible to reduce friction and wear. However, the invention may for example be applied to the proximal (upper) portion, for example the upper third, of the femoral stem. Such an arrangement can promote bone ingrowth and enhanced fixation in the femur where it is desirable and needed.

For a joint part for use in other applications, especially non-medical applications, it may be acceptable or even desirable for a bearing surface of the joint part to be porous, for example to provide a path for lubricant to reach the bearing surfaces.

In the case where the joint part or implant includes a solid portion, the solid portion may be formed by the solid freeform fabrication technique, and the solid portion and the porous portion are preferably made in one piece. Thus, the method of the invention may be one in which the joint part or implant includes a solid portion and a porous portion, the solid portion and the porous portion being formed in the same process of solid freeform fabrication to provide a one-piece integrated structure.

The invention may in particular be employed in an acetabular cup for a hip joint. Thus, in an especially preferred form the invention may provide an acetabular cup

having an inner cup-shaped surface and a porous portion that extends outwardly to a peripheral outer porous surface, the porous portion being defined by a multiplicity of solid regions where material is present and a remaining multiplicity of pore regions where material is absent, at least most of the multiplicity of regions where material is present being defined by one or more mathematical functions. Similarly, the invention may provide a method of making an acetabular cup, having an inner cup-shaped surface and a porous portion that extends outwardly to a peripheral outer porous surface, the porous portion being defined by a multiplicity of solid regions where material is present and a remaining multiplicity of pore regions where material is absent, the method including the step of depositing solid material in the multiplicity of solid regions during a process of solid freeform fabrication in which one or more mathematical functions are used to determine at least most of the multiplicity of regions where material is present.

Whilst certain features of the invention have been described in relation to a bone implant or joint part and not described in relation to a method of making an implant or joint part, it should be understood that those features may be used in the method. Similarly features described only in relation to the method may also be applied to an implant according to the invention. Finally, features described in relation to a bone implant may be used in a joint part and *vice versa*.

By way of example embodiments of the invention will now be described with reference to the accompanying drawings of which:

Fig. 1 is a view of a complete acetabular cup;

Fig. 2 is a sectional view of the acetabular cup; and

Fig. 3 is an end view of the acetabular cup.

The drawings show, by way of example, the application of the invention to one particular implant, namely an acetabular cup. The complete cup is shown in Fig. 1 and generally comprises an inner cup-shaped portion 1 and an outer porous portion 2. The inner cup-shaped portion 1 has a generally hemispherical concave surface 3 which provides a bearing surface of the socket of a hip joint. The inner cup-shaped portion 1 is not porous and has a thickness chosen to impart sufficient strength and rigidity to the bearing surface 3. The porous portion 2 has a porosity which increases gradually from zero to a significant level toward an outer surface 4 of the cup. The sizes of the individual pores also increase toward the outer surface 4 of the cup.

Three dimensional modelling of a part such as the porous portion 2 is traditionally carried out by adding primitives such as spheres, cylinders, boxes and other shapes, by rotating two dimensional shapes to form solids of revolution, and by making use of Boolean operations such as union, intersection or subtraction on the solids created. Parts created in this manner will then have measurable values of porosity and strength, but it is not

easy to predict how altering the part will alter its porosity and shape, nor is it easy to provide for a continuous smooth transition in the properties of the part from one region to another.

In accordance with the present invention, the three dimensional modelling of the acetabular cup is carried out using mathematical functions. The functions chosen can be relatively simple whilst still providing the desired properties. Of particular advantage for the modelling are the triply periodic surfaces that can be defined simply in mathematical functions using x, y and z coordinates. Three such surfaces are the primitive (P) surface, the diamond (D) surface and the gyroid (G) surface, having interconnectivity orders respectively equal to 6, 4 and 3 respectively. The primitive surface can be defined by the equation:

$$a_1(\cos x + \cos y + \cos z) + a_2(\cos x \cos y + \cos y \cos z + \cos z \cos x) + 1 = 0$$

Similarly, the diamond surface can be defined by the equation:

$$a_3(\sin x \sin y \sin z + \sin x \cos y \cos z + \cos x \sin y \cos z + \cos x \cos y \sin z) + \\ + a_4[\cos(4x) + \cos(4y) + \cos(4z)] + 1 = 0$$

And the gyroid (G) surface can be defined by the equation:

$$a_5(\cos x \sin y + \cos y \sin z + \cos z \sin y) + \\ + a_6[\cos(2x)\cos(2y) + \cos(2y)\cos(2z) + \cos(2z)\cos(2x)] + 1 = 0$$

Where the constants a_1 to a_6 are chosen according to the particular surface of given topology that is to be defined.

As will be appreciated, the porous portion defined by the Primitive surface has the topological characteristic of 6 struts per node, the diamond surface has the topological characteristic of 4 struts per node and the gyroid surface has the topological characteristic of 3 struts per node (the minimum). These surfaces can be used, in accordance with the invention, to define the boundary between the solid material and the pores. In that way a complex structure can be defined in relatively simple mathematical terms. It is then possible to modify the structure by adjustment of the constants a_1 to a_6, and to analyse the changes in porosity and strength that any such changes to the constants cause.

The approach set out immediately above is further explained below with reference to Figs. 1 to 3. In those examples an acetabular cup defined by gyroid (G) surfaces is shown. More specifically the locations of the solid regions of the cup are defined by the following set of inequalities:

$$z > 0$$

$$x^2 + y^2 + z^2 > r_i^2$$

$$\cos r \sin n\theta + \cos n\theta \sin n\phi + \cos n\phi \sin r + ar - b < 0$$

where

$$r = \sqrt{x^2 + y^2 + z^2} \qquad \theta = \arctan\frac{y}{x} \qquad \phi = \arctan\frac{z}{\sqrt{x^2 + y^2 + z^2}}$$

with the parameters:

r_i internal radius of the porous portion of the cup

n circumferential resolution (number of features)

a porosity gradient

b porosity offset

Shapes that can be generated by these inequalities are shown in Figs. 1 to 3. As can be seen the porosity of the porous portions and the sizes of the pores increase outwardly, facilitating the natural incursion of material into the implant when it is in use and thus providing secure fixing of the implant.

As will now be understood the porosity gradient can readily be changed simply by changing the value of a in the inequality above and the porosity offset, that is the thickness of the inner, non-porous part, can readily be changed simply by changing the value of b in the inequality above.

Because the locations of the solid regions are defined by simple mathematical functions it is straightforward to program a rapid prototyping machine to make the cup. For example machines using Laser or electron beam energy sources to melt the raw material in powder may be employed. As will be understood those machines make the entire cup of Fig. 1, including both the solid inner portion and the porous outer portion, in a single process.

If it is then desired to produce a cup having different properties of porosity and strength one or more of the constants in the inequalities given above can be altered to produce a predictable variation in the properties. Since the structure shape is mathematically

defined it is relatively easy to analyse its porosity and other properties.

In the example given above, simple mathematical functions have been described but it will be understood that it is within the scope of the invention to adopt more complex functions, for example to produce more complex shapes, if desired.

Claims:

1. A joint part having a porous portion that is defined by a multiplicity of solid regions where material is present and a remaining multiplicity of pore regions where material is absent, the locations of at least most of the multiplicity of solid regions being defined by one or more mathematical functions.

2. A joint part according to claim 1, in which all the solid regions of the implant are defined mathematically.

3. A joint part according to claim 1 or 2, in which the one or more mathematical functions define a periodic nodal surface as a boundary surface between solid and pore regions.

4. A joint part according to claim 3, in which the periodic nodal surface is selected from the group comprising the primitive (P) surface, the diamond (D) surface and the gyroid (G) surface having interconnectivity orders equal to 6, 4 and 3 respectively.

5. A joint part according to any preceding claim, in which the part includes a porous portion and a solid portion which are part of the same single piece.

6. A joint part according to claim 5, in which the porous portion has a porosity in the region bordering the solid region substantially equal to the porosity of the solid portion and increases in porosity away from the solid portion.

7. A joint part according to any preceding claim, which is a ball and socket joint.

8. A joint part according to claim 7, in which the porous part defines a socket of the ball and socket joint.

9. A joint part according to claim 8, in which the socket has a concave load-bearing cup portion which is solid and a porous portion extending outwardly from the cup portion to a peripheral outer surface.

10. A joint part according to claim 7, in which the porous part defines a ball of the ball and socket joint.

11. A joint part according to claim 10, in which the ball has a convex load-bearing ball portion which is solid and a porous portion extending away from the ball portion.

12. A joint part according to any preceding claim, in which the joint part is a load-bearing implant suitable for implanting in a human body.

13. A load-bearing implant having a porous portion that is defined by a multiplicity of solid regions where material is present and a remaining multiplicity of pore regions where material is absent, the locations of at least most of the multiplicity of solid regions being defined by one or more mathematical functions.

14. A load-bearing implant according to claim 13, in which all the solid regions of the implant are defined mathematically.

15. A load-bearing implant according to claim 13 or 14, in which the one or more mathematical functions define a

periodic nodal surface as a boundary surface between solid and pore regions.

16. A load-bearing implant according to claim 15, in which the periodic nodal surface is selected from the group comprising the primitive (P) surface, the diamond (D) surface and the gyroid (G) surface having interconnectivity orders equal to 6, 4 and 3 respectively.

17. A load-bearing implant according to any of claims 13 to 16, in which the implant is made of metal.

18. A load-bearing implant according to any of claims 13 to 16, in which the implant is made of ceramic material.

19. A load-bearing implant according to any of claims 13 to 16, in which the implant is made of polymeric material.

20. A load-bearing implant according to any of claims 13 to 19, in which the implant includes a porous portion and a solid portion which are part of the same single piece.

21. A load-bearing implant according to claim 20, in which the porous portion has a porosity in the region bordering the solid region substantially equal to the porosity of the solid portion and increases in porosity away from the solid portion.

22. A load-bearing implant according to any preceding claim, in which the solid portion defines a cup which provides part or all of the socket of a ball and socket joint.

23. A load-bearing implant according to claim 22, in which the cup has a concave load bearing cup portion which is

solid and a porous portion extending outwardly from the cup portion to a peripheral outer surface.

24. A load-bearing implant according to claim 22 or 23, in which the cup is an acetabular cup.

25. A load-bearing implant according to any of claims 13 to 22, in which the solid portion defines a ball which provides part or all of the ball of a ball and socket joint.

26. A load-bearing implant according to claim 25, in which the ball has a convex load bearing ball portion which is solid and a porous portion extending away from the ball portion.

27. A load-bearing implant substantially as herein described with reference to and as illustrated by the accompanying drawings.

28. A method of making a joint part having a porous portion defined by a multiplicity of solid regions where material is present and a remaining multiplicity of pore regions where material is absent, the method including the step of depositing solid material in the multiplicity of solid regions during a process of solid freeform fabrication in which one or more mathematical functions are used to determine at least most of the multiplicity of regions where material is present.

29. A method according to claim 28, further including the step of modifying one or more of the mathematical functions to vary the porosity and/or strength of the porous portion, calculating the porosity and/or strength of the modified

porous portion and making the joint part with the modified porous portion, the method including the step of depositing solid material during a process of solid freeform fabrication in which the one or more modified mathematical functions are used to determine at least most of the multiplicity of regions where material is present.

30. A method according to claim 28 or 29, in which the implant includes a solid portion and a porous portion, the solid portion and the porous portion being formed in the same process of solid freeform fabrication to provide a one-piece integrated structure.

31. A method according to any of claims 28 to 30, in which the joint part is as claimed in any of claims 2 to 12.

32. A method according to any of claims 28 to 30, in which the joint part is a load-bearing implant as claimed in any of claims 13 to 27.

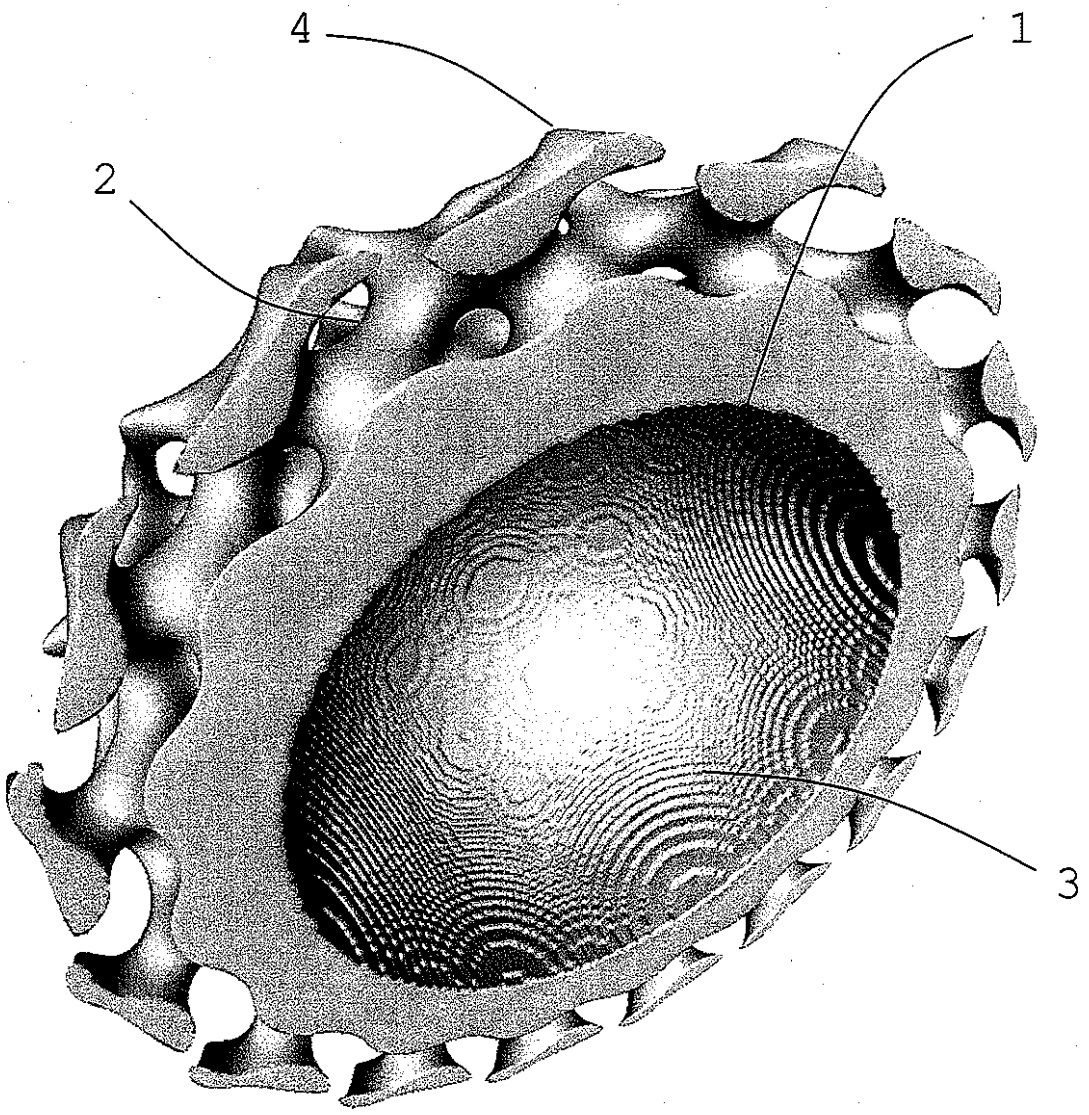

Fig 1

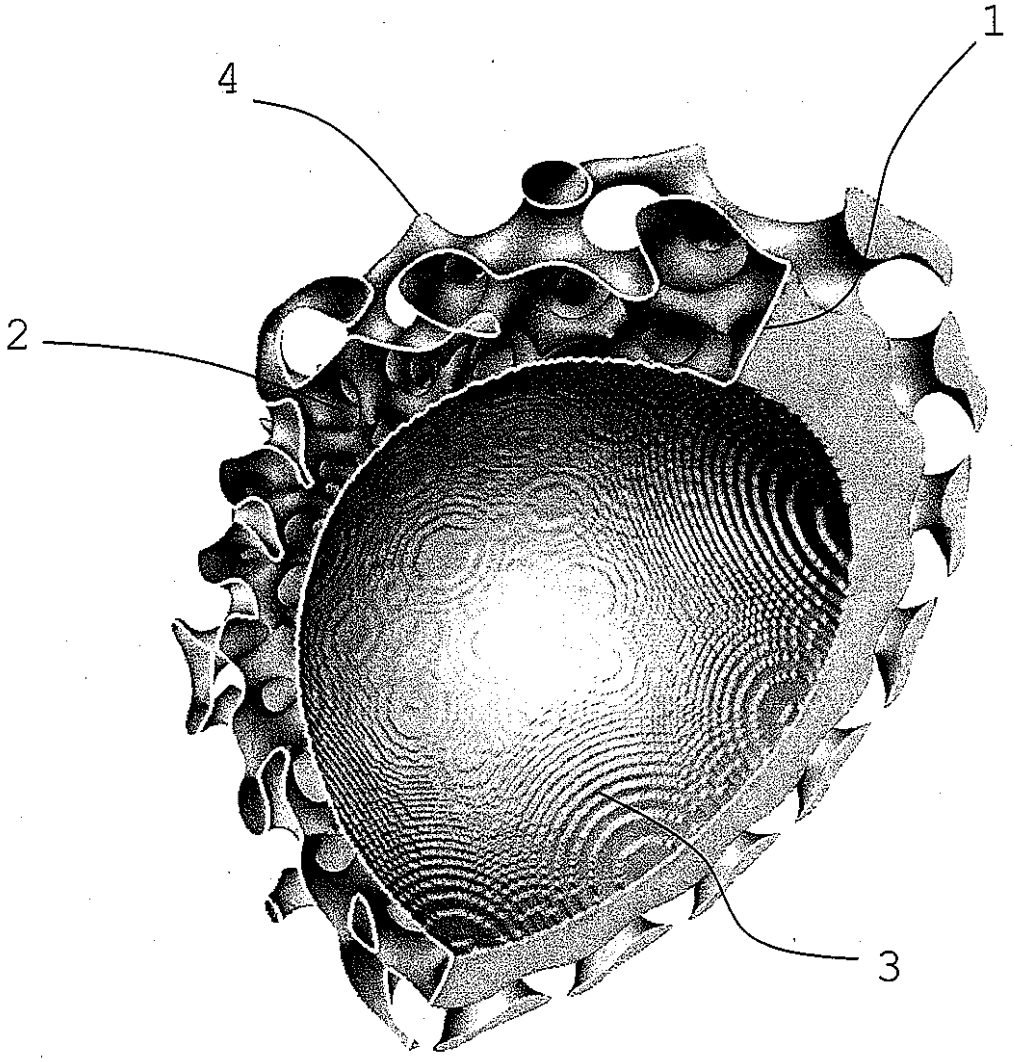

Fig 2

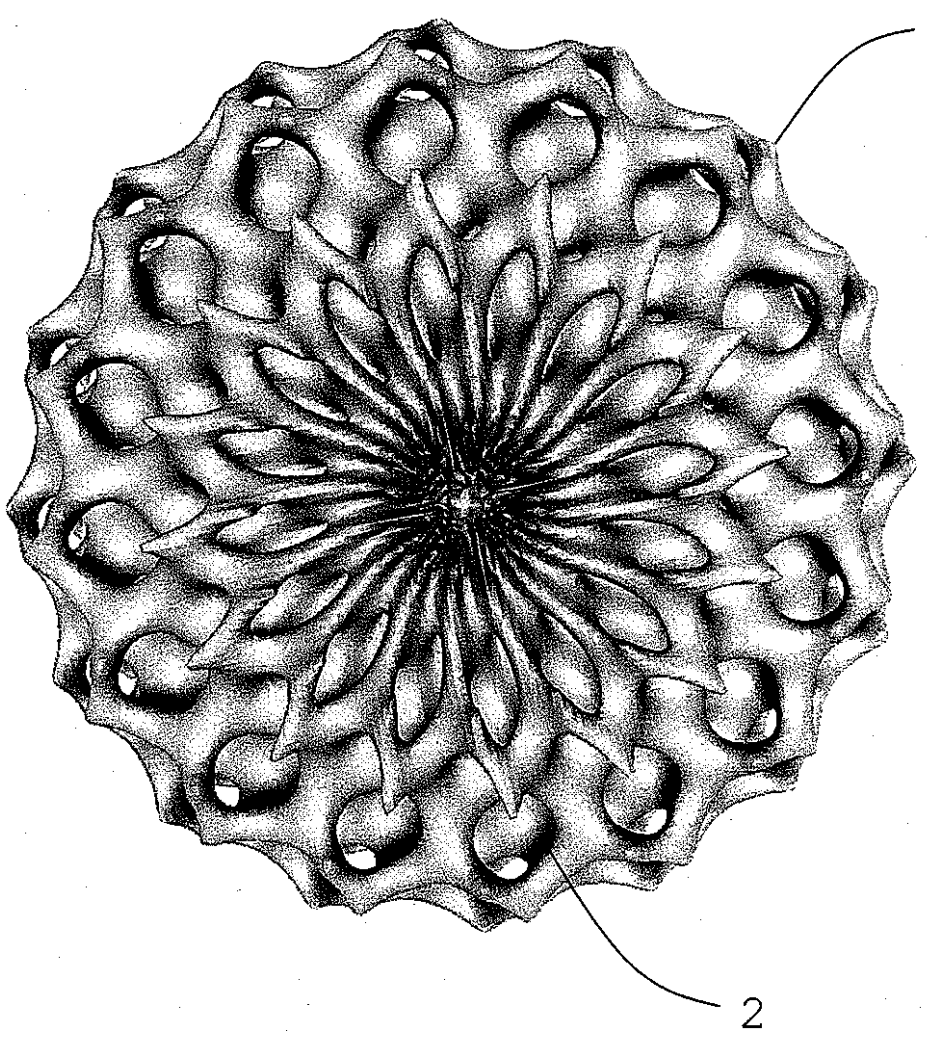

Fig 3

Appendix C

Invited Lectures and Seminars

Below is the complete list of invited talks, branched by subject. Each item includes the name of the person who sent the invitation, followed by date, place, name of the main event (if present), and School where the event/seminar took place. A selected list of talks, mainly held at conferences or meetings, is also included. Lists are provided in reverse chronological order.

- The geometry of foams
  - Katia Bertoldi, 24 Jun 2009: Enschede, The Netherlands - Multi Scale Mechanics - University of Twente, Faculty of Engineering Technology
- Periodic point sets from a differential equation
  - Stephen Hyde, 11 Dec 2008: Kioloa, Australia - Materials and Complexity VI - The Australian National University, Department of Applied Mathematics

- A new counter-example to Kelvin's conjecture on minimal surfaces
  - Chrystelle Egger, 14 May 2009: Keele, UK - RSC Advancing the Chemical Sciences - Keele University, Research Institute for the Environment, Physical Sciences & Applied Mathematics
  - Arrigo Cellina, 25 Mar 2009: Milan, Italy - Università di Milano Bicocca, Dipartimento di Matematica e Applicazioni
  - Barry Ninham, 8 Dec 2008: Canberra, Australia - Barry Ninham Chair of Natural Science - The Australian National University, Research School of Physical Sciences and Engineering
- Space partitions from a pattern forming equation
  - David Lloyd, 3 Dec 2008: Guilford, UK - University of Surrey, Department of Mathematics
  - Randall Kamien, 12 Nov 2008: Philadelphia, PA - Natural Sciences Seminars, Condensed Matter - University of Pennsylvania, Department of Physics and Astronomy
  - Thomas C. Hales, 6 Nov 2008: Pittsburgh, PA - Algebra, Combinatorics and Geometry Seminars - University of Pittsburgh, Department of Mathematics
- The Kelvin problem
  - Michael O'Keeffe, 8 Aug 2008: Santa Barbara, CA - Summer School on Periodic Structures and Crystal Chemistry - University of California at Santa Barbara, International Center for Materials Research
- Sphericity of simple polyhedra with 13 and 14 faces

  - Simon J. Cox, 23 Jul 2007: Aberystwyth, UK - Aberystwyth University, Institute of Mathematics and Physics

Other Lectures and Seminars

- The shape of soap bubbles
  - 23 Oct 2008 - University of Bath, Bridging the Gaps
  - 2 Jul 2008 - University of Bath, Department of Chemistry
- The shape of soap bubbles in foams
  - 2 Jun 2008 - University of Bath, Meeting of Minds
- Development of modelling methods for materials to be used as bone substitutes
  - 28 Feb 2008 - University of Bath, Stryker UK visit
  - 24 Oct 2007 - Nantes, Bioceramics20
- Porous matter design for load bearing capacity
  - 10 Sep 2007 - Brighton, European Conference on Biomaterials ESB2007
- Porous matter design
  - 22 May 2007 - Trinity College Dublin, Foams and Complex Systems